This is to certify that the

thesis entitled

A New Microporous Silica:
Its Intercalation in Magadiite
presented by

Astrid Bavière

has been accepted towards fulfillment
of the requirements for

Master's degree in Chemistry

Thomas J. Pinnavaia
Major professor

Date July 30, 1992

A NEW MICROPOROUS SILICA: ITS INTERCALATION IN MAGADIITE

By

Astrid Bavière

A THESIS

Submitted to
Michigan State University
in partial fulfillment of the requirements
for the degree of

MASTER OF SCIENCE

Department of Chemistry

1992

ABSTRACT

A NEW MICROPOROUS SILICA: ITS INTERCALATION IN MAGADIITE

By

Astrid Bavière

The study of magadiite evidenced the structural importance of water in the intergallery space. Removal of water from Na-magadiite by heat treatment is equivalent to proton exchange with regard to effects on stacking order. The loss of order in H-magadiite was assigned to a rearrangement of the gallery space due to the absence of water molecules.

The acid-catalyzed hydrolysis-polymerization of tetraethylorthosilicate in the presence of alkylamines generates precursors, which, when calcined, afford highly microporous silica. The pore size is controlled by the alkylamine chain length.

The polymerization of tetraethylorthosilicate into alkylamine-swollen layered silicic acid affords materials with large surface areas, due to the silica-intercalated porosity. The hydrolysis is catalyzed by the interlayer protons. Alkylamines are used to swell the layers in order for the protons to be accessible, but they also play a role in designing the pores of the silica-intercalated magadiite.

To my family

ACKNOWLEDGMENTS

I would like to acknowledge here advisor Prof. T. J. Pinnavaia for the opportunity I was given to realize this project. I really appreciated his comments and suggestions as well as his everyday good spirit. Also, thanks should go to the members of my Guidance Committee, Prof. H. A. Eick and Prof. G. J. Blanchard for their helpful advice on writing this thesis. I am also appreciative of Prof. H. A. Eick's help on X-ray analysis and electron diffraction.

I want to say a big 'Thank you' to the Pinnavaia's group members, who made these two years in the laboratory enjoyable, even if, sometimes, chemical smell could be detected, glassware was missing, but it was all fun. I really want to thank all of them for being understanding when I was monopolizing the Macintosh for drawing my figures. I especially want to thank Dr. Laurent Michot for his research spirit and for trying to communicate it through his friendly behavior. I will also remember Dr. Antonio Lara for caring about me coming back late from the Chemistry Building. No words can describe Dr. Wang and the nice feeling just to know that his smiling face was around. Also, thanks should go to Dr. Jay Amaratsekara and Dr. Ravi Kukkadapu for helping me to transfer files, for discussing science and keeping me informed on sport events (especially basketball).

I will also remember all my friends that made my two years at Michigan State University enjoyable. Among them, a special thank goes to my Summer '92 roommates, Raul (the future president of the Philippines) and Takayo, for being there when I needed breaks and for making me taste Filipino and Japanese food. I also want to acknowledge Arvind and Sanjay for their presence. I will always remember Petra for making fun of my French accent. Also to be cited are Hyon, the little Korean doll who wanted to fly and Greg the Greek who wanted to teach her how to.

Furthermore, special thanks should go to the 'French delegation'. Among them to Anne, with two 'é' in her last name, the first person I met when I arrived at Lansing Airport. Other members of the connection include Betty, Sophie, Sylvie, Pascal 1 and 2, and Frédéric. Frédéric will always be 'The French Cook' to me and his home 'The French Party House'.

Finally, but not least, I want to thank Jean-Rémi for being there everyday: to help me in the laboratory, to correct the first draft of this thesis, to paste the captions under the figures, to believe in me and much more...

TABLE OF CONTENTS

LIST OF TABLES

LIST OF FIGURES

ABBREVIATIONS

DSC: Differential Scanning Calorimetry

DTA: Differential Thermic Analysis

FTIR: Fourier Transform Infra Red

NMR: Nuclear Magnetic Resonance

SEM: Scanning Electron Microscopy

TEM: Transmission Electron Microscopy

TEOS: Tetraethylorthosilicate $Si(OCH_2CH_3)_4$

TGA: Thermo Gravimetric Analysis

TMS: Tetramethylsilane $Si(CH_3)_4$

XRD: X-Ray Diffraction

b: broad (XRD)
film: film with preferred 001-orientation (XRD)
n: narrow (XRD)
pwd: randomly oriented powder (XRD)
s: strong (FTIR)
sh: shoulder (FTIR)
vs: very strong (FTIR)
vs.: *versus* (NMR)
vw: very weak (FTIR)
w: weak (FTIR)

RESEARCH OBJECTIVES

There is a considerable interest in obtaining microporous and mesoporous materials of controlled sizes. The outstanding properties of zeolites as adsorbent and catalysts have encouraged researchers to search for new microporous and mesoporous materials, especially with pore openings larger than 10 Å. Layered materials can lead to porous materials when the sheets are propped apart by intercalative species. The general pillaring method is to insert gallery guests that are sufficiently robust to expand the host layer and laterally separated to provide a two-dimensional pore structure.[1] A new route to create microporous materials has been recently discovered that involves the hydrolysis and condensation-polymerization of metal alkoxides in the gallery of alkylammonium-exchanged derivatives of layered host.[2,3,4] Unlike conventional pillaring methods,[5,6] the use of metal alkoxides allows for the formation of the pillars *in situ*, reducing the number of steps in the pillaring process. This very promising new approach produces porous materials, but the processes

involved are still not understood. The goal of this work is to gain a better understanding of the reaction in order to predict pore sizes depending on the reaction conditions. To this end, magadiite has been intercalated by the reaction of tetraethylorthosilicate (TEOS) in presence of alkylamines as swelling agents.

Na-magadiite ($Na_2 Si_{14} O_{28} (OH)_2 . 8 H_2O$), and more particularly, its acid form, H-magadiite has been chosen in this study as a starting layered material. Indeed, magadiite belongs to the hydrous sodium silicate minerals family. Conclusions drawn for magadiite are likely to be applicable to other members of the family. Furthermore, magadiite is easily synthesized[7] by hydrothermal reaction and its swelling properties have been extensively studied.[8] However, as magadiite structure is still unknown, we first decided to carefully study Na-magadiite, and its acid form H-magadiite, to better elucidate the interlayer space where the intercalation will occur.

The silica intercalation reaction makes use of *in situ* hydrolysis and condensation-polymerization of TEOS. After obtaining some knowledge about the nature of the layered host, we investigated the sol-gel process involved during the intercalation of TEOS by conducting alkylammonium-mediated TEOS hydrolysis experiments in the absence of magadiite.

Finally, we studied the intercalation of magadiite by TEOS hydrolysis..

EXPERIMENTAL

SYNTHESIS

Na-magadiite

Na-magadiite was prepared by the reaction of NaOH and SiO_2 under hydrothermal conditions according to the procedure of Fletcher and Bibby.[9] The starting molar ratios were 1:3:50 for $NaOH:SiO_2:H_2O$. Deionized water (300.0 mL, 16.7 mol) was used to dissolve sodium hydroxide (13.3 g, 0.33 mol) in a Teflon-lined 1-liter Parr reactor. Davisil-62 silica (60.0 g, 0.99 mol) was added to the 1.1 M NaOH solution. The suspension was heated to 150°C at a rate of 1°C/min, and stirred at that temperature for 42 hours. The solid Na-magadiite product was separated by centrifugation after 10 min at 10,000 rev/min. It was then washed once with 200 mL of deionized water before being redispersed in deionized water and air-dried, at room temperature, on a polyethylene film.

H-magadiite

H-magadiite was obtained by titration of synthetic Na-magadiite with HCl according to the method described by Lagaly et al..[10] Na-magadiite was dispersed in water at a ratio of 25 ml of deionized water per gram of Na-magadiite (9<pH<10). The suspension was titrated with a 0.1 M solution of hydrochloric acid to lower the pH to less than 1.9. The titration rate was about 3 ml/min. The pH of the suspension was maintained at a value of 1.9 for a period of one day. H-magadiite was separated by centrifugation after 10 min at 10,000 rev/min and washed with deionized water until the supernatant was free of chloride ions, according to the silver nitrate test. Three washings with 30 mL of deionized water per gram of magadiite were necessary. The solid was then redispersed in deionized water and air-dried, at room temperature, on a polyethylene film. The mass of Na-magadiite titrated ranged from 2 g ($1.9*10^{-3}$ mol) to 42 g ($3.9*10^{-2}$ mol).

Amine-solvated magadiite

Three amines were used to prepare amine-solvated magadiite: hexylamine, octylamine and decylamine. The amine was added to H-magadiite in an approximately 27:1 amine:magadiite molar ratio to form a gel. For the silica-pillaring experiments, the resulting amine-solvated magadiite was freshly prepared and used after 5 to 10 min of aging in the excess amine. For the amine-swelling experiments, the amine was allowed to react with H-magadiite for one day in a sealed vial before being air-dried on a glass plate at room temperature.

Siloxane-intercalated magadiite

The wet amine-solvated magadiite gel was mixed with tetraethylorthosilicate (TEOS) in three different TEOS:amine:magadiite molar ratios: 50:27:1, 100:27:1 and 200:27:1. The suspensions were stirred for one day before being separated by centrifugation after 10 min at 10,000 rev/min. The siloxane-intercalated magadiite reaction products were redispersed in ethanol and air-dried on a glass plate at room temperature. Where indicated, the product was washed once with absolute ethanol. The mass of H-magadiite used for these preparations ranged from 0.5 g ($5.6*10^{-4}$ mol) to 20 g ($220*10^{-4}$ mol).

Silica-intercalated magadiite

To obtain a silica-intercalated magadiite, the siloxane-intercalated magadiite was calcined at 450°C for 4 hours in a programmable oven at a heating rate of 5°C/min. The powder was slowly cooled to room temperature. A preliminary survey of calcination temperatures at 100°C, 250°C, 450°C and 800°C indicated that the optimal surface area was achieved at 450°C.

TEOS-derived silica precursor

An alkylamine/alkylammonium solution was prepared by adding the desired amount of concentrated hydrochloric acid to the neat liquid amine. Tetraethylorthosilicate (TEOS) was then added to the ammonium/amine solution in three different TEOS:amine:HCl:H_2O molar ratios: 50:27:2:7, 100:27:2:7 and 200:27:2:7. The suspension was stirred for one day before being separated by centrifugation after 10 min at 10,000 rev/min. The

solution containing the TEOS-derived silica precursor was then air-dried on a glass plate at room temperature to obtain a white powder.

TEOS-derived silica

To obtain a TEOS-derived silica, the TEOS-derived silica precursor was calcined at 450°C for 4 hours in a programmable oven at a heating rate of 5°C/min. The powder was slowly cooled to room temperature.

ANALYSIS

Chemical analyses

Elemental analysis (Na, Si)

A 50-mg of sample was fused with 300 mg ($6*10^{-3}$ mol) of lithium borate for 10 min at 1000°C in a preignited graphite crucible. The resultant molten glass was transferred to 50 ml of 6% wt nitric acid solution. This solution was stirred until dissolution of the glass was complete and then further diluted to 100 mL with deionized water. The solution was analyzed by induced coupled plasma atomic emission spectrometry (ICP), at the Inorganic Laboratory of the Michigan State University Toxicology Department, on a Jarnell-Ash atom-comp instrument.

C, H, N analyses

Carbon, hydrogen and nitrogen analyses were performed at the University of Illinois Microanalysis Laboratory by oxidation of the elements and chromatographic detection of the gases produced.

Thermal analyses

Thermogravimetric analysis (TGA)

The thermogravimetric curves were obtained on a Cahn TG system 121 analyzer. The starting temperature was held at 30°C for 5 min. The sample was then heated to 800°C at 5°C/min. The furnace cooling fan was switched off at 500°C.

Differential scanning calorimetry (DSC)

The calorimetric data were obtained on a Dupont-9900 thermal analyzer, at a heating rate of 5°C/min .

Structural analysis

X-ray powder diffraction (XRD)

The basal spacings were determined by X-ray powder diffraction, using a Rigaku Rotaflex diffractometer equipped with a rotating copper anode producing K_α radiation. The current and voltage used to operate the anode were 45 mA and 100 kV, respectively. The scan speed was set to 2°/min. The temperature dependences of the XRD patterns were performed *in situ* in a specially designed high temperature aluminum attachment. Samples were prepared by spreading the powder on powder glass holders, or, when indicated, by air-drying the sample suspension on a microscope slide.

Nitrogen adsorption-desorption (surface and porosity)

Nitrogen adsorption-desorption experiments were performed on an Omnisorb 360 CX sorptometer after outgassing the samples for 12 hours at the specified temperature (75°C, 100°C, 150°C and 300°C) under vacuum.

Helium gas was used for volumetric calibration. Surface area values and pore data were obtained by the BET equation and the t-plot method.[11]

Infrared spectroscopy (FTIR)

The Fourier transform infrared spectra were recorded on an IBM IR44 spectrophotometer, using the KBr pressed pellet technique or by preparing pressed pellets of the pure material. Some experiments were run, under a flow of helium gas, under reduced pressure, at 150°C. The sample was cooled *in situ* before recording the spectrum.

^{29}Si nuclear magnetic resonance (NMR)

The solid state ^{29}Si NMR experiments were performed on a Varian 400 VXR solid state NMR spectrometer operated at 79.5 MHz. A Bruker multinuclear MAS probe equipped with zircon rotors was used for the measurements. The spectra were obtained using a 4.6 μs 90° pulse width, a 4 kHz spinning rate, a delay time of 600 s and by accumulating 12 scans, unless otherwise specified.

Scanning electron microscopy (SEM)

The scanning electron microscopy images were obtained on a JEOL JSM-25 microscope at the Michigan State University Center for Electron Optics.

Transmission electron microscopy (TEM)

The transmission electron microscopy images and the electron diffraction patterns were recorded on a JEOL JEM-100CX microscope at the Michigan State University Center for Electron Optics.

MAGADIITE CHARACTERIZATION

INTRODUCTION

The hydrous sodium silicate minerals family includes four members: kanemite ($Na\ H\ Si_2\ O_4\ (OH)_2\ .\ 2\ H_2O$),[12-14] makatite ($Na_2\ Si_4\ O_8\ (OH)_2\ .\ 4\ H_2O$),[12-16] magadiite ($Na_2\ Si_{14}\ O_{28}\ (OH)_2\ .\ 8\ H_2O$)[7,12,15-17] and kenyaite ($Na_2\ Si_{22}\ O_{44}\ (OH)_2\ .\ 9\ H_2O$).[13,15-18] Some of these minerals have been synthetically prepared by early workers.[19,20] Magadiite and kenyaite were first found in 1967 by Eugster, near Lake Magadi, Kenya.[17] Makatite was found in 1969 by Sheppard and Gude, at the same place[15]; its name comes from the Masaï (Kenya) word *emakat*, which means soda, in reference to the high sodium content of the mineral. Kanemite was found in 1971 by Maglione, near Lake Chad, Chad, in the Kanem region.[12]

Other silicates are more or less related to this silicate mineral family. These include: natrosilite ($Na_2\ Si_2\ O_5$)[13,21] which is an anhydrous sodium silicate mineral ; sodium octosilicate ($Na_2O\ .\ 8\ SiO_2\ .\ 9\ H_2O$)[16,22,23] which is only known as a synthetic hydrous sodium silicate, and some synthetic

potassium silicates such as K H $Si_2 O_5$,[24] $K_2 Si_{14} O_{29}$. x H_2O and $K_2 Si_{20} O_{41}$. y H_2O.[25]

The above sodium silicate minerals have been studied in their natural and synthetic forms. They are easily synthesized by hydrothermal reaction of aqueous sodium hydroxide with silica at various SiO_2/Na_2O molar ratios. Reaction composition, reaction temperature and reaction time determine the final product.[8,22,25] Among this family of silicates, only magadiite has a natural silicic acid analog, named silhydrite.[2,6] The materials exhibit a broad range of properties, such as, the sorption of interlamellar water and polar organic molecules, cation exchange of internal sodium cations, intracrystalline swelling, grafting and transformation into crystalline layered silicic acids by proton exchange.[7,8,13,16,25,27-32] Those specific properties promote their application as adsorbents, catalysts, catalyst supports, cation exchangers or molecular sieves.

Owing to their intercalation properties and potential use for material application, the layer structure of these silicates has been well studied. The negative charge of the layers is compensated by sodium cations, which are solvated by water molecules. Adjacent layers are held together by electrostatic interactions between the layers and the gallery cation and/or by hydrogen bonding with interlayer water.[14,16,22,30,33,34] However, except for makatite,[16] their crystal structure is still unknown due to the lack of suitable single crystals. Recently, some structures have been proposed,[22,35] based on spectroscopic data, such as infrared spectroscopy and solid state ^{1}H, ^{23}Na, ^{29}Si nuclear magnetic resonance.

In this work, we obtain a better understanding of the magadiite composition and structure by carefully studying Na-magadiite, H-magadiite

and the titration process that leads to the formation of the proton-exchanged silicic acid derivative.

RESULTS AND DISCUSSION

Syntheses

Like the other sodium silicate minerals, Na-magadiite is easily synthesized by hydrothermal reaction:[9]

$$4.7\ NaOH + 14\ SiO_2 + 233\ H_2O \rightarrow Na_2\ Si_{14}\ O_{28}\ (OH)_2\ .\ 8\ H_2O + NaOH_{aq}$$

(150°C, 42 hours)

The suspension containing Na-magadiite is centrifuged. If the white powder is redispersed in water and air-dried without further treatment, unwashed Na-magadiite containing excess NaOH is obtained. However, if the white powder is washed once with 200 mL of water before being redispersed in water and air-dried, Na-magadiite, more or less close to the ideal composition is obtained (Table 1). The magadiite acid form H-magadiite is obtained by acid titration of Na-magadiite. Figure 1 illustrates the acid titration curve for Na-magadiite and the samples that were analyzed at various stages of the titration.

TABLE 1. Na-magadiite formulae

sample		formula
	ideal	$Na_{2.0}\ Si_{14}\ O_{28}\ (OH)_{2.0}\ .\ 8.0\ H_2O$
this work	unwashed synthetic	$Na_{4.3}\ Si_{14}\ O_{28}\ (OH)_{4.3}\ .\ 8.7\ H_2O$
this work	synthetic	$Na_{2.3}\ Si_{14}\ O_{28}\ (OH)_{2.3}\ .\ 7.8\ H_2O$
this work	synthetic	$Na_{1.9}\ Si_{14}\ O_{28}\ (OH)_{1.9}\ .\ 7.0\ H_2O$
this work	synthetic	$Na_{1.6}\ Si_{14}\ O_{28}\ (OH)_{1.6}\ .\ 5.5\ H_2O$
Dailey[4]	unwashed synthetic	$Na_{2.3}\ Si_{14}\ O_{28}\ (OH)_{2.3}\ .\ 8.4\ H_2O$
Rojo et al.[34]	*natural: CA	$Na_{2.3}\ Si_{14}\ O_{28}\ (OH)_{2.3}\ .\ 8.9\ H_2O$
Garces et al.[22]	*natural: CA	$Na_{2.2}\ Si_{14}\ O_{28}\ (OH)_{2.2}\ .\ 4.6\ H_2O$
Lagaly et al.[7]	*natural: CA	$Na_{2.1}\ Si_{14}\ O_{28}\ (OH)_{2.1}\ 10.3\ H_2O$
McAtee et al.[36]	*natural: CA	$Na_{2.1}\ Si_{14}\ O_{28}\ (OH)_{2.1}\ .\ 7.5\ H_2O$
Garces et al.[22]	synthetic	$Na_{2.1}\ Si_{14}\ O_{28}\ (OH)_{2.1}\ .\ 3.2\ H_2O$
Lagaly et al.[7]	synthetic	$Na_{2.0}\ Si_{14}\ O_{28}\ (OH)_{2.0}\ .\ 10.3\ H_2O$
Schwieger et al.[18]	synthetic	$Na_{2.0}\ Si_{14}\ O_{28}\ (OH)_{2.0}\ .\ 9.1\ H_2O$
McAtee et al.[36]	*natural: OR	$Na_{2.0}\ Si_{14}\ O_{28}\ (OH)_{2.0}\ .\ 8.3\ H_2O$
McAtee et al.[36]	*natural: CA	$Na_{2.0}\ Si_{14}\ O_{28}\ (OH)_{2.0}\ .\ 8.2\ H_2O$
McCulloch[19]	synthetic	$Na_{2.0}\ Si_{14}\ O_{28}\ (OH)_{2.0}\ .\ 7.8\ H_2O$
Garces et al.[22]	synthetic	$Na_{2.0}\ Si_{14}\ O_{28}\ (OH)_{2.0}\ .\ 3.4\ H_2O$
Eugster[17]	*natural: K	$Na_{1.9}\ Si_{14}\ O_{28}\ (OH)_{1.9}\ .\ 7.8\ H_2O$
Dailey[4]	synthetic	$Na_{1.7}\ Si_{14}\ O_{28}\ (OH)_{1.7}\ .\ 7.6\ H_2O$

* K: Kenya, CA: California, OR: Oregon

Chemical compositions

The formulae have been determined using the elemental analysis and the thermogravimetric data. From the general Na-magadiite formula:

$$Na_n\ Si_{14}\ O_x\ (OH)_y\ .\ z\ H_2O$$

we are going to obtain the formulae for Na/H-magadiites (Table 2):

$$Na_n\ H_h\ Si_{14}\ O_{28}\ (OH)_{y'}\ .\ z\ H_2O$$

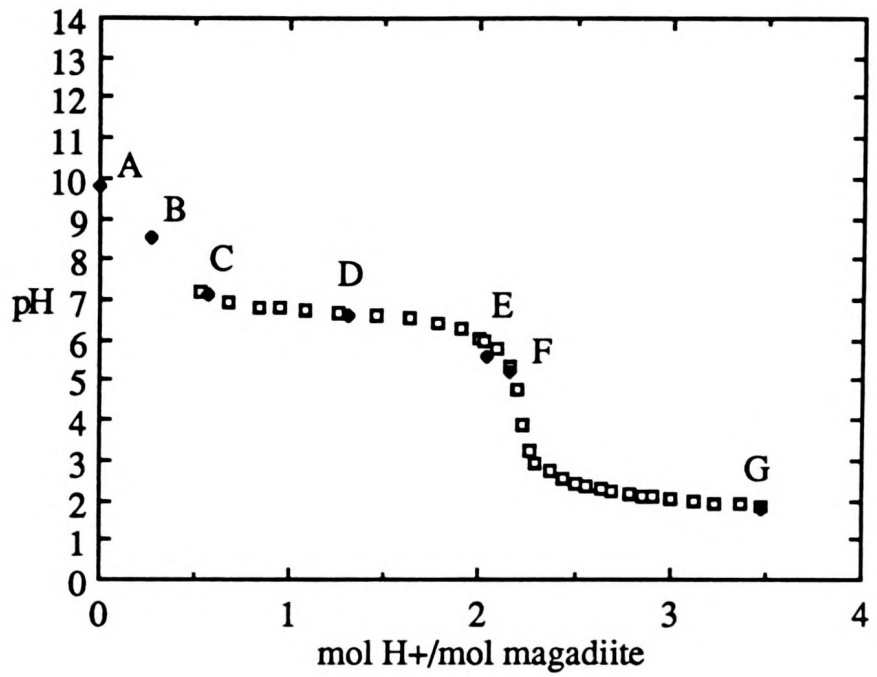

FIGURE 1. Magadiite titration curve
(3 g of Na-magadiite in 75 mL of deionized water, HCl 0.1 M, addition rate: 3 mL/min)

The molar mass M_t is:

$$M_t = n*23.0 + 14*28.1 + x*16.0 + y*(16.0+1.0) + z*(2*1.0+16.0)$$

The elemental analysis provides the molar ratio of silicon to sodium. Let's consider the ratio 14:n.

The thermogravimetric curve (Figure 2) shows that the weight loss can be divided into three main steps : room temperature to 170°C, 170°C to 450°C and 450°C to 800°C. We assigned the mass loss below 170°C to physisorbed

and interstitial water (z), and the loss between 170°C and 800°C to condensation-dehydroxylation of silanols groups (y). The assignment of the high temperature limit for water loss differs slightly from those found in the literature. Eugster[17] took 110°C, Rojo et al. 200°C[30,33] or 250°C[34] and Dailey[4] 200°C for water loss from Na-magadiite and 300°C from H-magadiite. We limited the water loss to temperature below 170°C because it matches both Na-magadiite and H-magadiite thermogravimetric curves.

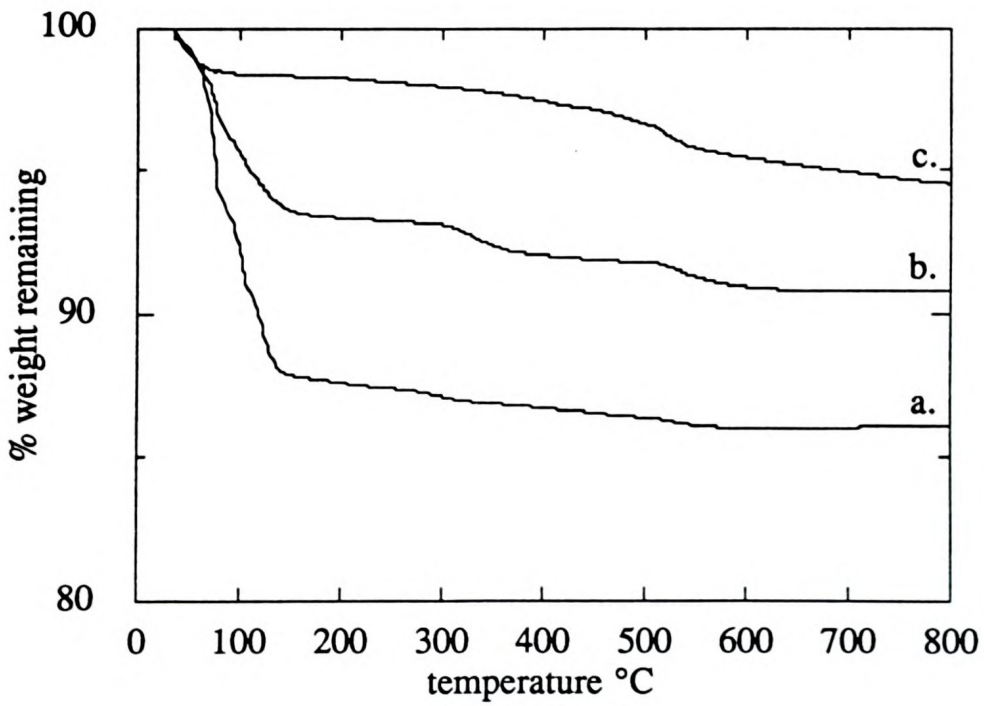

FIGURE 2. Magadiite thermogravimetric analysis curves
a. Na-magadiite, b. sample D as identified in the titration curve shown in Figure 1, c. H-magadiite

Let's consider Z, the weight loss below 170°C:

$$Na_n\ Si_{14}\ O_x\ (OH)_y\ .\ z\ H_2O \quad \text{---------->} \quad Na_n\ Si_{14}\ O_x\ (OH)_y$$

$$Z = 18.0 * \frac{z}{M_t}$$

For Y, the weight loss between 170°C and 800°C, we have:

$$Na_n\ Si_{14}\ O_x\ (OH)_y \quad \text{---------->} \quad Na_n\ Si_{14}\ O_{(x+y/2)}$$

$$Y = 9.0 * \frac{y}{M_t}$$

The fourth equation needed to solve the four-unknown system is derived from electroneutrality:

$$0 = n*1 + 14*4 + x*(-2) + y*(-1)$$

The solutions to this set of equations are:

$$M_t = \frac{31*n + 60.1*14}{1 - Y - Z}$$

$$z = Z * \frac{M_t}{18}$$

$$y = Y * \frac{M_t}{9}$$

$$x = \frac{n + 4*14 - y}{2}$$

The parameter x is then adjusted to 28, with $h = 28-x$ and $y' = y-28+x$

to obtain the final formula: $Na_n H_h Si_{14} O_{28} (OH)_{y'} . z H_2O$

The formulae found for Na-magadiite by this method (Table 1) are in good agreement with those generally found in the literature. We can notice that Lagaly et al.[7] generally find high water contents while Garces et al.[22] find low water contents for both natural and synthetic samples. The chemical compositions depend on two parameters: the sample by itself and the analytical method. The synthetic route and washing procedure,[7,37] as well as the conditions used to store the product will give products with various compositions. Too much sodium can be explained by some occluded NaOH molecules ; a low sodium content can be understood as the consequence of hydrolysis due to washing with water.[34] Those variations of sodium content in comparison to the theoretical value have also been observed for kanemite.[13] Enhanced water content can be explained by an increased hydrophilicity of the surfaces. A low water content can only be understood by cross-linkage between the layers which impedes the water molecules from occupying the gallery. We can see, for our samples, that the amount of sodium can be either smaller or larger than the theoretical value of 2. The large amount of sodium can be explained by the sodium hydroxide being trapped between the sheets during the synthesis. The small amount of sodium is due to too much washing. That is why the unwashed Na-magadiite: $Na_{4.3} Si_{14} O_{28} (OH)_{4.3}. 8.7 H_2O$ (that can be alternatively written as: $Na_{2.0} Si_{14} O_{28} (OH)_{2.0}. 8.7 H_2O. 2.3$ NaOH) looses more than half its sodium content upon washing. Then, the washed product Na-

magadiite: $Na_{1.9}\ Si_{14}\ O_{28}\ (OH)_{1.9}.\ 7.0\ H_2O$ has a smaller amount of sodium in comparison to the expected value of 2.

According to Figure 1, the titration of Na-magadiite occurs in two steps. The first inflexion point occurs at pH=8.5, for the addition of 0.3 mol H^+/mol magadiite (14%), and the second one occurs at pH=4.3, for the addition of 2.2 mol H^+/mol magadiite (100%). This two-step titration curve is characteristic of the hydrous sodium silicates: for kanemite,[13] pH=8.5 (70%) and pH=5 (100%) and for sodium octosilicate,[23] pH=7.0 (50%) and pH=4.5 (100%). Rojo et al.[34] found for magadiite: pH=9 (5%) and pH=5 (100%). This difference in percent exchanged at the first inflexion point is due to the variation in the amount of occluded sodium hydroxide present in between the layers.

TABLE 2. Composition of the samples formed at various stages in the acid titration of Na-magadiite

sample	formula	composition Na_2O: SiO_2: H_2O	%H^+ exchange
A*	$Na_{1.9}\ H_{0.0}\ Si_{14}\ O_{28}\ (OH)_{1.9}\ .\ 7.0\ H_2O$	0.95 : 14 : 7.95	0.0
B	$Na_{1.4}\ H_{0.2}\ Si_{14}\ O_{28}\ (OH)_{1.6}\ .\ 6.4\ H_2O$	0.70 : 14 : 7.30	12.5
C	$Na_{1.3}\ H_{0.4}\ Si_{14}\ O_{28}\ (OH)_{1.7}\ .\ 5.9\ H_2O$	0.65 : 14 : 6.95	23.6
D	$Na_{0.7}\ H_{1.1}\ Si_{14}\ O_{28}\ (OH)_{1.8}\ .\ 3.4\ H_2O$	0.35 : 14 : 4.85	61.1
E	$Na_{0.1}\ H_{1.7}\ Si_{14}\ O_{28}\ (OH)_{1.8}\ .\ 1.0\ H_2O$	0.05 : 14 : 2.75	94.4
F	$Na_{0.1}\ H_{1.8}\ Si_{14}\ O_{28}\ (OH)_{1.9}\ .\ 0.8\ H_2O$	0.05 : 14 : 2.65	94.7
G*	$Na_{0.0}\ H_{1.8}\ Si_{14}\ O_{28}\ (OH)_{1.8}\ .\ 0.7\ H_2O$	0.00 : 14 : 2.50	100.0

* A: Na-magadiite, G: H-magadiite

Several trends can be noted from the compositions isolated from the titration of Na-magadiite (Table 2). The amount of hydroxide remains

almost constant while the sodium content keeps on decreasing with increasing added H^+. The amount of sodium, hydrogen and water are correlated : the disappearance of sodium and water is compensated by the appearance of hydrogen. In the first stage of the reaction, corresponding to the transition from sample A to B (Figure 1), the amounts of sodium and hydroxide decrease in relatively the same proportions, while the hydrogen content remains almost constant. This corresponds to the titration of the sodium hydroxide trapped in between the layers during the Na-magadiite synthesis.[34] Upon further titration to pH~6.6, the amount of hydroxide remains constant, but the sodium amount decreases sharply while the hydrogen amount increases (compare samples B to E). The plateau on the titration curve is assigned to the sodium-proton exchange reaction. At the same time, the water content exactly follows the decrease in sodium: the water molecules leave the solid together with the sodium cations. It is an evidence for the presence, at this point, of water molecules only in the form of an hydration sphere around the sodium cations. The last step (samples E to G) corresponds to the second equivalence point. The hydroxide concentration remains constant at its initial value. Gradually, the sodium content reaches 0 while the hydrogen content reaches the initial sodium value, and, the water content still decreases a little. During this step, the exchange process is completed, but the water content decreases from 1.0 to 0.7. Our chemical composition for H-magadiite has a relatively low water content in comparison to the ones found in the literature (Table 3).

TABLE 3. H-magadiite formulae

sample	formula $SiO_2 : H_2O$
this work	14 : 2.5
Dailey[4]	14 : 2.0
Rojo et al.[33]	14 : 3.7
Lagaly et al.[28]	14 : 5.4

According to the Na-magadiite formula, there are 1.9 moles of sodium per Si_{14} unit. However, according to the titration curve, 2.2 moles of H^+ are required to titrate one mole of Na-magadiite (0.3 moles for interlayer sodium hydroxide and 1.9 moles for sodium cations). There is thus a 14% deviation in the sodium content, which might be due in part to experimental errors and to titration of dissolved CO_2. Contamination by CO_2 is plausible since the titration was carried out over a period of one day.

To better understand the various slopes before 170°C on the Na-magadiite TGA curve, we ran some DSC experiments up to 300°C. The Na-magadiite and H-magadiite DSC curves are displayed in Figure 3. H-magadiite DSC curve only exhibits a weak endothermic phenomenon starting at about 75°C. This thermal process is assigned to water loss from external surfaces. Its weak intensity reflects the H-magadiite low water content: 14 SiO_2 . 2.5 H_2O. The Na-magadiite DSC curve shows five distinct endothermic phenomena at the approximate onset temperatures of 120°C, 155°C, 180°C, 205°C and 240°C. Kanemite DTA analysis[12] to 800°C displayed three endothermic peaks at 160°C, 220°C and 600°C and

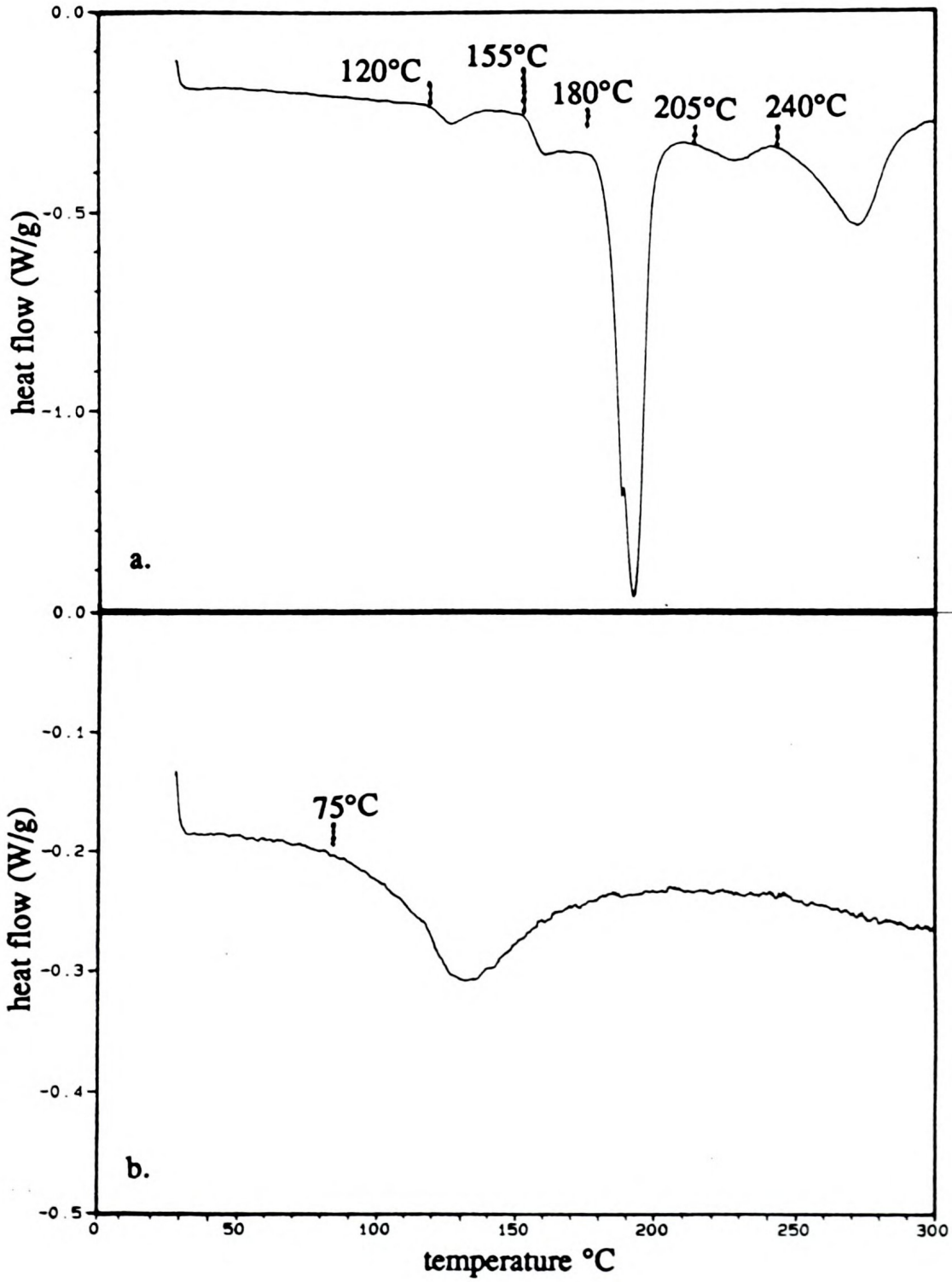

FIGURE 3. Magadiite differential scanning calorimetry spectra (heating rate: 5°C/min)
a. Na-magadiite (4.5 mg), b. H-magadiite (4.7 mg)

one broad exothermic peak at 655°C. The endothermic peaks have been assigned respectively to elimination of water molecules, dehydroxylation of silanol groups and a further dehydration ; the exothermic peak has been assigned to the recrystallization of the amorphous product. Makatite DTA analysis[15] to 1000°C displayed five endothermic peaks at 80°C, 100°C, 185°C, 530°C and 810°C and one broad exothermic peak at 675°C. So, like makatite, Na-magadiite displays three peaks below 200°C which have been assigned to water desorption. The 120°C and 155°C peaks are tentatively assigned to external water and excess water in the interlayer space, respectively. The sharp and intense peak at 180°C can be assigned to the loss of water from the sodium hydration sphere. The last two peaks at 205°C and 240°C might be due to structural rearrangements accompanied by dehydroxylation, because of the stabilizing effect loss of the hydration sphere.

X-ray powder diffraction

A careful study of the oriented powder X-ray diffraction patterns of Na-magadiite, H-magadiite and intermediate samples (samples B to F) has been achieved. The basal spacing, or d-spacing, or d_{001}, given by the X-ray diffraction analysis, is the sum of the layer thickness (11.2 Å)[38] and the gallery height (Figure 4).

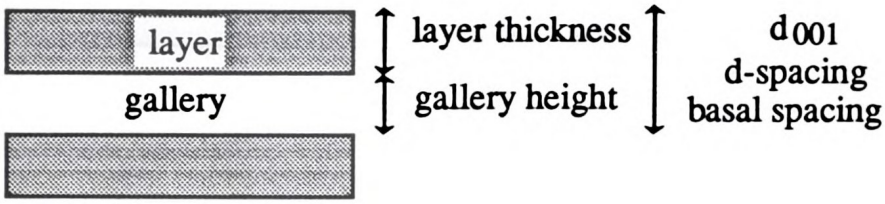

FIGURE 4. Schematic illustration of the structural definitions of basal spacing, gallery height and layer thickness

Na-magadiite X-ray powder diffraction patterns have been recorded using two preparatory methods: 1) a more or less randomly oriented powder (pwd) and 2) an air-dried sample on a microscope slide in order to make a film with preferred 00l-orientation (film). The patterns are displayed in Figures 5 and 6. The spacings are gathered with the indexed reference[38] in Table 4. Also displayed in Table 4 are the spacings for H-magadiite (pwd). The H-magadiite X-ray powder diffraction pattern is shown in Figure 7.

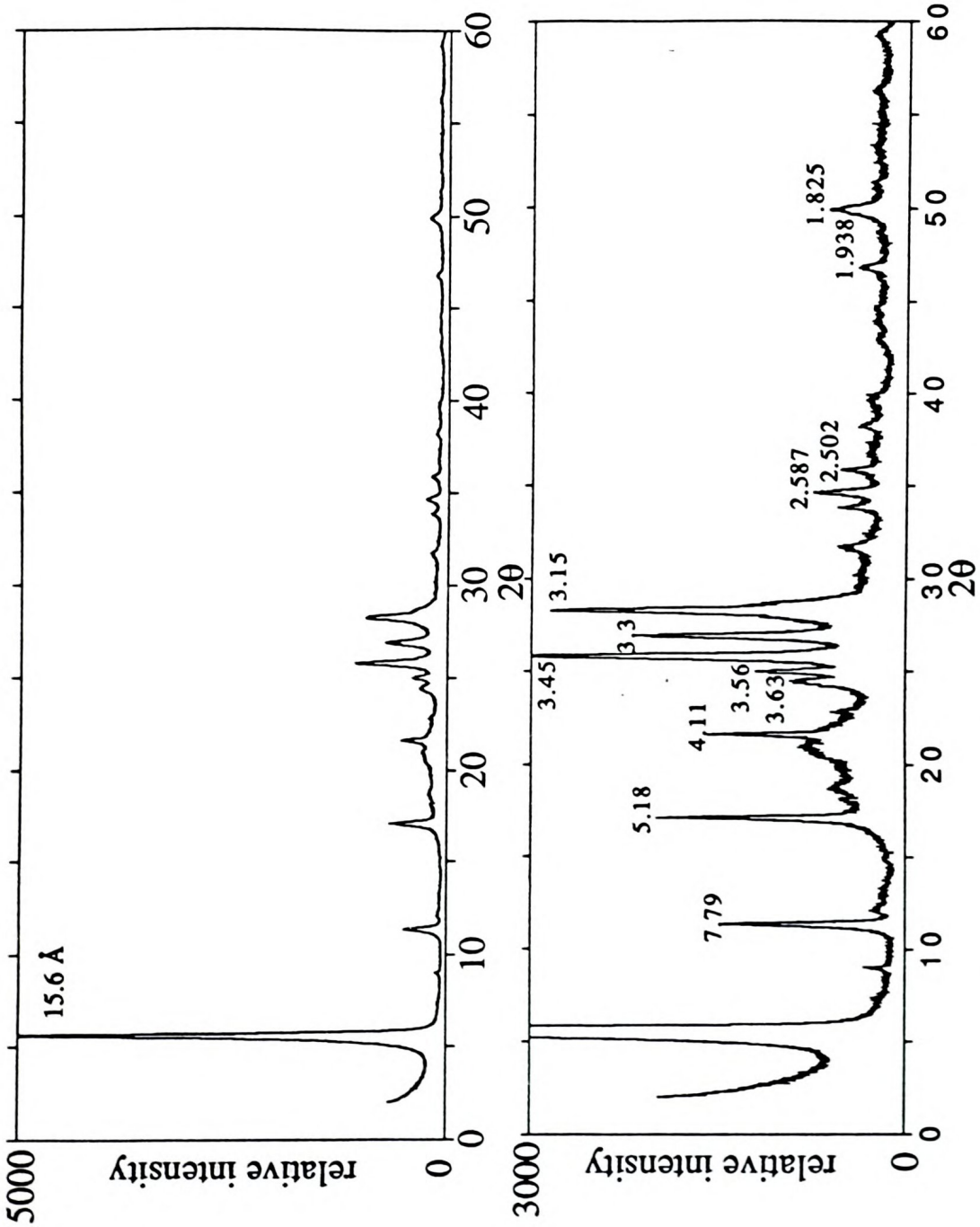

FIGURE 5. Na-magadiite X-ray powder diffraction pattern (pwd)
(the bottom pattern is an expanded scale of the top pattern)

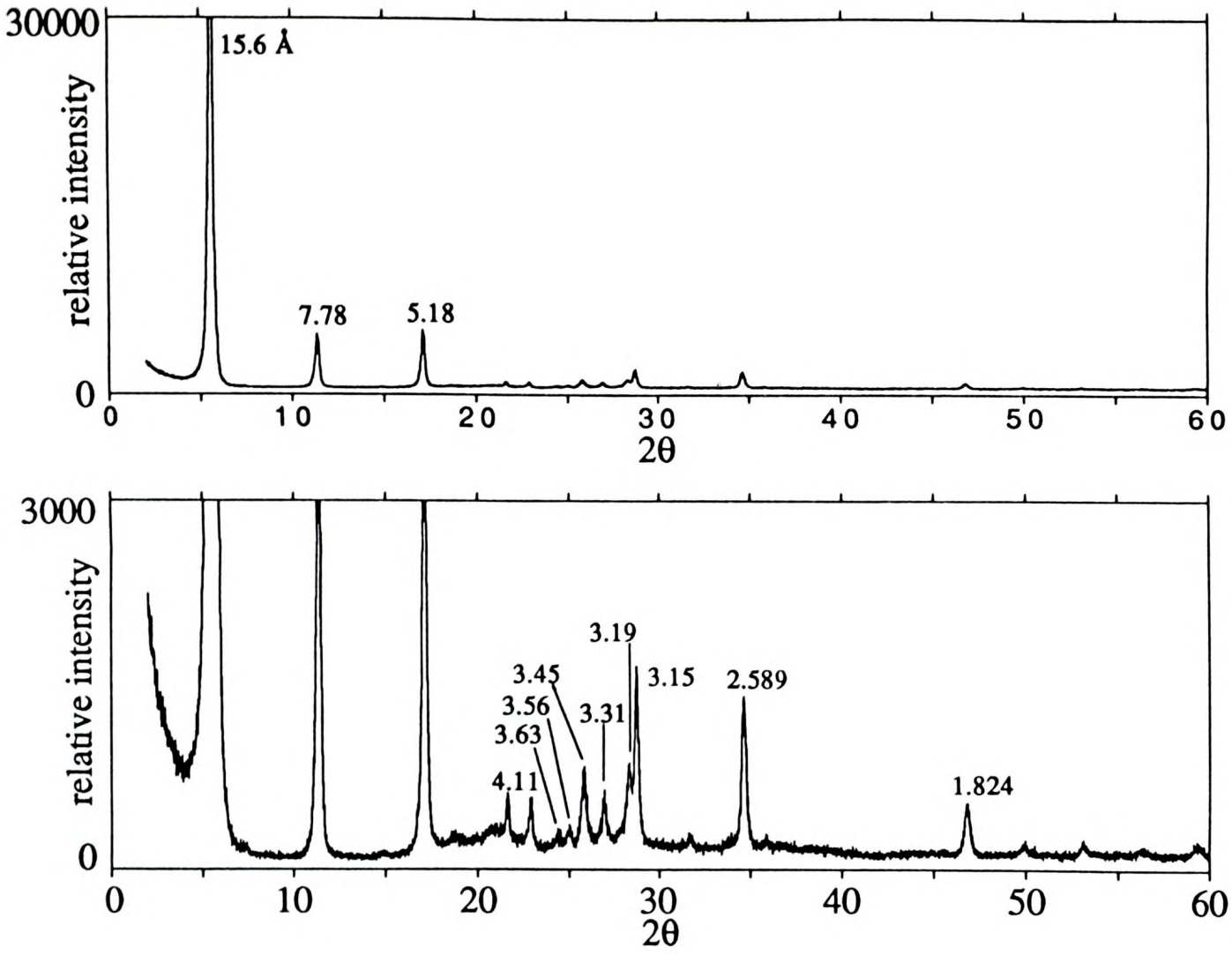

FIGURE 6. Na-magadiite X-ray powder diffraction pattern (film)
(the bottom pattern is an expanded scale of the top pattern)

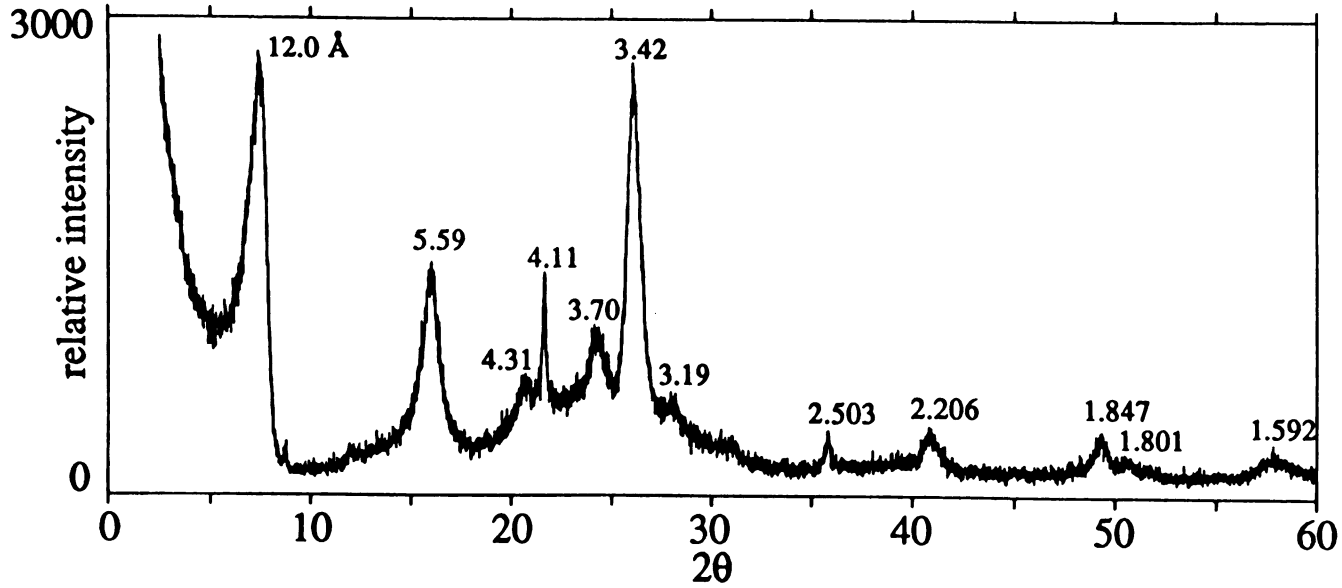

FIGURE 7. H-magadiite X-ray powder diffraction pattern (pwd)

TABLE 4. X-ray diffraction data for Na-magadiite and H-magadiite

	Na	ref	Na	pwd	Na	film		H	pwd
hkl	d (Å)	I/I_{001}	d (Å)	I/I_{001}	d (Å)	I/I_{001}	hkl	d (Å)	I/I_{001}
001	15.6	100	15.60	100	15.60	100	001	12.00	100
002	7.77	10	7.79	9	7.78	9			
010	7.24	6	7.32	1					
102	5.64	4					002	5.59	45
003	5.19	18	5.18	11	5.18	10			
102	5.01	14	4.80	1					
111	4.70	6	4.70	1					
103	4.47	18							
013	4.23	4	4.28-4.22	2				4.31	14
			4.11	7	4.11	1	hk0	4.11	39
103	4.01	8							
004	3.92	4	3.88	1	3.88	1			
020	3.63	14	3.63	3	3.63	-	003	3.70	16
021	3.54	20	3.56	4	3.56	-			
014	3.43	75	3.45	18	3.45	1		3.42	96
022	3.30	40	3.31	11	3.31	-			
121	3.20	12			3.19	-		3.19	7
203	3.15	60	3.15	16	3.15	1			
005	2.989	6							
015	2.866	6							
123-204	2.821	10	2.818	2	2.822	-			
105	2.735	4							
024-214	2.639	2	2.647	2					
006	2.599	2	2.587	3	2.589	3			
106-205	2.528	2							
			2.502	2			hk0	2.503	13
030-301	2.406	2							
106	2.353	4	2.354	1					
131-310	2.270	2	2.272	1				2.206	11
027	2.103	2	2.103	1					
034	2.067	2	2.067	1					
206	1.997	4	2.029	1					
008-304	1.97-1.94	2	1.938	1	1.941	1			
118	1.873	2							
108-316	1.822	8	1.825	3	1.824	-		1.847	12
-	1.785	2	1.778	1				1.801	5
-	1.74-1.70	2			1.722	-			
-	1.674	2							
-	1.642	2	1.630	1	1.635	-			
			1.562	1	1.558	-		1.592	7

Table 4 compares the spacings for the two Na-magadiite X-ray powder diffraction sample preparations. The randomly oriented powder sample affords for more crystallographic data, but the film preparation allowed us to resolve a peak at 3.19 Å that was obscured by a 3.15 Å reflection. From the randomly oriented powder pattern in Figure 5, we see that the two peaks overlap because of the broad base of the sharp 3.15 Å peak, but the line could not be determined. Some refection lines for Na-magadiite are missing in comparison with the lines found in the X-ray powder diffraction handbook data,[39] but, interestingly, there is one extra reflection line at 4.11 Å. We first thought it could be due to an impurity, but this spacing corresponds closely to the measured a=b=4.16 Å value for the electron diffraction pattern shown in Figure 8c (Appendix A). The electron diffraction pattern also gave us a β angle of 93.94°. Furthermore, that reflection line was also present in the Na-magadiite patterns taken at different temperatures (Figure 9 and Table 5) and in the H-magadiite pattern. We thus tentatively assigned this reflection, as well as the 2.503 Å line, to an hk0 reflection line. Unfortunately, we were not able to index satisfactorily our Na-magadiite X-ray powder diffraction data with the measured parameters a=b=4.16 Å, c= 15.6 Å and β=93.94°. Thus, in our following study, we will still use the reference values found by Brindley[38] instead of the ones found by Garces et al.[22] and Eugster[17]. For a monoclinic system, Garces et al.[22] found for its hypothetical unit cell a=27.50 Å, b=9.20 Å, c=7.52 Å, β=101°, while Brindley[38] used a=b=7.25 Å, c=15.69 Å, β=96.80°, even though he did not try the possibility for the unit cell to be triclinic. Earlier, Eugster[17] assumed a tetragonal symmetry to obtain a=b=12.62 Å and c=15.57 Å. The Na-magadiite X-ray powder diffraction pattern is characterized by a cluster of five peaks between 3.63

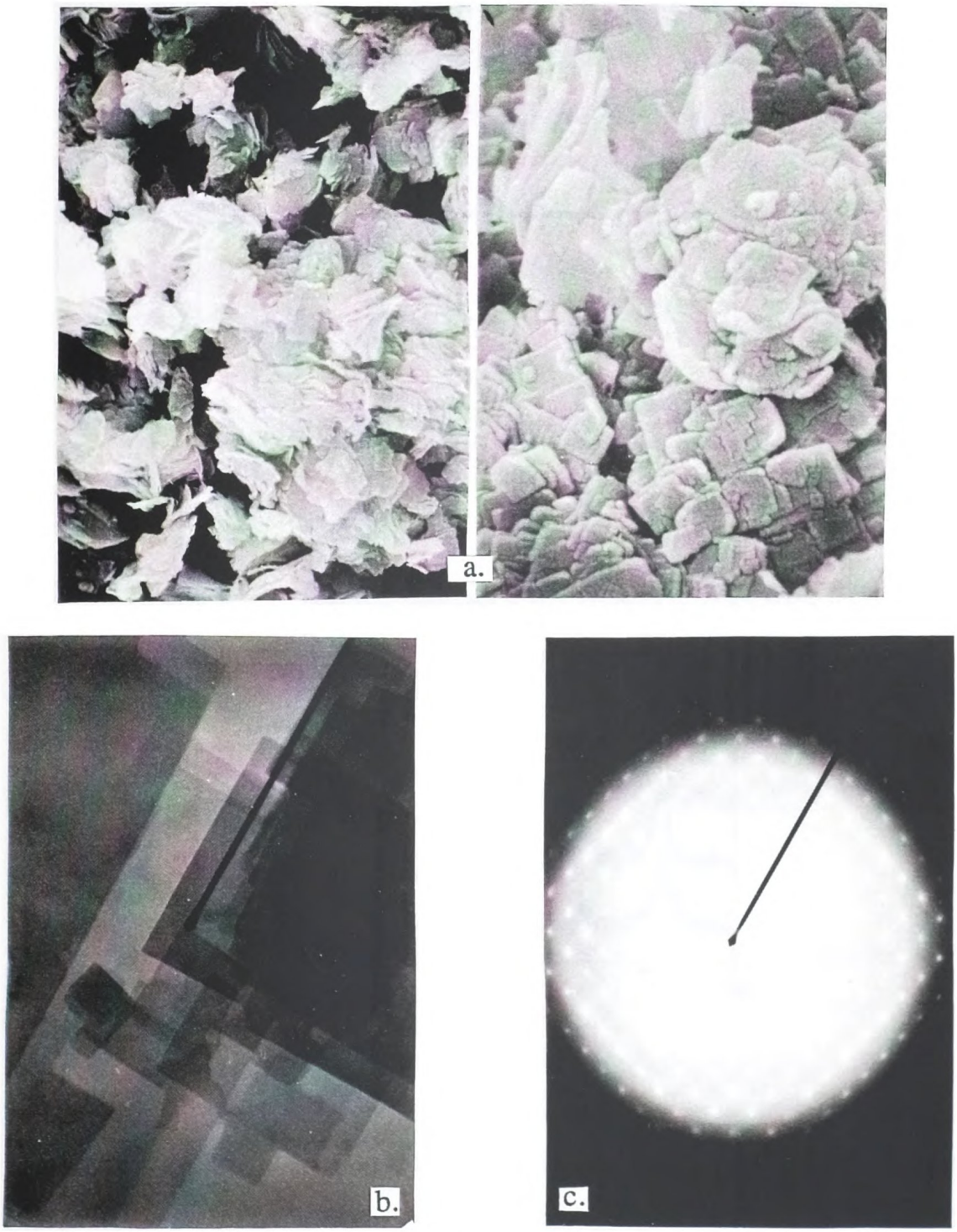

FIGURE 8. Na-magadiite electron micrographs
a. Scanning electron micrographs (left: x3,600: 1cm=2.78μm, right: x15,000: 1cm=0.667μm)
b. Transmission electron micrograph (x48,000: 1cm=0.208μm)
c. Electron diffraction micrograph (camera length=83cm: 1cm=1.53Å)

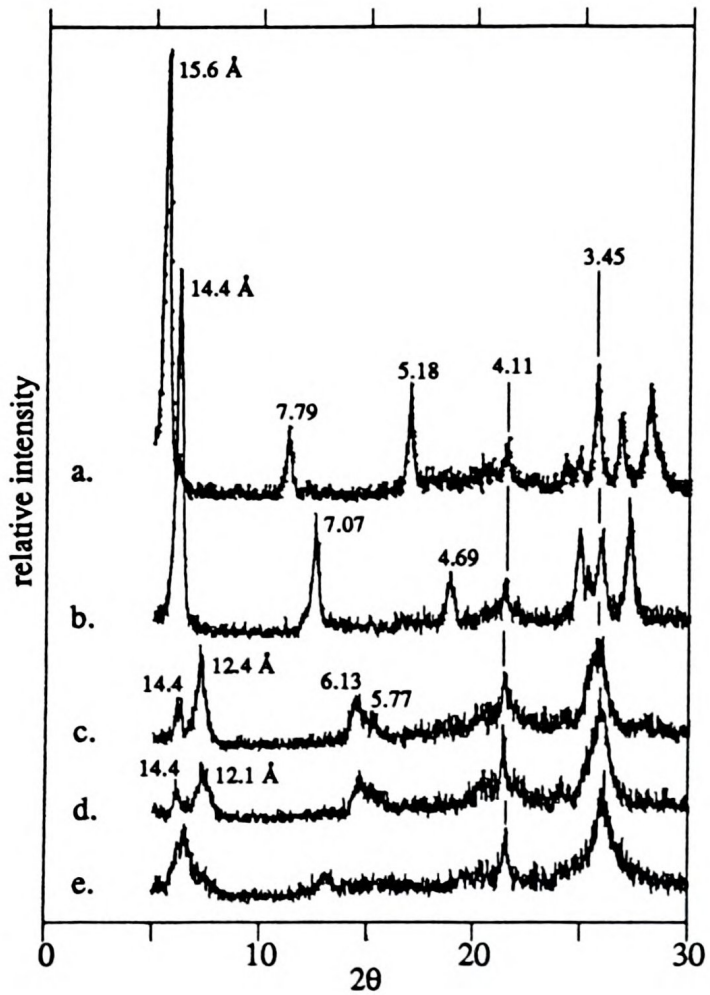

FIGURE 9. Na-magadiite X-ray powder diffraction patterns (pwd) at various temperatures

a. room temperature
b. 75°C
c. 150°C
d. 300°C
e. back to room temperature

Å and 3.15 Å.[37] With the resolution of the 3.19 Å reflection thanks to the film preparation, this cluster is more precisely made of six peaks. In contrast, the H-magadiite X-ray powder diffraction pattern is characterized by an intense reflection line at 3.42 Å. The exceptional intensity of this line can be understood by considering the Na-magadiite patterns taken at various temperatures (Figure 9 and Table 5).

TABLE 5. Selected X-ray powder diffraction reflections for Na-magadiite at various temperatures and for H-magadiite

	d (Å)				
	Na-25°C	Na-75°C	Na-150°C	Na-300°C	H-25°C
			14.4	14.4	
d_{001}	15.6	14.4	12.4	12.1	12.0
hk0	4.11	4.11	4.11	4.15	4.11
	3.63	3.58			
	3.56	3.52	3.49		
	3.45	3.44	3.43	3.44	3.42
	3.31	3.27			
	3.15				

It should to be noticed that our d_{001}-values for Na-magadiite at various temperatures are somewhat different from the ones found by Lagaly et al..[7] The values reported by Lagaly et al. are: up to 100°C d_{001}=15.6 Å, from 100°C to 200°C d_{001}=13.5 Å, from 200°C to 400°C d_{001}=11.6 Å, from 400°C to 500°C d_{001}=11.5 Å. Na-magadiite is converted to quartz at 500°C and to tridymite at 700°C while H-magadiite is converted to cristobalite at 900°C.[7] As can be seen from the d_{001}-values in Table 5, by heating Na-magadiite to 150°C or beyond, we eliminate the water molecules, and so the d_{001} value decreases. Heating the Na-magadiite:

$Na_{1.9}\ Si_{14}\ O_{28}\ (OH)_{1.9}$. 7.0 H_2O decreases the amount of water present in between the layers as does exchanging the sodium cations by protons to obtain the H-magadiite: 14 SiO_2 . 2.5 H_2O. We can see on the Na-magadiite heating experiences that the five reflection lines shift and get overlayed to one another. Thus, we can assume that the intense 3.42 Å line on the H-magadiite pattern is the sum of several overlaying lines. An other interesting point, though not understood, can be noted from the Na-magadiite pattern at various temperatures. A 14.4 Å line appears after heating at 75°C. Perhaps this reflection is hidden by the 15.6 Å d_{001} line at room temperature. In that case, this 14.4 Å line could be assigned to a hk0 reflection.

The X-ray diffraction patterns of the Na/H-magadiite compounds formed by acid titration of Na-magadiite are displayed in Figure 10. Table 6 provides the basal spacing for each derivative and the scattering domain size or crystallinity along the c-axis. The latter quantity was determined from the Scherrer equation (Appendix B).

TABLE 6. Basal spacings and crystallinity for Na/H-magadiite samples prepared by acid titration of Na-magadiite. The samples correspond to those identified in the titration curve shown in Figure 1

sample	%H^+ exchange	d_{001} (Å)	crystallinity (Å)	number of layers orderly stacked
unwashed Na-magadiite		15.6	400	26
A*	0.0	15.6	400	26
B	12.5	15.6	400	26
C	23.6	15.6	400	26
D	61.1	15.6 and 13.4	340 and -	
E	94.4	12.4	50	4
F	94.7	12.4	50	4
G*	100.0	12.0	50	4

* A: Na-magadiite, G: H-magadiite

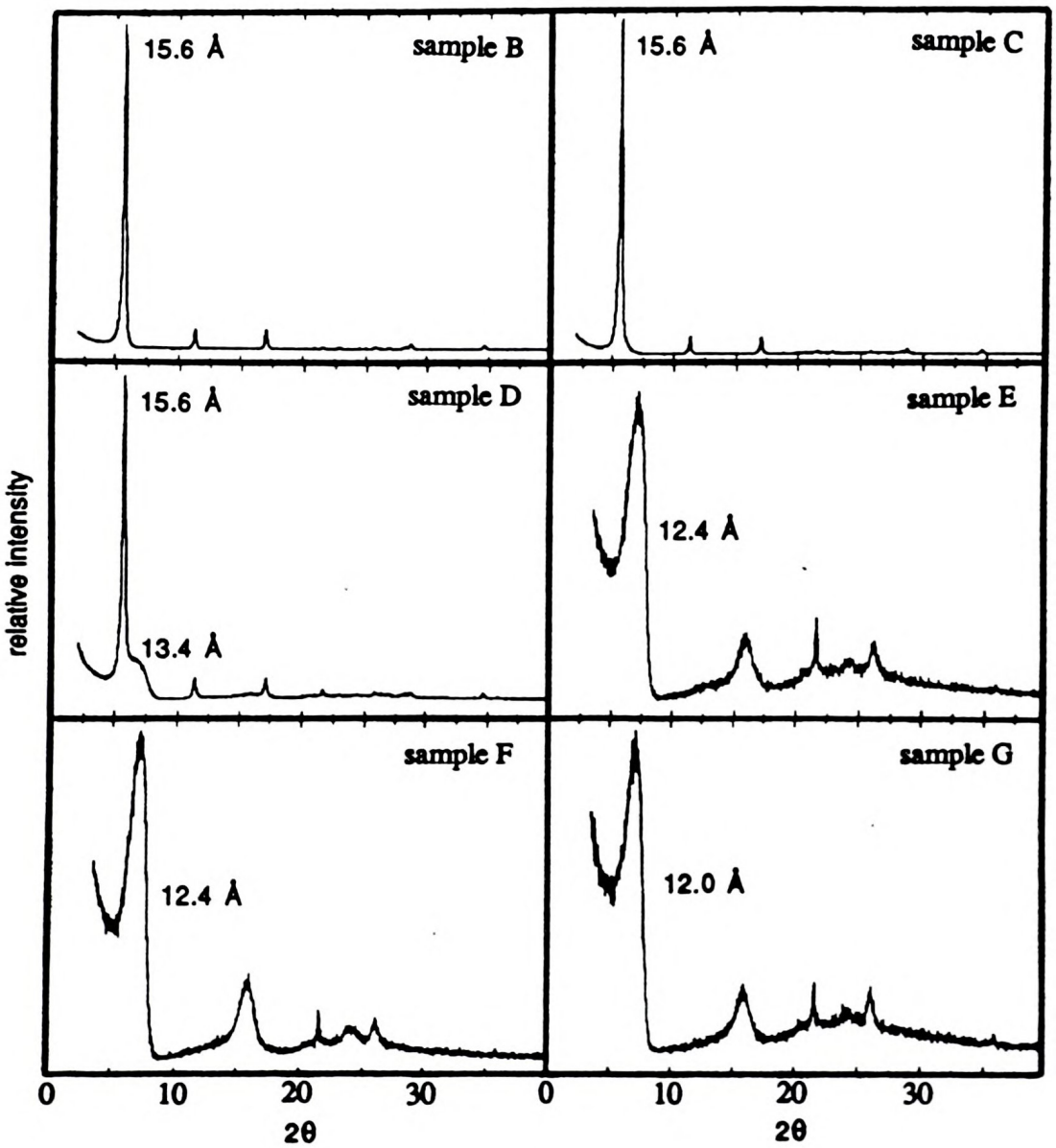

FIGURE 10. X-ray powder diffraction patterns (film) for mixed Na/H-magadiite samples prepared by acid titration of Na-magadiite. The samples correspond to those identified in the titration curve shown in Figure 1

A 15.6 Å basal spacing and a high crystallinity along the stacking direction are associated with Na-magadiite, while H-magadiite exhibits a 12.0 Å basal spacing and a lower crystallinity, as judged by the width of the d_{001} reflection. For the Na-magadiite structure, the basal spacing and crystallinity are identical from the unwashed Na-magadiite (Figure 11) with a composition of $Na_{4.3}\ Si_{14}\ O_{28}\ (OH)_{4.3}\ .\ 8.7\ H_2O$ to sample C with a composition of $Na_{1.3}\ H_{0.4}\ Si_{14}\ O_{28}\ (OH)_{1.7}\ .\ 5.9\ H_2O$. The gallery height is insensitive to variations in Na^+ and H_2O contents over this range. For the H-magadiite structure, the basal spacing varies only slightly with the water content, while the crystallinity remains the same: compare samples E ($Na_{0.1}\ H_{1.7}\ Si_{14}\ O_{28}\ (OH)_{1.8}\ .\ 1.0\ H_2O$) to G ($H_{1.8}\ Si_{14}\ O_{28}\ (OH)_{1.8}\ .\ 0.7\ H_2O$). Interestingly, as was already noticed by Rojo et al.,[34] sample D ($Na_{0.7}\ H_{1.1}\ Si_{14}\ O_{28}\ (OH)_{1.8}\ .\ 3.4\ H_2O$) is the only compound displaying two phases ; the 15.6 Å peak represents the Na-magadiite structure, while the shoulder at about 13.4 Å represents H-magadiite. The crystallinity of the 15.6 Å phase is of the same order as the previous ones (340 Å *versus* 400 Å), but, the crystallinity of the 13.3 Å phase could not be determined because of poor resolution. When two thirds of the sodium have been exchanged (sample D), the Na-magadiite structure remains unchanged for most layers. The Na-magadiite structure is stable over a wide range of sodium and water content. This stability might be due to the sodium cations stabilized by their hydration sphere. This large entity is able to prop apart the layers even though some of the sites are already exchanged: the intercalated sodium cation surrounded by its hydration sphere is robust. Furthermore, as can be seen from the data for the unwashed Na-magadiite ($Na_{4.3}\ Si_{14}\ O_{28}\ (OH)_{4.3}\ .\ 8.7\ H_2O$), the intercalated space can accommodate some extra molecules like water and sodium hydroxide in excess of the ideal formula

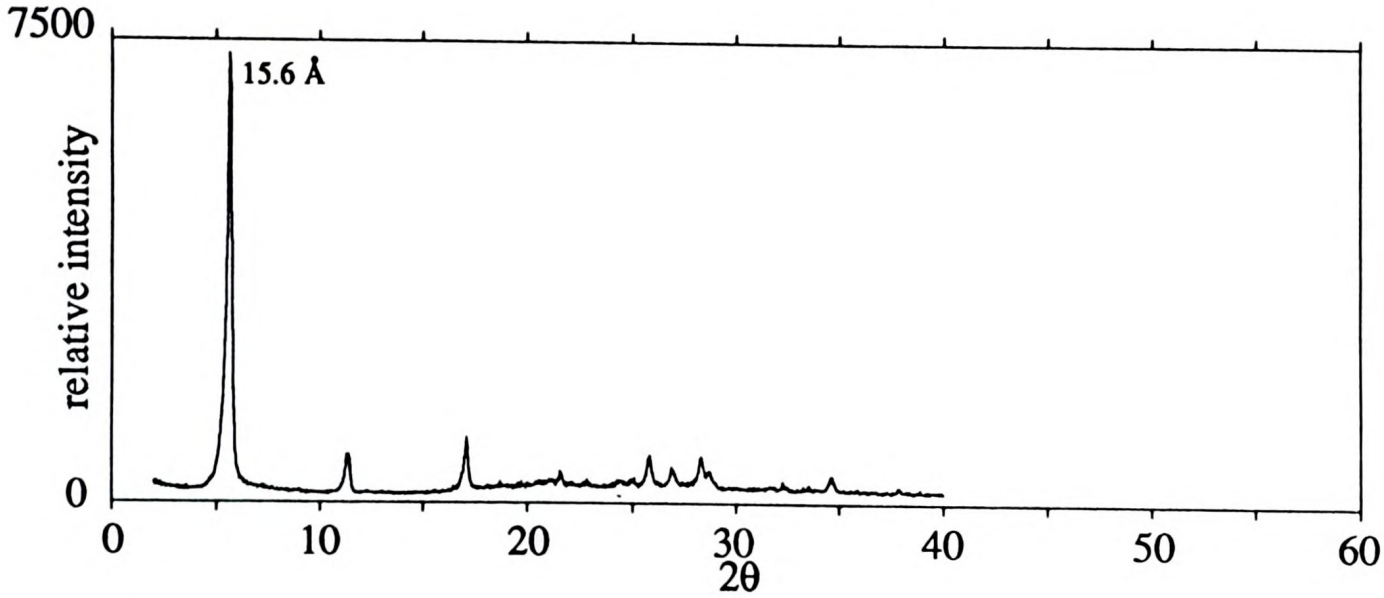

FIGURE 11. Unwashed Na-magadiite X-ray powder diffraction pattern (film)

$Na_{2.0}\,Si_{14}\,O_{28}\,(OH)_{2.0}$. 8.0 H_2O. For the H-magadiite structure, the amount of gallery water contributes to the basal spacing. That is, the basal spacing found for H-magadiite (12.0 Å) is not equal to the layer thickness (11.2 Å)[38] because of the presence of some water molecules. The presence of the two phases for sample D with 61% H^+ exchanged is a further evidence for the assignment of sodium to proton exchange with retention of structure on the titration plateau (~ pH=7). The two distinct phases present in the pattern can be understood thanks to the magadiite morphology and the assumption of a diffusion process for the proton exchange. Na-magadiite and H-magadiite have a rosette-like structure (Figure 8a).[2,4,8,18,20,22,29,38] It is formed by the stacking of thin square plates (Figure 8a and b). This morphology has also been seen for most of the elements of the hydrous sodium silicate family.[12,17,24] The layers on the edges of the rosette might be completely converted into the acid form, while only some sodium cations have already been exchanged in the internal layers. Even though the layer charge is no longer exclusively balanced by sodium cations, the gallery is still propped by the dimensions of the hydrated sodium cations.

The crystallinity, or coherent domain is associated with the sharpness of the peaks and the number of reflection lines. Peak broadening and disappearance of reflection lines are the consequences of stacking disorder.[13,34] The Na-magadiite structure crystallinity is equal to 400 Å, corresponding to about (400/15.6) 26 layers orderly stacked. The H-magadiite structure crystallinity equals 50 Å, corresponding to about (50/12.0) 4 orderly stacked layers. This loss of crystallinity, as well as the retention of the sodium structure up to some extent of proton exchange, has also been noted for kanemite[13] and octosilicate.[23] There is thus a

reorganization of the Na-magadiite structure, with retention of the crystal morphology, upon proton exchange. This change in crystallinity is indicated by the disappearance of most of the hkl reflections. This same effect on the X-ray diffraction patterns could also be seen upon heating Na-magadiite (Figure 9). Thus, the loss of crystallinity for H-magadiite is associated with the loss of the water molecules, which play an important role in Na-magadiite stability and structure .

Infrared spectroscopy

In order to obtain a better appreciation of the structure changes occurring upon converting Na-magadiite to H-magadiite, we studied next our samples (Na-magadiite, mixed Na/H-magadiite sample D and H-magadiite) by infrared spectroscopy (Table 7). Figure 12 provides the FTIR spectra for those samples.

TABLE 7. Magadiite infrared data

	infrared absorption bands (cm^{-1})										
	A		B	C		D	E		F	G	
Na-magadiite	414		547	692	782		1036	1172	1631	3291	3662
	443		579	706	811	949	1060	1205	1664	3470	
	460	483	620		821		1078	1239		3581	
sample D	414	423	542	692	785	902		1182	1631	3291	3662
	443	450	579	706		957		1200	1653	3458	
	460	483	620		821		1078	1229		3581	
H-magadiite		423	542	692	789	902		1189	1631	3291	
		450	579	706		975		1200		3440	
		483	613		821		1078	1226		3581	

A: Si-O bend[22,37]
B: double ring[22,37]
C: Si-O symmetric stretch[22,37] and Si-O-H bend[40]
D: lattice vibration[23]
E: Si-O asymmetric stretch[22,37]
F: O-H bend[12,33-37]
G: O-H stretch[12,22,33-35,40]

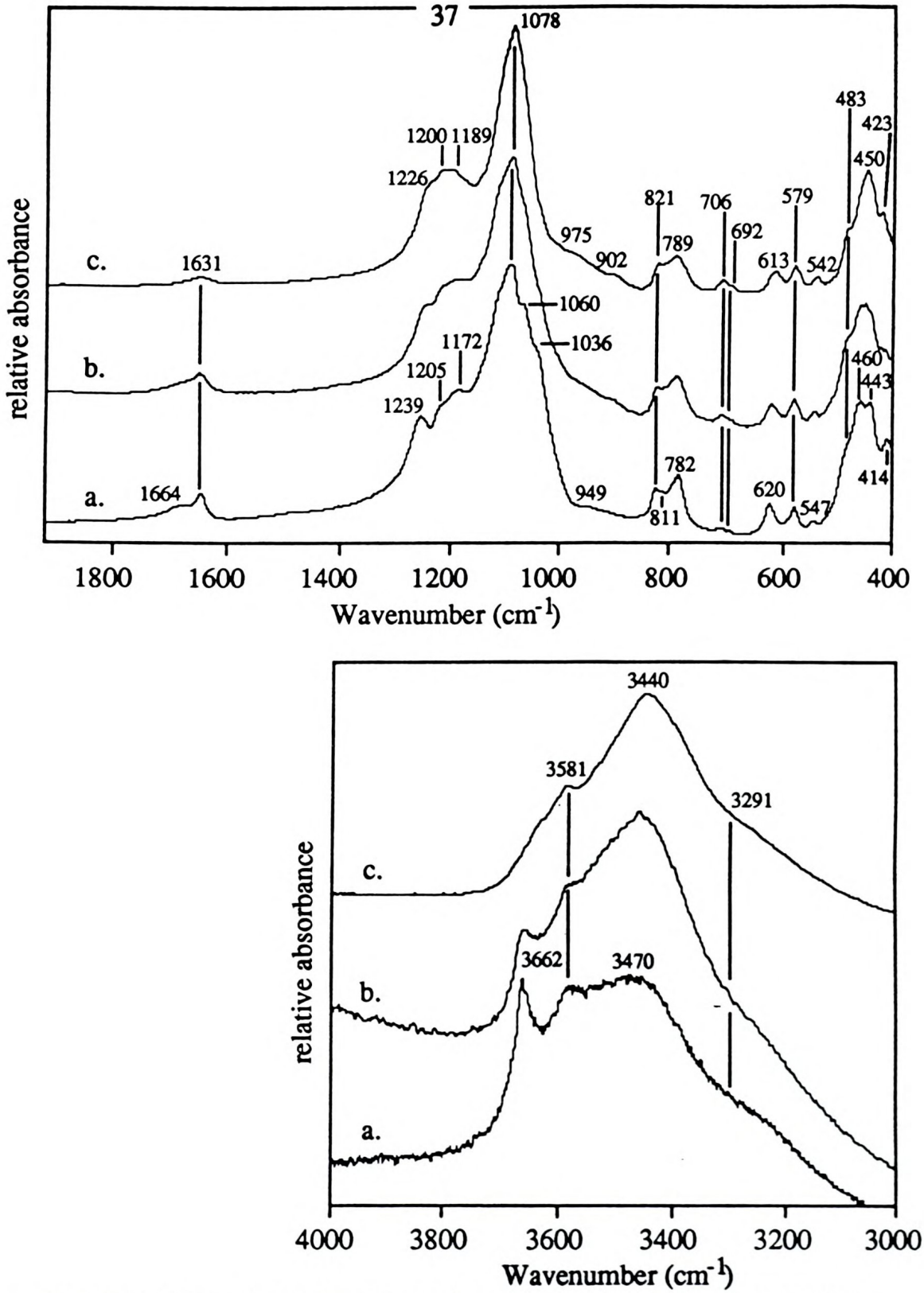

FIGURE 12. Magadiite infrared spectra (KBr pellet, room temperature)
a. Na-magadiite c. H-magadiite
b. sample D as identified in the titration curve shown on Figure 1

The infrared data obtained for Na-magdiite are close to those reported by Garces et al.[22] and by Scholzen et al..[37] By comparing his data with the 1225 cm^{-1} characteristic vibration of some zeolites, Garces et al.[22] assigned bands at 1237, 1210 and 1175 cm^{-1} to the presence of SiO_4 units forming five-member rings. He also assigned the 576 and 546 cm^{-1} bands to type B structural blocks analogous to those found in high silica zeolites. The 949 cm^{-1} band in the Na-magadiite lattice vibration region has also been reported by Borbély et al.[23] for octosilicate. The 975 cm^{-1} vibration is known to be a Si-OH stretching band for isolated silanols.[40] The O-H bend vibration at 1664 cm^{-1}, and the 1172 and 460 cm^{-1} bands of the Si-O stretch and bend vibrations, respectively, have been noted for kanemite.[12] The two latter bands might be due to the same kind of SiO_4 tetrahedra. The Na-magadiite and H-magadiite absorption lines are similar, yet distinguishable. Furthermore, sample D displays the features characteristic of the two structures. H-magadiite has a smaller number of SiO_4 tetrahedra bands (see Si-O bend and Si-O stretch regions). However, the layer double ring structure is identical. Also, there are changes in the O-H bend and stretch regions. The lower number of SiO_4 tetrahedra types in H-magadiite can be due to the conversion of $O_3Si\text{-}O^- Na^+$ into $O_3Si\text{-}O\text{-}H$ sites that were already present in the Na-magadiite structure. The changes in the O-H environments on passing from Na-magadiite to H-magadiite are due to the loss of the hydration sphere around the sodium cation, to the creation of new silanol groups and to the formation of siloxane bridges. Many bands are present in the O-H stretch region of both Na-magadiite and H-magadiite, but all the hydroxyl peaks are broadened and shifted to lower wavenumbers because of the presence of water molecules that create hydrogen bonds.

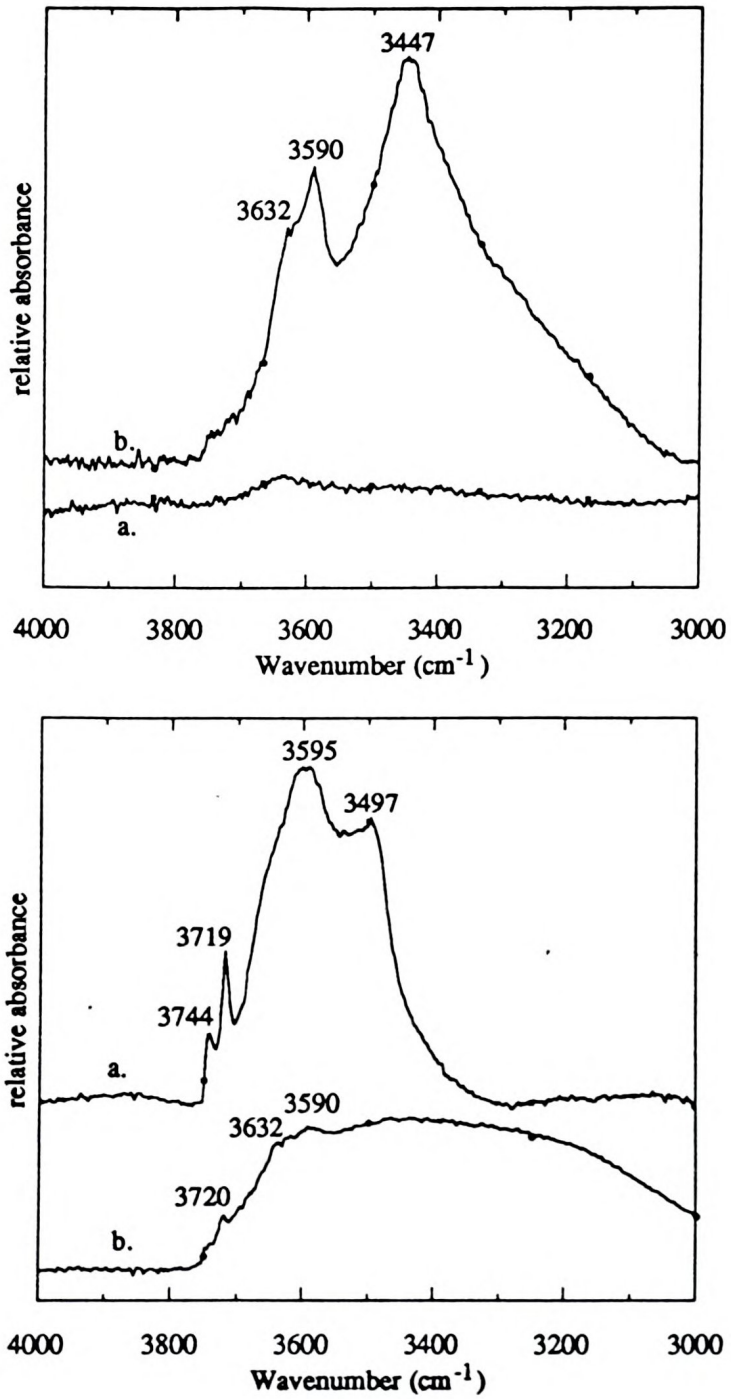

FIGURE 13. Magadiite hydroxyl stretch FTIR bands under vacuum at 150°C
top: pristine pressed pellet (a: 20 mg ; b: 10 mg)
bottom: 1 mg of sample in a 100 mg KBr pressed pellet
a: Na-magadiite, b. H-magadiite

We attempted to eliminate physisorbed water molecules by running some experiments under vacuum at 150°C (Figure 13 and Table 8).

TABLE 8. Magadiite hydroxyl stretch FTIR data under vacuum at 150°C

	infrared absorption bands (cm^{-1})							
	Na-magadiite				H-magadiite			
pristine pellet	3744	3719	3595	3497	3720	3632	3590	-
in KBr pellet	-	-	-	-	-	3632	3590	3447

Two preparative methods, which give complementary information, have been used. As a KBr pellet, the Na-magadiite reacts and looses all its water and silanol groups at 150°C. This reaction is reversible: when the pellet is put back into atmosphere and set back into the instrument, the O-H stretches appear again. The pristine Na-magadiite pellet gives more information: upon loosing its extra physisorbed water molecules, four peaks can be determined at 3744, 3719, 3595 and 3497 cm^{-1}. The KBr pellet gives more information in the case of the H-magadiite sample: three peaks can be identified at 3632, 3590 and 3447 cm^{-1}. However, when the pristine H-magadiite powder is compressed into a pellet in absence of KBr, the water cannot escape the sample. The peaks are then overlayed by the broad water peak, but an extra peak appears at 3720 cm^{-1} and the 3632 and 3590 cm^{-1} peaks can be observed. The multiple O-H stretching bands in the 4000-3000 cm^{-1} region are indicative of O-H bonds in different environments. Several O-H groups can be present in magadiite: physically adsorbed water, which is removed at 150°C under vacuum, interlayer

water molecules participating to the structure and silanol groups. Silanol groups can be on the internal or external surfaces, hydrogen bonded with other silanol groups or with water molecules. By comparison of the magadiite spectra taken before and after treatment at 150°C, we can assign the 3291 cm^{-1} shoulder to external physisorbed water. Upon complete departure of water, the Na-magadiite silanol groups are accessible and very reactive toward substitution when the pellet is diluted by KBr. Possible reactions are as follow:

$$\text{Si-O-H} + \text{KBr} \xrightarrow[-H_2O]{\text{150°C, vacuum}} \text{Si-Br} + \text{KOH} \xrightarrow[+H_2O]{\text{room temperature}} \text{Si-O-H} + \text{KBr}$$

or

$$\text{Si-O-H} + \text{KBr} \xrightarrow[-H_2O]{\text{150°C, vacuum}} \text{Si-O}^- \text{K}^+ + \text{HBr} \xrightarrow[+H_2O]{\text{room temperature}} \text{Si-O-H} + \text{KBr}$$

However, when the pristine Na-magadiite is pressed to a pellet in the absence of KBr, only external water can desorb. In that case, the structure does not change and the silanol groups can clearly be seen. For H-magadiite, when the pellet is pure, the water molecules cannot desorb at all and the spectrum displays a broad peak. However, when the sample is prepared as a KBr pellet, water can escape and then the silanol groups can be determined. There is thus a completely different behavior for Na-magadiite and H-magadiite in the presence of KBr at 150°C. The substitution reaction which occurs for Na-magadiite is a diffusion process that can not happen in the small H-magadiite gallery. The 3744 cm^{-1} band disappears upon proton exchange. This might be due to non hydrogen-

bonded internal silanol groups, due to the presence of gallery sodium cations and large gallery height. After proton exchange, some hydrogen bonds arise from neighboring silanols because the average H-H distance between O-H groups decreases from ~4 Å in Na-magadiite to ~2.5 Å in H-magadiite.[34] Then, a new band at 3632 cm^{-1} appears which is due to silanols from adjacent layers interacting with each other. The sharp 3744 cm^{-1} band has also been observed on the surface of silica for isolated silanols.[40] The 3719 cm^{-1} band might be due to isolated silanols on the external surfaces ; this band is shifted to lower wavenumbers due to some interparticle contact. This band is very weak in the pristine H-magadiite spectrum and completely absent in the KBr pellet sample of H-magadiite. As for Na-magadiite, reaction with KBr can occur because this silanol is outside the gallery. The 3595 and 3590 cm^{-1} bands might be due to hydrogen-bonded silanols while the 3497 and 3447 cm^{-1} bands might be due to interlayer water molecules. It should be noted that Rojo et al.[33] found different OH stretching bands for H-magadiite at 150°C depending on whether the starting Na-magadiite was natural or synthetic. For the natural mineral, the bands were located at 3640, 3380, 3260 and 3180 cm^{-1} while for the synthetic derivative, he found just two bands at 3620 and 3440 cm^{-1}. Conversion of his natural Na-magadiite to H-magadiite gave two types of silanols: some (H_B) interacting with the opposite layer (3380, 3280 and 3180 cm^{-1}) and the others (H_A) not (3660-3640 and 3490 cm^{-1}).[33,34]

^{29}Si nuclear magnetic resonance

To obtain more information on the Si-OH groups, we studied next the layer structure of the magadiite by solid state ^{29}Si nuclear magnetic resonance (Figure 14 and Table 9).

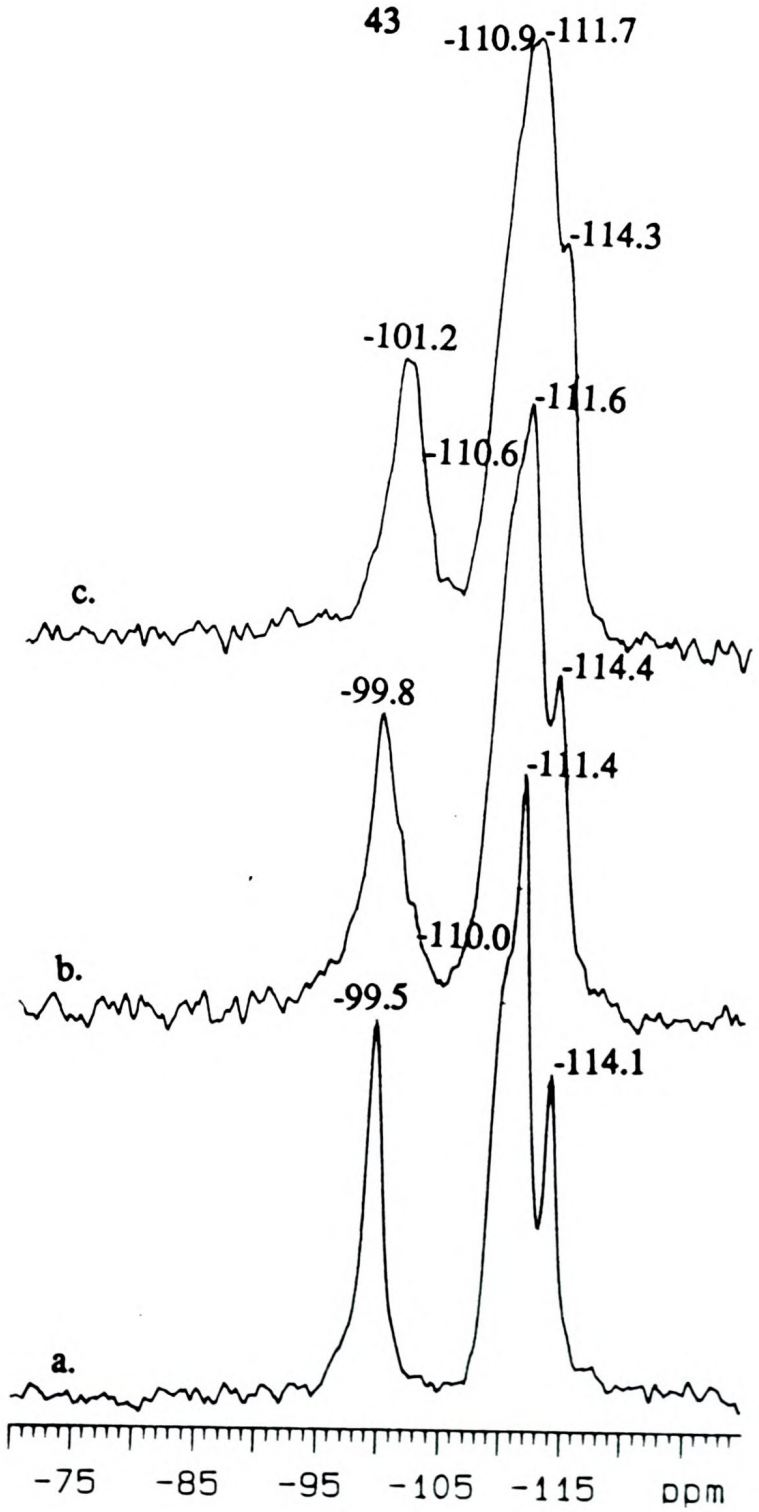

FIGURE 14. Magadiite solid state ^{29}Si nuclear magnetic resonance spectra (delay time: 1200 seconds for Na-magadiite and 600 seconds for sample D and H-magadiite, line broadening: 40, 12 scans)

a. Na-magadiite c. H-magadiite

b. sample D as identified in the titration curve shown on Figure 1

TABLE 9. Magadiite solid state ^{29}Si nuclear magnetic resonance data

sample	Si chemical shifts (ppm *vs.* TMS)				Q^3/Q^4 ratio	per Si_{14} unit cell	
	Q^3	Q^4				Q^3	Q^4
Na-magadiite	-99.5	-110.0	-111.4	-114.1	0.39	3.9	10.1
D	-99.8	-110.6	-111.6	-114.4	0.32	3.4	10.6
H-magadiite	-101.2	-110.9	-111.7	-114.3	0.29	3.2	10.8

^{29}Si NMR allows for the differentiation of SiO_4 tetrahedra environments and relative abundance of the environments. The spectra of magadiite exhibits Q^3 and Q^4 sites, according to Lippma and al. nomenclature.[41] Silicon atoms chemical shifts are governed by their bonding angles and length.[37] Q^4 sites mean the silicon atoms are coordinated to four O-Si units. They are represented as $\underline{Si}(OSi)_4$ units. The Q^3 silicon atoms are coordinated to three O-Si units, the last bond being made up of O-H or O^-Na^+ groups. We can express a Q^3 environment as $(H\text{-}O)\underline{Si}(OSi)_3$ or $(Na^+O^-)\underline{Si}(OSi)_3$.

The spectra for Na-magadiite, sample D and H-magadiite are similar. Upon proton exchange, the Q^3 peak broadens with a full width at half maximum in the range 1.6-3.8 ppm and shifts from -99.5 ppm to -101.2 ppm. This broadening and shifting of the peaks are a consequence of hydrogen bondings between the layers.[30] Indeed, a hydrogen-bond between layers will make the two silicon tetrahedra which are sharing the proton more Q^4-like. For the three samples, the Q^4 peak is divided into three components at -110.9, -111.7 and -114.3 ppm, with relative intensities of 98:100:65 for H-magadiite. For the sample D, the chemical shifts are -110.6, -111.6 and -114.4 ppm, with relative intensities of 89:100:55. For

Na-magadiite, the shifts are at -110.0, -111.4 and -114.3 ppm, with relative intensities of 70:100:52. The three H-magadiite Q^4 peaks have been missed by some authors[4,14,30] (Table 10) because the first two peaks are of the same intensity. An excessive smoothing of the spectra will only allow the determination of one peak positioned in between the two peaks of the same intensity. As the magadiite structure is still unknown, the three Q^4 peaks have not yet been assigned. There are four possible Q^4 sites: $Q^4(4Q^4)$, $Q^4(3Q^4,1Q^3)$, $Q^4(2Q^4,2Q^3)$ and $Q^4(1Q^4,3Q^3)$. The -110.9 ppm peak is sensitive to the presence of $O\text{-}Na^+$, because, after proton exchange, it shifts and its intensity increases to equal the -111.7 ppm peak. The -111.7 and -114.3 ppm peaks do not change upon proton exchange. We may postulate that they are Q^4 silicon tetrahedra that are preferentially connected to Q^4 rather than Q^3 silicon tetrahedra: $Q^4(4Q^4)$ or $Q^4(3Q^4,1Q^3)$.

The Q^3/Q^4 ratio is equal to 0.39 for Na-magadiite. This ratio can be translated, for a unit cell of 14 silicon atoms, into 10.1 Q^4 sites and 3.9 Q^3 sites. This ratio is in good agreement with the Na-magadiite formula found by chemical analysis : $Na_{1.9}\ Si_{14}\ O_{28}\ (OH)_{1.9}\ .\ 7.0\ H_2O$. This latter formula is showing 1.9 $Si\text{-}O\text{-}Na^+$ groups and 1.9 Si-O-H groups, for a total of 3.8 Q^3 silicon sites. The Q^3/Q^4 ratio is equal to 0.32 for the sample D, and equal to 0.29 for H-magadiite. This latter ratio can be translated, for a unit cell of 14 silicon atoms, into 10.8 Q^4 sites and 3.2 Q^3 sites. The Q^3/Q^4 ratio depends on the condensation of Q^3 SiOH groups. If there was no layer condensation, the Q^3/Q^4 ratio would be constant. In our case, it appears that 0.7 (18%) silanols condensed per unit cell upon proton exchange. As the Q^3/Q^4 ratio decreases from Na-magadiite to H-magadiite and the intensity of the Q^4 peak at -110.9 ppm increases, we can assign the latter peak to Q^4 sites formed by condensation of silanol groups. Condensation of silanols

groups also occurs during the proton exchange of kanemite.[42] Indeed, as kanemite is made of a single sheet of SiO_4 tetrahedra, its ^{29}Si NMR spectrum only displays a Q^3 peak. However, upon proton exchange, a Q^4 peak appears due to some silanol condensation.[42]

Various Q^3/Q^4 ratio have been reported in the literature (Table 10). Dailey[4] noticed that Na-magadiite has unusually long relaxation times: 160 seconds for Q^3 and 280 seconds for Q^4 ; for H-magadiite, both Q^3 and Q^4 relaxation times are 95 seconds. To obtain quantitative analysis, the delay time should be five time larger than the relaxation times for a 90° pulse. Scholtzen et al.[37] state that the delay time should be equal or greater than 60 seconds. A short relaxation time will enhance the Q^3 signal relative to the Q^4 signal.

TABLE 10. Various magadiite ^{29}Si NMR data

sample	ref	Si chemical shifts (ppm *vs.* TMS)				Q^3/Q^4 ratio	delay time s
		Q^3	Q^4				
Na-magadiite	22	-99.1	-109.4	-110.6	-113.2	1	10
Na-magadiite	22	-99.7	-109.5	-111.2	-113.6	0.83	10
Na-magadiite	18	-101.0	-112.2	-114.8	-117.5	0.48	20
Na-magadiite	37	-99.2	-110.1	-111.0	-113.5	0.43	7
Na-magadiite	37	-99.3	-110.0	-111.2	-113.9	0.42	7
Na-magadiite	4	-99.3	-110.1	-111.3	-113.9	0.36	~1250
Na-magadiite	14	-102			-113	0.33	4
Na-magadiite	31	-99.0	-110.7				7
H-magadiite	30	-98	-109.3			0.37	4
H-magadiite	14	-105		-111.5		0.3	4
H-magadiite	4	-100.4		-110.8	-113.7	0.28	~1250

Sample D ($Na_{0.7}\ H_{1.1}\ Si_{14}\ O_{28}\ (OH)_{1.8}\ .\ 3.4\ H_2O$) does not exhibit the Q^3/Q^4 ratios or chemical shift values of Na-magadiite or H-magadiite. The

observed values are intermediate between those of Na-magadiite and H-magadiite. So, the chemical shifts and Q^3/Q^4 ratio depends on the amount of protons in between the layers.

Generally speaking, we can say that the Na-magadiite and H-magadiite exhibit the same layer framework based on NMR spectra. But, it is somehow surprising that the Na-magadiite Q^3 peak is narrower than H-magadiite one, even though, in the Na-magadiite case, the Q^3 sites are created by two kinds of tetrahedral silicon units, namely, $(Na^+O^-)Si(OSi)_3$ and $(HO)Si(OSi)_3$. The broader H-magadiite Q^3 peak may be the result of reduced interlayer order due to some silanol condensation and the formation of hydrogen bonds.

^{23}Na and ^1H NMR experiments have also been carried out by other workers.[29,33,34] Rojo et al.[34] found two kinds of sodium in Na-magadiite at +6.7 and -1.8 ppm *vs.* NaCl. He assigned the +6.7 ppm peak to NaOH because it disappeared completely at the beginning of the titration. The -1.8 ppm peak, which decreases to zero upon complete titration, was assigned to $Na^+{-}OSi\equiv$. On the basis of relaxation time studies, Lagaly[29] found two kinds of hydrogen in H-magadiite. One due to water molecules, the other one to silanol protons. Rojo et al.[34] found three different proton environments in Na-magadiite and two in H-magadiite. Upon heating, Na-magadiite and H-magadiite lose two and one proton environment, respectively. These resonances were assigned to water molecules. For Na-magadiite, the two kinds of water can be external physisorbed water molecules and interlayer water molecules in the hydration sphere of Na^+.

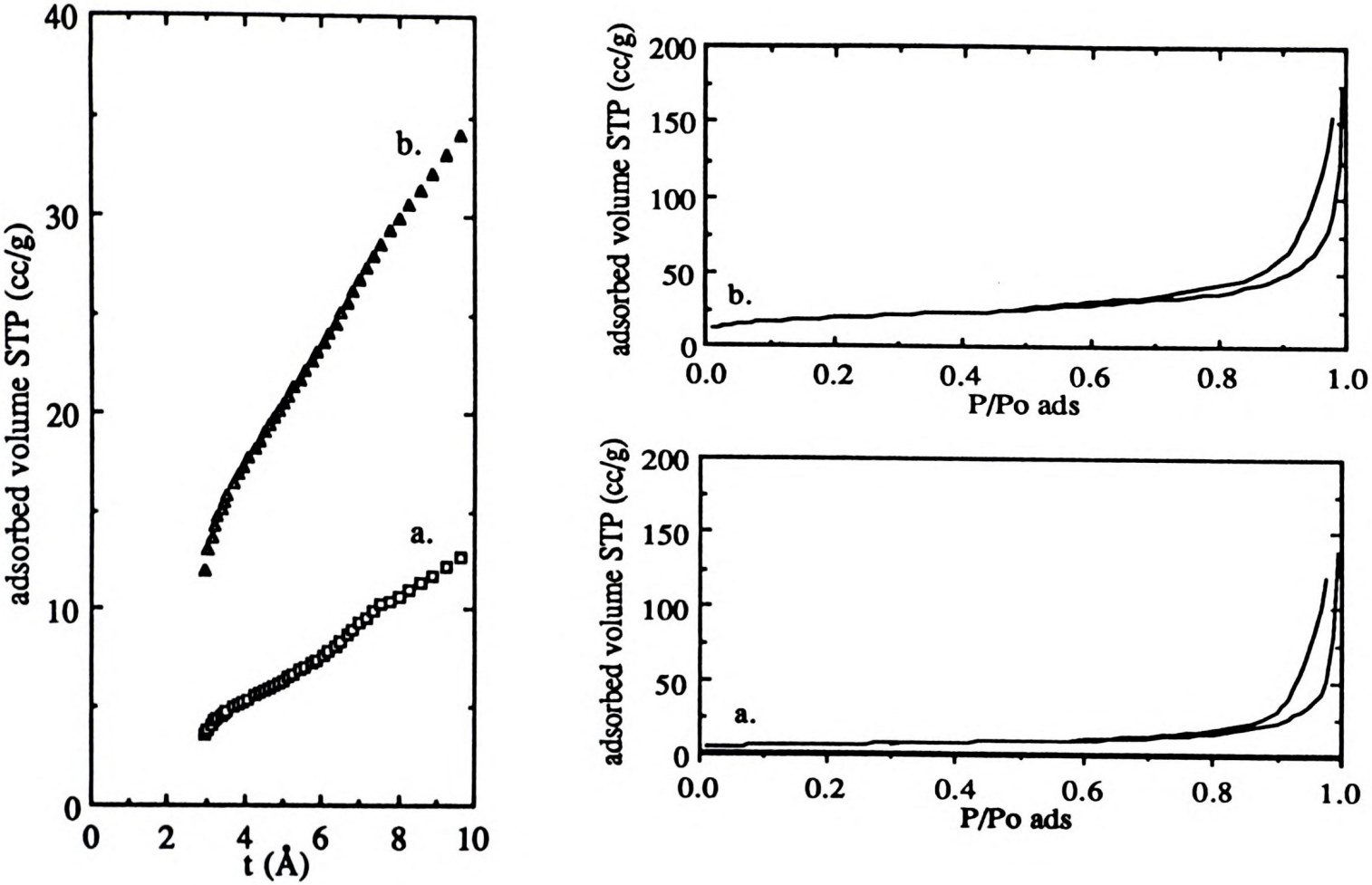

FIGURE 15. Magadiite N_2 adsorption-desorption curves ; outgassing was carried out under vacuum at 150°C
left: N_2 adsorption-desorption isotherm, right: t-plot
a. Na-magadiite, b. H-magadiite

Nitrogen adsorption-desorption

We also studied the magadiite surfaces by gas adsorption-desorption[11] (Appendix C). The isotherms and t-plots are displayed on Figure 15 and the data are gathered in Table 11.

TABLE 11. Magadiite N_2 adsorption-desorption data

		BET[43]	t-plot[44]		
sample	outgassing temperature ℃	total surface m^2/g	total surface m^2/g	microporous surface m^2/g	non microporous surface m^2/g
Na-magadiite	75	20			
Na-magadiite	150	21	21	0	21
Na-magadiite	300	20			
H-magadiite	150	70	70	48	22
H-magadiite	300	69			

Na-magadiite exhibits a total surface area of 21 m^2/g, with no micropores, regardless of the outgassing temperature over the range 75-300°C. At various outgassing temperatures, H-magadiite shows a higher total surface area of 70 m^2/g, due to the presence of micropores. Dailey[4] found a surface area of 24 m^2/g and 45 m^2/g for Na-magadiite and H-magadiite, respectively, outgassed at 120°C. Lagaly et al.[8] found a surface area of 83 m^2/g for H-magadiite which he assigned to interparticle pores. It is also worth noticing that the surface area found for H-kanemite is of the same magnitude: 50 m^2/g after outgassing at 700°C.[42] According to the t-plot, it is unlikely that the microporosity we observe for H-magadiite arises from interparticle pores. Although the basal spacing decreases with increasing outgassing temperatures (Table 5: from 14.4 Å to 12.1 Å), the Na-

magadiite surface area does not change. The increase in surface area upon proton exchange (d_{001}=12.0 Å), which arises due to the presence of micropores, indicates a different organization of the layers.

Structure discussion

The recent development of some analytical techniques such as FTIR and solid state NMR have allowed some authors[18,22] to propose some structure for magadiite. The two models assumed the formation of layers by superposition of three tetrahedra SiO_4 sheets.

Schwieger et al.[18] made use of the single-sheet makatite structure to derive structures for octosilicate, magadiite and kenyaite. The crystal structure of makatite has been determined, in 1982, by Annehed et al..[16] It is made of continuous sheets of highly folded Q^3 tetrahedra, condensed to form six membered rings (Figure 16). The study is based on basal spacing values, found by X-ray powder diffraction, and on high resolution solid state ^{29}Si nuclear magnetic resonance spectroscopy. The derived structures consist of two, three and five combined makatite-monolayers (Figure 16 and Table 12).

TABLE 12. Experimental and theoretical data for layered Na-silicate structures according to Schwieger et al.[18]

	experimental			model		
silicate	SiO_2/Na_2O molar ratio	d_{001} (Å)	Q^3/Q^4 ratio	SiO_2/Na_2O molar ratio	d_{001} (Å)	Q^3/Q^4 ratio
makatite	4	9.05	∞	4	9.10	∞
octosilicate	8	11.0	1.12	8	14.1	1.00
magadiite	14	15.8	0.48	12	19.1	0.50
kenyaite	20	19.7	0.25	20	29.2	0.25

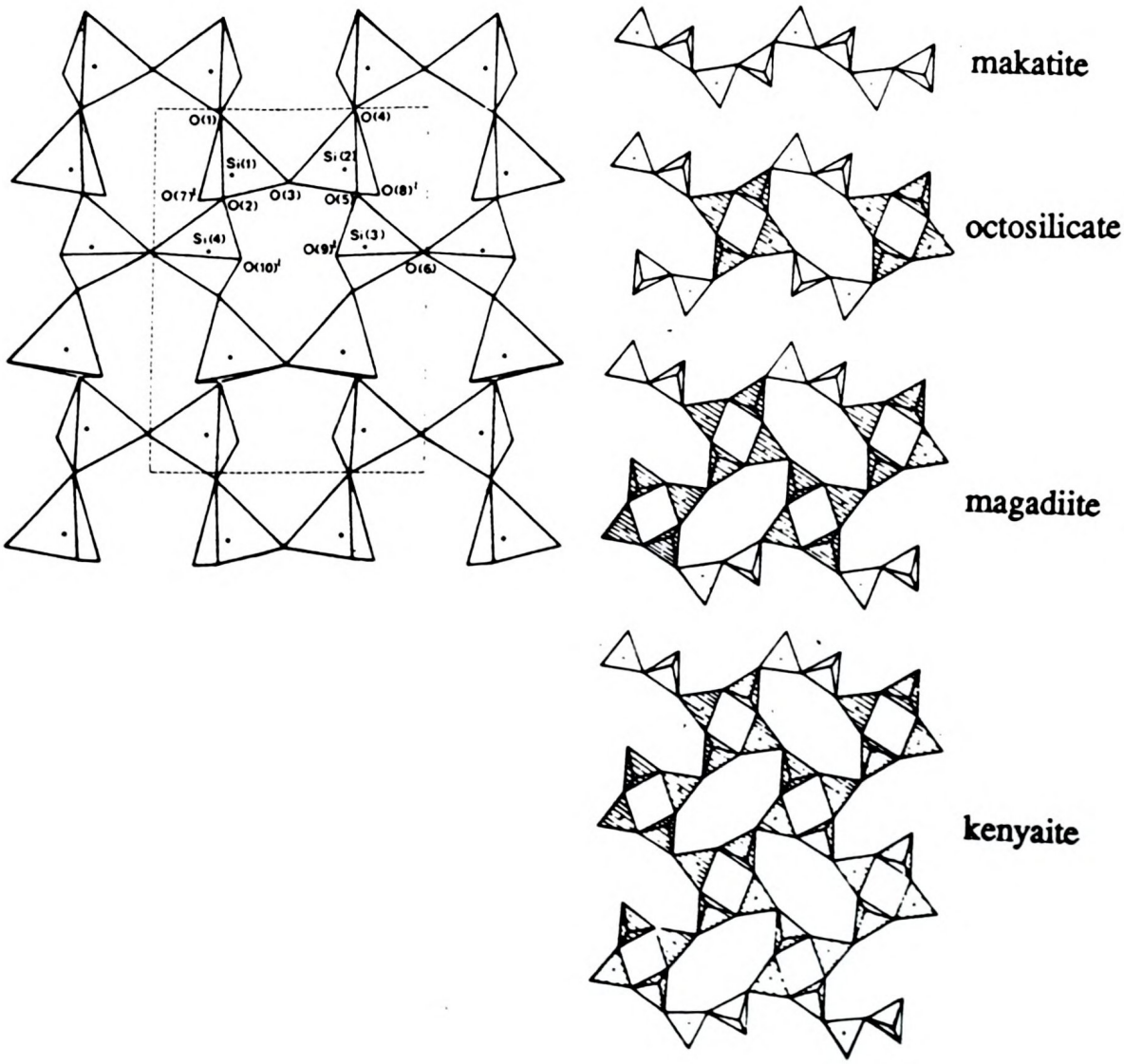

FIGURE 16. Structure of makatite and the postulated stuctures for octosilicate, magadiite and kenyaite (Schwieger and al.[18])
left: top view of the makatite single-sheet surface[16]
right: edge-on view

Table 12 clearly indicates that experimental basal spacing data are smaller than theoretical ones. The basal spacing derived from the model is the sum of the makatite layer thickness (5.02 Å), times the number of makatite monolayers, plus the makatite gallery height (4.08 Å):[18]

$d_{001} = n*5.02 + 4.08$
n=1,2,3,5 for makatite, octosilicate, magadiite and kenyaite, respectively.

The difference in basal spacings between experimental and theoretical values was explained by a condensation of Si-OH units between the makatite-monolayers. However, a discrepancy between experimental and theoretical Si/Na ratio for magadiite was pointed out, but not explained.

The hypothetical magadiite structure developed by Garces et al.[22] is based on X-ray powder diffraction data, infrared and NMR spectroscopies and comparison with mordenite- and pentasil-group zeolites. The structure is based on the experimentally derived value of Q^3/Q^4 ratio equal to unity and on the presence of an infrared peak at 1225 cm^{-1} characteristic of zeolites containing five-member rings. The Garces model consists of 'layers of six-member rings of tetrahedra and blocks containing five-member rings attached to both sides of the layers' (Figure 17). However, this model does not take into account the non-equivalent Q^4 seen in NMR.

The Schwieger and Garces models for Na-magadiite do not agree with one another. This is mainly due to the different values found for the Q^3/Q^4 ratios. The 20-second delay time taken by Schwieger et al.[18] and the 10-second delay time taken by Garces et al.[22] are too short for the spin relaxation times of 160 seconds and 280 seconds for Q^3 and Q^4,

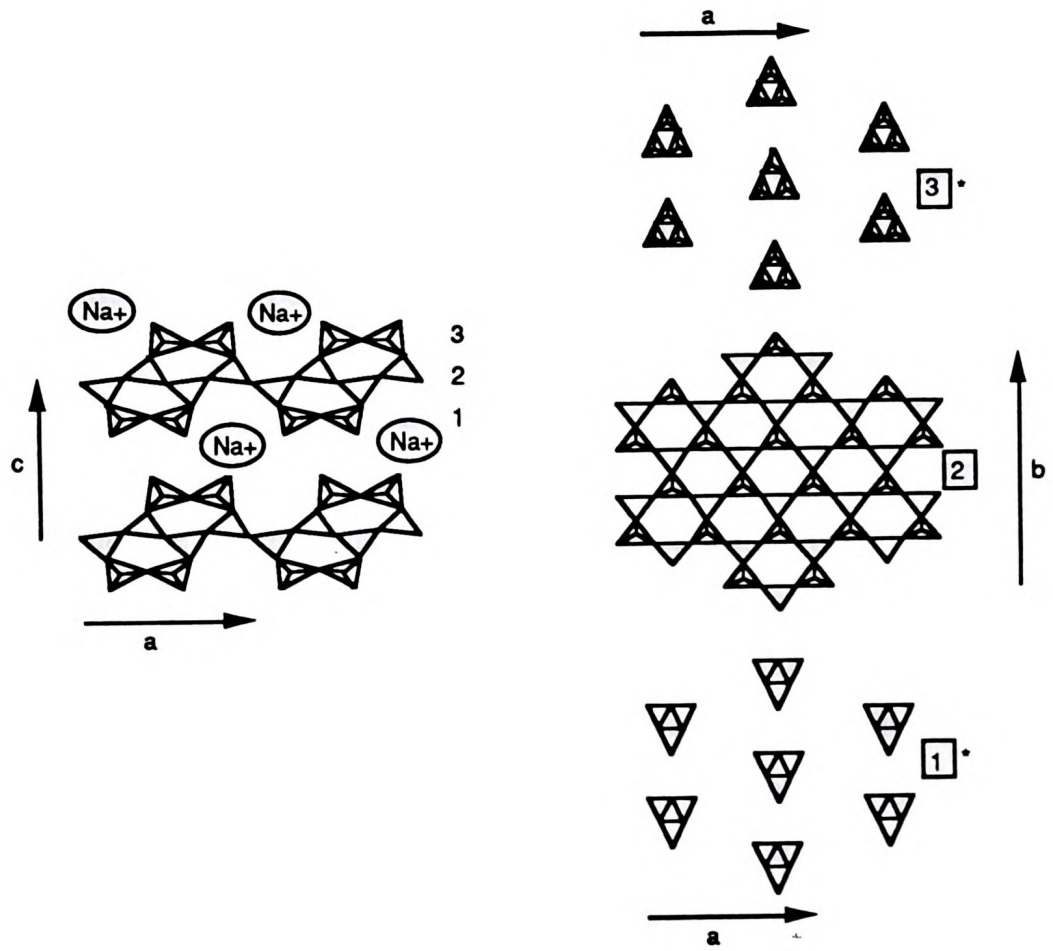

FIGURE 17. Magadiite structure postulated by Garces et al.[22]
left: edge-on view
right: top view
* possible arrangement for the level

respectively.[4] The quantitative use of the NMR data was thus, most probably, incorrect due to insufficient delay time between pulses.

Unfortunately, we are not able to propose a Na-magadiite structure that will account for our NMR data. However, on the basis of our results for the structure stabilizing effect of the hydration sphere (chemical composition, DSC) around the sodium cation, we can postulate a well-defined site for the sodium cation and its hydration sphere in the interlayer space. Indeed, an imperfect layer stacking orientation along the c-axis due to the disappearance of the stabilizing effect of the sodium hydration sphere upon proton exchange will affect the scattering of the X-rays (XRD). Such disorder has no consequence on the sheet lattice vibrations (FTIR, ^{29}Si NMR) and the morphology of the product (SEM, TEM). This loss of stabilization upon proton exchange will allow some stacking disorder that will create some intragallery micropores and then increase the surface area (gas adsorption). Thus, the disorder seen by some techniques is not due to a change of the layer structure, but to a change of the interlayer stacking arrangement. Furthermore, when the water molecules disappear, the layers become close to one another. This allows some silanol condensation, giving rise to the formation of siloxane bridges (NMR). Those bridges could explain the disappearance of some of the silanol absorption bands (FTIR).

It is also noteworthy to notice that, ideally, the sodium to water ratio is equal to 4 for the Na-magadiite: $Na_{2.0}\ Si_{14}\ O_{28}\ (OH)_{2.0}\ .\ 8.0\ H_2O$. So, the sodium cation can be located in the center of 4 water molecules. Moreover, we can recall the similarities between the 185-190°C endothermic peaks assigned to the loss of the hydration sphere on makatite[15] and magadiite. In the makatite structure,[16] sodium cations are either in the center of an

octahedra formed by water molecules, or in the center of a distorted trigonal bipyramid formed by two water molecules and three oxygen atoms, one coming from a layer, the two other from the opposite layer. So, derived from that known makatite structure, we can postulate that the sodium cations occupy positions within the layer that might be octahedral sites created by 6 oxygen atoms: 4 from the water molecules, 1 as an hydroxide from a silanol and the last one bearing the negative charge (Figure 18). This importance of the hydration sphere around the sodium cation might as well be relevant for the other members of the hydrous sodium silicate minerals family, as H-kanemite was also found to be less organized than its sodium counterpart.[42]

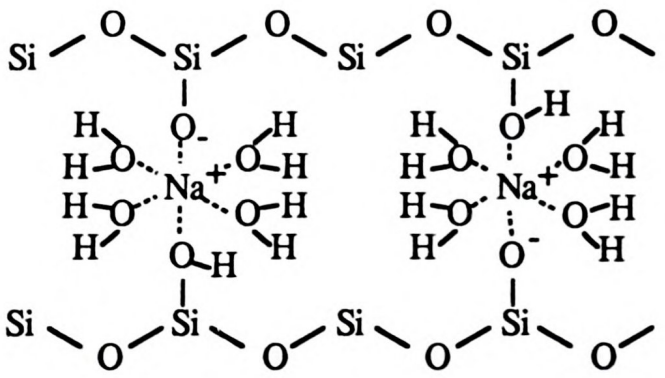

FIGURE 18. Hypothetical proposed sodium site in the magadiite

CONCLUSION

The acid titration of Na-magadiite is not a simple cation exchange reaction. The replacement of Na^+ by H^+ is accompanied by a structural change in the interlayer space and a condensation of the interlayer silanols groups. Although there is retention of the layer framework structure, the reaction is not rigorously topotactic.

Upon proton exchange, as well as upon heating Na-magadiite, the amount of gallery water decreases and the layer stacking structure becomes less organized. This stacking disorder is due to the changes in the interlayer space. Thus, the water molecules might occupy specific sites in between the layers and play a stabilizing role even after the replacement of two thirds of the sodium cations. The Na-magadiite stability is promoted by these water molecules that form the hydration spheres around the sodium cations.

ACID CATALYZED TEOS POLYMERIZATION IN THE PRESENCE OF ALKYLAMINES: SYNTHESIS OF A NEW POROUS SILICA

INTRODUCTION

A new approach has been recently developed for the metal oxide pillaring of certain types of lamellar solids.[2-4] The conventional pillaring synthesis[45,46] takes advantage of ion exchange properties of the host. The approach can be described as a two-stage reaction. In a first step, a polycationic pillaring species is intercalated by ion exchange in presence of the layered material. Secondly, the newly intercalated pillar is converted to a nanoscopic metal oxide aggregate by calcination (Figure 19). In the new approach, a condensation-polymerization reaction of an alkoxide $M(OR)_x$, (eg., tetraethylorthosilicate $Si(OCH_2CH_3)_4$ (TEOS)), is carried out in the gallery of an acid form of the layered material. The gallery height of the acidic layered material is expanded by an intercalation of alkylamine and protonated alkylammonium cations ; the $M(OR)_x$ molecules can then access

the interlayer space and proton-catalyzed hydrolysis can occur to form a metallo-organic polymer. The product is finally calcined to eliminate the organic molecules and to stabilize the intercalating species as an oxide (Figure 20). The final product displays extremely high surface areas.

In this work, we elucidate the mechanism of that new pillaring reaction that yields such microporous materials. To achieve this goal, we performed experiments in the same conditions as for the pillaring reactions, but without the presence of the layered material. The chemical effect of the layered compound was mimicked by the addition of acid. The studied reaction in that part is thus an acid catalyzed TEOS polymerization in presence of alkylamine.

BACKGROUND

Many references can be found in the literature concerning TEOS polymerization.[47-60] Most of them deal with the TEOS/water/solvent ternary system in presence of acid or base catalyst.[58] The most studied solvent is ethanol. This system is studied in order to better understand the sol-gel processing of metal alkoxides.[47] Their polymerization enable the synthesis of glasses, ceramics and composites[50-52,56] at low temperature.[55,59] They can be produced as homogeneous and pure[51] powders, films, fibers and monolithic products.[55,57-59] The studies are done in order to obtain a fundamental knowledge about the sol-gel processes: hydrolysis, condensation-polymerization, gelation, drying and densification.[47] The investigators studied in particular the effects of temperature, TEOS concentration, solvent, pH, catalyst, amount of water[50,53,55,59] on the reaction rate and mechanism[49,51,56,59] in order to derive models. They usually use nitrogen adsorption, small angle scattering, liquid ^{1}H, ^{13}C, ^{29}Si

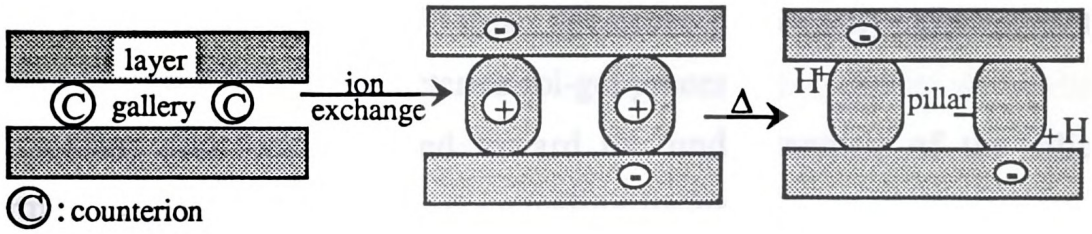

FIGURE 19. Ion exchange pillaring

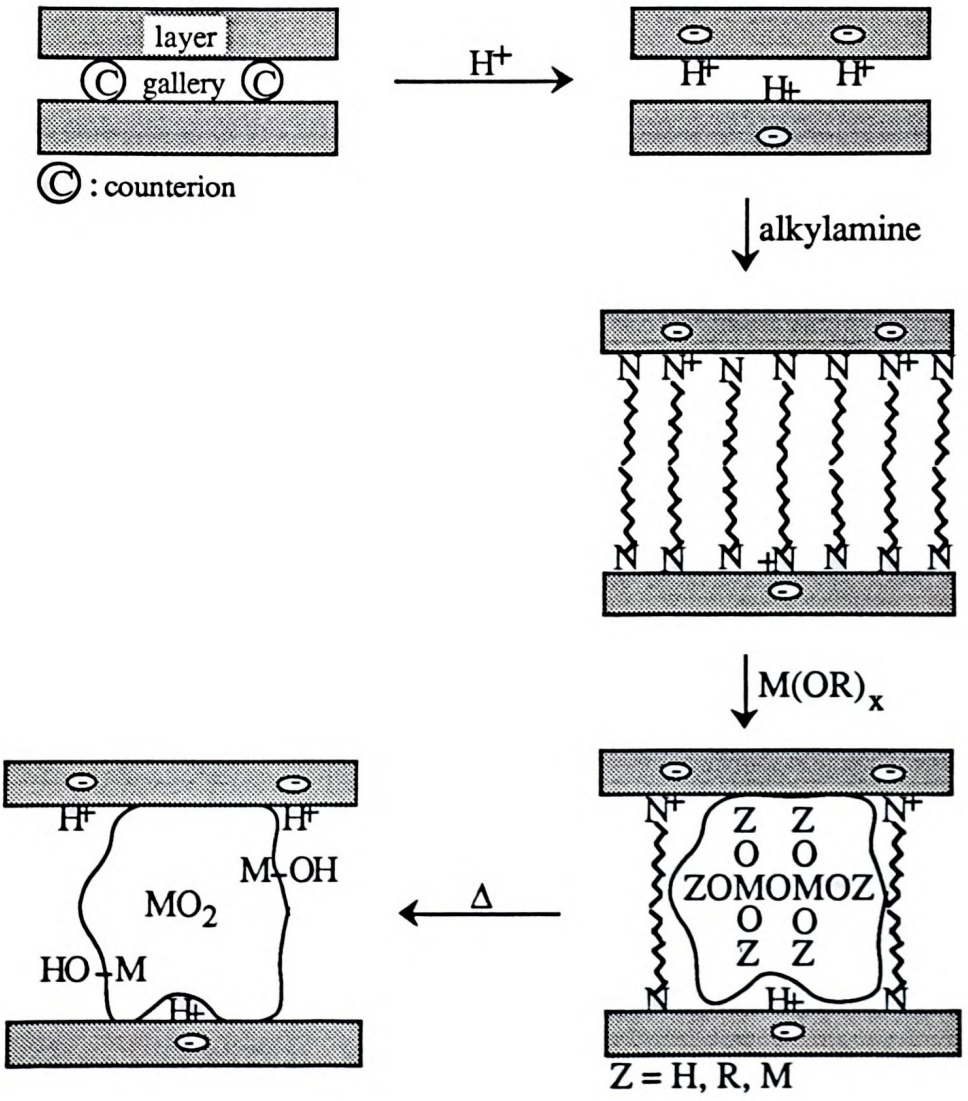

FIGURE 20. Alkoxide polymerization pillaring

NMR, gas chromatography, Raman spectroscopy, density and viscosity measurements[48,50,60] to characterize sol-gel processes.

Our work was oriented toward the understanding of the silica formed in between the layer of magadiite by hydrolysis of TEOS in the presence of alkylamine, its condensation-polymerization and calcination at 450°C. To our knowledge, no TEOS polymerization has been studied in presence of alkylamines.

THE SOL-GEL PROCESSING OF SILICATES[47]

The sol-gel process involves a solution or sol that undergoes a sol-gel transition. At that point, the one-phase solution becomes a two-phase system due to destabilization, precipitation or supersaturation. The mechanism is not yet understood, but can be divided into five steps: hydrolysis, condensation-polymerization, gelation, drying and densification. The overall chemical reaction can be express in the case of TEOS as:

$$Si(OCH_2CH_3)_4 + 2\,H_2O \text{ -----> } SiO_2 + 4\,CH_3CH_2OH$$

Hydrolysis

In the hydrolysis reaction of metal alkoxides such as TEOS, water molecules displace alkoxy (eg. ethoxy) groups to create silanols:

$$\equiv Si(OCH_2CH_3) + H_2O \text{ -----> } \equiv SiOH + CH_3CH_2OH$$

The reaction is an electrophilic substitution in presence of acid, but a nucleophilic substitution in a basic solution. The complete hydrolysis would produce silicic acid $Si(OH)_4$, but some condensation-polymerization occurs simultaneously.

Condensation-polymerization

The way in which the species hydrolyze and polymerize determines the propagation of the linking units:

$$\equiv Si(OCH_2CH_3) + \equiv SiOH \text{ -----> } \equiv SiOSi\equiv + CH_3CH_2OH$$

$$\equiv SiOH + \equiv SiOH \text{ -----> } \equiv SiOSi\equiv + H_2O$$

Under acidic condition, the first hydrolysis causes the subsequent hydrolysis of the same unit to be more difficult, so that linear polymer growth will be favored. Furthermore, acid catalyzed reactions in solutions containing a low water concentration produces linear polymers, while solutions containing high water concentration produces cross-linked polymers or branched clusters. Under basic conditions, subsequent hydrolysis of the alkoxy groups of the starting species is easier, so that branched cluster growth is promoted.

Gelation

Gelation is related to the diffusion of the oligomer species and the viscosity of the solution. It can occur before the end of hydrolysis and condensation-polymerization. Gelation is defined by the time-to-gel parameter. Dilute solutions exhibit long time-to-gel, while concentrated solutions have short time-to-gel. Increasing temperature also decreases time-to-gel. The sol-gel transition is reached when the one-phase liquid becomes a two-phase system composed of a solid and a liquid that can be converted into a two-phase system of a solid and a gas.

Drying

The solvent phase can be removed by low-temperature evaporation, to form xerogels or by hypercritical evacuation, to create aerogels.

Condensation-polymerization can still occur during the solvent removal. Drying provokes shrinkage, but the gel is not said to be dry until it is subject to heat treatment.

Densification

Densification occurs during the final heat treatment: trapped water and organic molecules are eliminated, residual organics are oxidized and silanols are condensed to form siloxane bridges and form pure silica.

RESULTS AND DISCUSSION

Reaction conditions

The reaction conditions for the hydrolysis of TEOS in the presence of alkylamines are summarized in Table 13.

It is worth noticing that the water quantity is less than stoichiometric for complete hydrolysis and polymerization of TEOS. Each TEOS molecule requires two water molecules for complete polymerization to form silica, whereas the actual amounts used were in the range 0.04-0.16 mol H_2O/ mol TEOS. The samples were furthermore exposed to atmosphere moisture during the air-drying process. Such low H_2O/TEOS ratios were selected in order to be as close as possible to the conditions for the silica intercalation into H-magadiite ($H_2 Si_{14} O_{29} . 1.5 H_2O$). The amount of water used in our preparations is the smallest possible, as water is coming from the concentrated hydrochloric acid (38% wt).

TABLE 13. Experimental conditions for the acid-catalyzed TEOS polymerization in the presence of alkylamines

sample	amine	calcination (4 hrs)	wt (g) amine	wt (g) HCl conc.	wt (g) TEOS	molar ratio TEOS/ amine	molar ratio TEOS/ H^+	molar ratio TEOS/ H_2O
HA50	hexyl	none	3.12	0.260	12.0	1.9	22	6.4
CHA50		450°C						
OA50	octyl	none	3.97	0.265	12.0	1.9	21	6.2
COA50		450°C						
DA50	decyl	none	4.82	0.270	12.0	1.9	21	6.1
CDA50		450°C						
HA100	hexyl	none	6.22	0.462	48.1	3.7	49	14
CHA100		450°C						
OA100	octyl	none	7.94	0.486	48.0	3.7	46	14
COA100		450°C						
DA100	decyl	none	9.66	0.498	48.0	3.7	45	13
CDA100		450°C						
HA200	hexyl	none	3.12	0.257	48.1	7.5	88	26
CHA200		450°C						
OA200	octyl	none	3.97	0.251	48.1	7.5	90	26
COA200		450°C						
DA200	decyl	none	4.84	0.243	48.1	7.5	93	27
CDA200		450°C						

The polymerization occurs immediately when TEOS is completely added to the amine/HCl/water mixture. The clear TEOS solution turned white, except for the HA50 sample which remained clear. During the rapid (~1 day) air drying process on glass plates, the samples form homogeneous films of thin white powder. After calcination at 450°C, even under flowing air, the thin powder turns brown due to residual carbon. The CDA samples were browner than the COA samples, which were also browner than the CHA samples. The yields of CHA100, COA100 and CDA100/TEOS exceed to 30%. They have been approximated as:

$$100 * \frac{\text{wt calcined product}}{M_{SiO_2}} \Big/ \frac{\text{wt TEOS}}{M_{TEOS}} = 100 * \frac{\text{wt calcined product}}{60.1} \Big/ \frac{\text{wt TEOS}}{208.33}$$

The reacting solutions containing the white particles were allowed to air dry without further treatments. New phenomena occured during the addition of ethanol as solvent to the hydrolyzed TEOS/amine solution. After centrifugation of the solutions containing the gel, the liquid mother was poured away and ethanol was added to the white gel. The gel, instead of becoming dispersed, dissolved. Upon air drying the clear ethanol solution, a thin white powder was formed.

Chemical compositions

The elemental analyses for TEOS-hydrolysis products, before and after calcination, are listed in Table 14. The results derived from thermogravimetric analysis (Figure 21) are displayed in Table 15.

TABLE 14. Chemical composition from elemental analysis for TEOS-hydrolysis products formed in the presence of alkylamines

	%wt element					%wt composition			
sample	%wt C*	%wt H*	%wt N*	%wt Si**	%wt O**	%wt amine**	%wt ethoxy**	%wt H_2O**	%wt SiO_2**
HA100	14	4.0	3.0	37	42	22	0.0	6.2	72
OA100	28	6.5	4.0	25	37	37	0.68	8.9	53
DA100	54	10	6.1	14	16	69	2.2	0.0	29
CHA100	0.23	1.3	0.17	42	56	1.2	0.0	10	89
COA100	0.86	1.3	0.11	42	56	1.0	0.20	9.7	89
CDA100	2.1	1.4	0.33	41	55	3.7	0.0	7.5	88

* measured from C, H, N analysis
** calculated according to the method explained in the text

The C, H, N results from the chemical analyses are given in ppm (µg/l) for C, H and N. By assuming a density of 1 g/l for the analyzed solutions, we can convert those results to %wt.

The amine content has been calculated from the %wt N, given by the analysis:

n_A: moles of nitrogen in 100 g = moles of amines in 100 g

$$n_A = \frac{\%\text{wt N}}{M_N} = \frac{\%\text{wt N}}{14}$$

$$\%\text{wt amine} = n_A * M_A$$

M_A = 101.19 g/mol for hexylamine

M_A = 129.25 g/mol for octylamine

M_A = 157.30 g/mol for decylamine

The ethoxy-ethanol content has been calculated using the %wt C left after subtraction of the carbon present in the amine:

n_{EtO} is defined as the number of moles of ethoxy groups and ethanol molecules trapped per 100 g of compound.

$$n_{EtO} = \left(\frac{\%\text{wt C}}{M_C} - c * n_A\right) / 2 = \left(\frac{\%\text{wt C}}{12} - c * n_A\right) / 2$$

c = 6 for hexylamine

c = 8 for octylamine

c = 10 for decylamine

$$\%\text{wt ethoxy} = n_{EtO} * M_{EtO} = n_{EtO} * 45$$

The water content has been calculated using the %wt H left after deduction of the hydrogen present in the amine and the ethoxy-ethanol groups:

n_{H2O} is defined as the number of moles of water created by silanols condensation and by desorption of water per 100 g of compound.

$$n_{H2O}=\left(\frac{\%wt\ H}{M_H} - h * n_A - 5 * n_{EtO}\right)/2 = \left(\frac{\%wt\ H}{1} - h * n_A - 5 * n_{EtO}\right)/2$$

h = 15 for hexylamine

h = 19 for octylamine

h = 23 for decylamine

$$\%wt\ H_2O = n_{H2O} * M_{H2O} = n_{H2O} * 18$$

The silicon content in 100 g of compound has been calculated, assuming that after the C, H, N analysis, the remaining product is silica SiO_2.

$$\%wt\ SiO_2 = 100 - \%wt\ amine - \%wt\ ethoxy - \%wt\ H_2O$$

If n_{SiO2} and n_{Si} represent the number of silica molecules and silicon atoms, respectively, in 100 g of compound:

$$\%wt\ SiO_2 = n_{SiO2} * M_{SiO2} = n_{SiO2} * 60.1$$

$$n_{Si} = n_{SiO2} = \frac{\%wt\ SiO_2}{60.1}$$

$$\%wt\ Si = n_{Si} * M_{Si} = n_{SiO2} * 28.1$$

Finally, the total oxygen content in 100 g of compound is determined to complete the elements weight % to 100:

$$\%wt\ O = 100 - \%wt\ C - \%wt\ H - \%wt\ N - \%wt\ Si$$

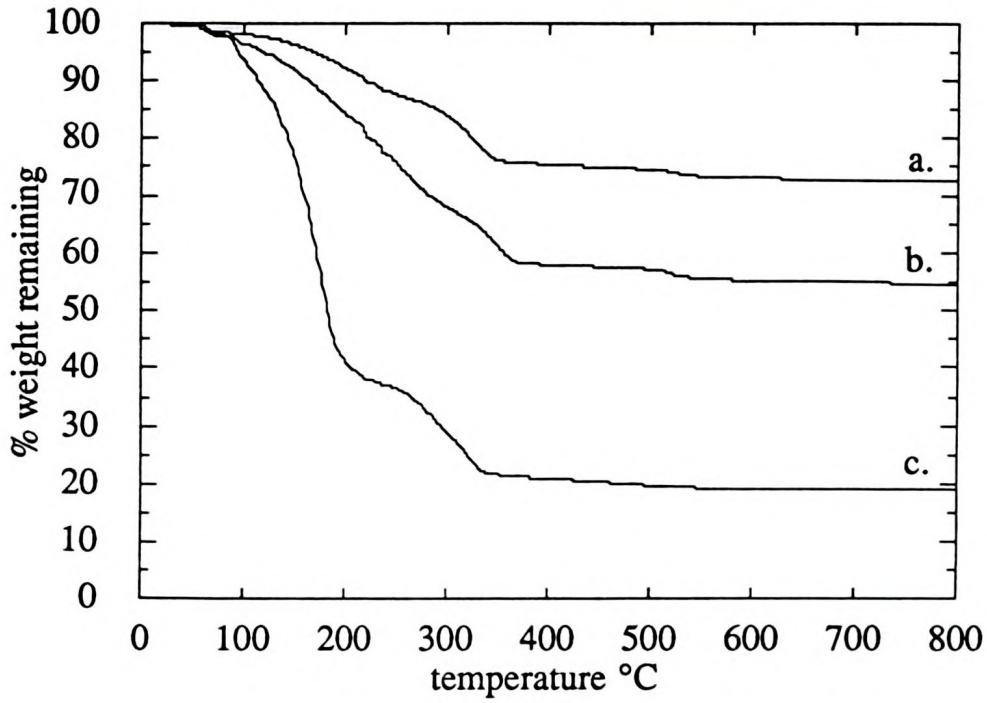

FIGURE 21. Thermogravimetric analysis for air-dried TEOS-hydrolysis products formed in the presence of alkylamines
a. HA100, b. OA100, c. DA100

The %wt SiO_2 determined from thermogravimetric analysis has been calculated assuming the remaining mass left after heating at 800°C is pure silica (Table 15).

TABLE 15. Chemical composition from thermogravimetric analysis for air-dried TEOS-hydrolysis products formed in the presence of alkylamines

sample	first %wt loss	from... to...°C	second %wt loss	from... to...°C	%wt SiO_2
HA100	12	30 to 250	16	250 to 800	72
OA100	33	30 to 300	12	300 to 800	55
DA100	62	30 to 225	19	225 to 800	19

The thermogravimetric curves show a two-step weight loss. The first increment increases with the amine length and can be assigned to some amine loss. The second increment is almost constant and might be due to the elimination of some bonded amines and to the loss of water from silanols condensation. The calcination temperature has been chosen according to those thermogravimetric curves: there is no more weight loss above 450°C.

The chemical compositions found by chemical analysis calculations and thermogravimetric analysis agree in general terms (Table 16).

TABLE 16. Comparison of chemical composition from elemental analysis and thermogravimetric analysis for air-dried TEOS-hydrolysis products formed in the presence of alkylamines

sample	chemical analyses		TGA	
	%wt volatiles	%wt SiO_2	%wt volatiles	%wt SiO_2
HA100	28	72	28	72
OA100	47	53	45	55
DA100	71	29	81	19

The amine content in the samples increases with the length of the alkyl chain due to lower vapor pressures. Surprisingly, there are almost no ethoxy groups left after the polymerization. The polymerization went all the way through to pure silica. Presumably, water from the atmosphere during air-drying contributes to the hydrolysis process. Water is present before and after calcination. After calcination, water is present as physisorbed water molecules in the pores. The presence of 6-9 wt% water

for HA100 and OA100 before calcination is more questionable. Indeed, as was noticed earlier, there are not enough water molecules in the initial reaction mixture to entirely polymerize TEOS. We thus should expect the polymerization to continue until no water remains.... The water present in the air-dried gel might be due to physisorbed external water which adsorbs from the atmosphere after drying and densification.

Infrared spectroscopy

The presence of amine and some water, as well as the absence of ethoxy groups, can also be verified from the infrared spectra (Figures 22, 23 and 24). The data are gathered in Table 17.

The bands in the 3000-2500 cm^{-1} region are due to symmetric and antisymmetric stretching vibrations of CH_2 and CH_3 groups.[61] In the octylamine spectrum (Figure 22b), the bands at 3370 and 1600 cm^{-1} have been assigned to N-H stretching and NH_2 bending, respectively.[61] The bands at 1469 and 955 cm^{-1} are due to C-C stretching and C-C bending, respectively.

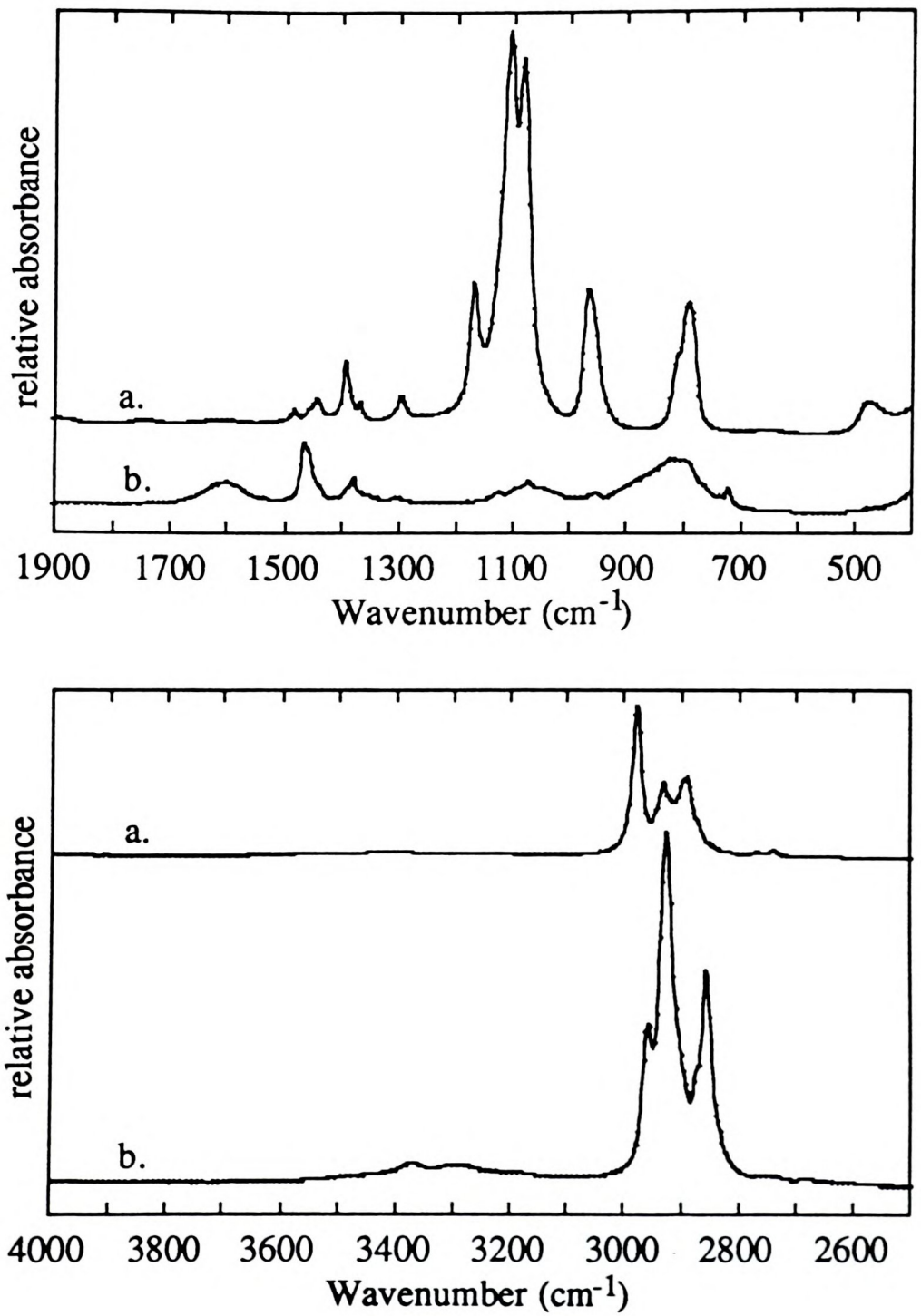

FIGURE 22. Infrared spectra of the starting materials (liquid film between KBr plates)

a. TEOS, b. alkylamine: octylamine

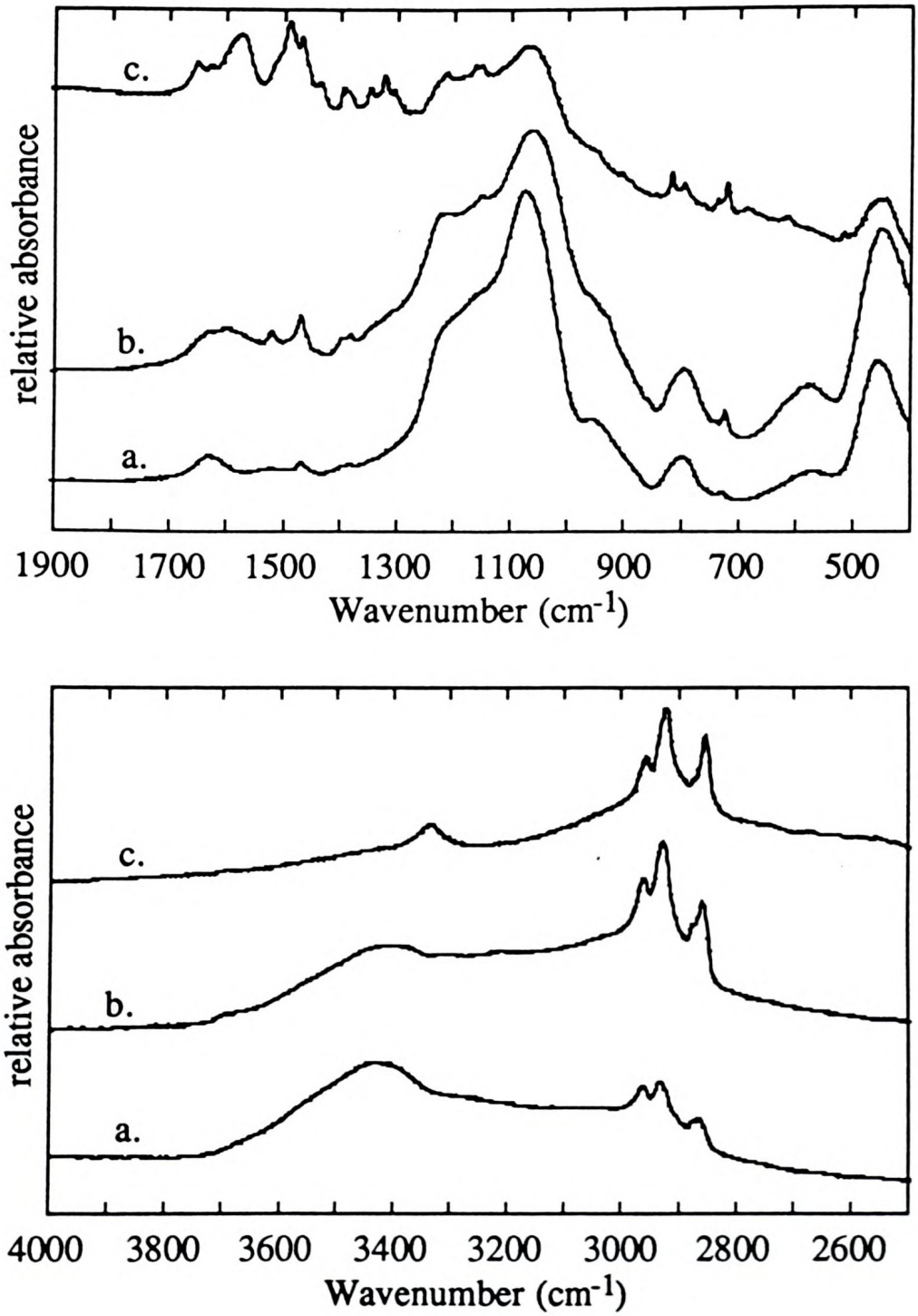

FIGURE 23. Infrared spectra of the air-dried TEOS-hydrolysis products formed in the presence of alkylamines (KBr pellet)
a. HA100, b. OA100, c. DA100

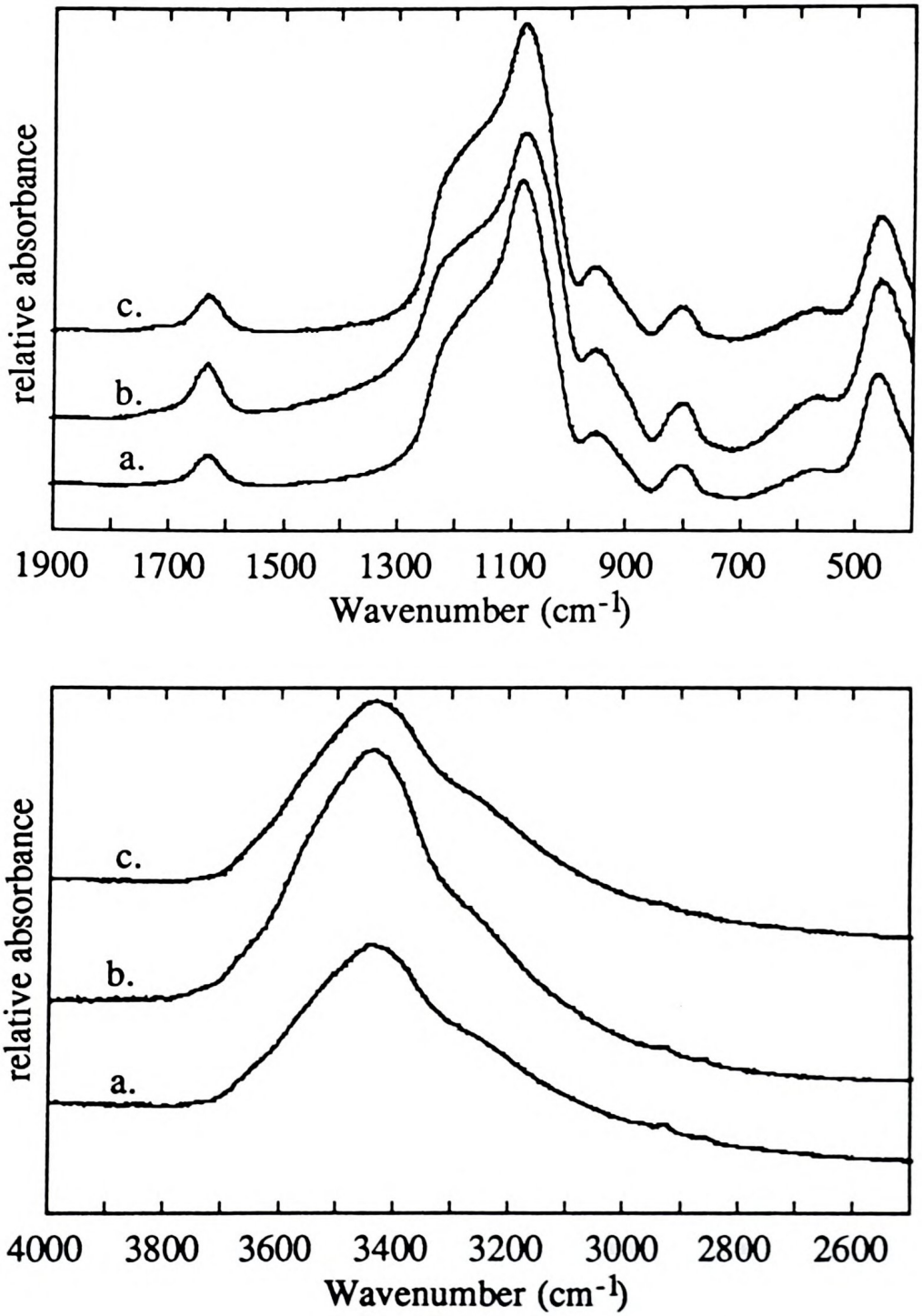

FIGURE 24. Infrared spectra of the calcined (450°C) TEOS-hydrolysis products formed in the presence of alkylamines (KBr pellet)
a. CHA100, b. COA100, c. CDA100

TABLE 17. Infrared data of the TEOS-hydrolysis reactants and products

sample	wavenumber (cm^{-1})									
TEOS		2977	2892		1485	1394	1296	1171	1084	966
		2930			1443	1366		1107		796
										476
octylamine	3370	2959	2872	1600	1469	1382				955
		2928	2857							824
										821
										724
Davisil-62 silica	3440			1631				1105		975
	3275									803
										542
										471
HA100	3428	2959	2872	1631	1469	1394			1074	959
		2928	2857			1382				796
										724
										576
OA100	3407	2959	2872	1631	1469	1394	1222	1152	1070	959
		2928	2857	1600		1382	1212			796
				1521						724
										576
DA100	3333	2959	2872	1651	1489	1394	1212	1163	1070	818
		2928	2857	1631	1469	1382		1152		796
				1576	1435	1346				759
						1321				737
						1306				724
										683
										617
										517
										505
CHA100	3434			1631					1080	953
COA100	3275									803
CDA100										567
										460

Before calcination of the TEOS-hydrolysis products (Figure 23), the different compounds exhibit the alkylamines' characteristic C-H vibrations at 2959, 2928, 2872 and 2857 cm^{-1}, and other alkyl groups modes at 1469, 1382, 1306 and 724 cm^{-1} bands (Figure 22). As was noticed during the analysis of the chemical compositions, the amount of amine incorporated

into the TEOS-hydrolysis products after air-drying increases from hexylamine to decylamine. All three air-dried amine-containing hydrolysis products exhibit the same four bands in the C-H vibration region with the same relative intensities ; those bands and their relative intensities are the same as the ones found for octylamine. The three characteristic peaks of the ethoxy groups (Figure 22) at 2977, 2930 and 2892 cm^{-1} cannot be seen. This is a further evidence for complete hydrolysis. HA100 and OA100 spectra display a broad hydroxyl and water peak centered at about 3420 cm^{-1}, but the DA100 spectrum shows a small peak at 3333 cm^{-1} that might be assigned to N-H vibration even though the octylamine spectrum only displays a peak at 3370 cm^{-1}. Again, the chemical composition values are correlated with the infrared data: only HA100 and OA100 exhibit some water molecules. In the region below 1600 cm^{-1}, a greater number of peaks appears in the DA100 spectrum than in the OA100 spectrum which also exhibits more peaks than the HA100 spectrum. This is the region expected for both Si-O and Si-N vibrations. Thus, the peaks in the DA100 spectrum which cannot be assigned to alkylamine, TEOS and which are not present in the HA100 spectrum might be due, not only to some new kinds of Si-O bonds, but also to Si-N vibrations. Indeed, silicon-nitrogen compounds have been known for a long time.[62,63] An easy way to synthesize them is to react silyl chloride with ammonia. Some of their infrared bands were assigned twenty five years ago.[64,65] For the cyclic $(H_3SiN\text{-}SiH_2)_3$, Wells and Schaeffer[64] assigned the bands at 945 (vs, sh) cm^{-1} to Si-N-Si deformation and the bands at 992 (vs, sh) and 1018 (s, sh) cm^{-1} to Si-N stretching. Bürger and Sawodny[65] assigned the Si-N stretching vibrations to the bands at 721 (vs) cm^{-1}, 741 (vs) and 686 (vs) cm^{-1}, 731 (vs) and 626 (vs) cm^{-1}, 710 (vs) cm^{-1} for the following dimethylamino-chlorosilanes: Cl_3Si

$[N(CH_3)_2]$, Cl_2 Si $[N(CH_3)_2]_2$ Cl_1 Si $[N(CH_3)_2]_3$ and Si $[N(CH_3)_2]_4$, respectively. For dimethylamino-methylsilanes, Si-N stretching vibrations were assigned to bands at 699 (vs) and 582 (vw) cm^{-1} for $(CH_3)_2$ Si $[N(CH_3)_2]_2$ and to 679 (s) cm^{-1} for (CH_3) Si $[N(CH_3)_2]_3$. For diethylamino-methylsilanes, Si-N stretching vibrations were assigned to bands at 599 (vw) cm^{-1}, 690 (s) and 600 (vw) cm^{-1}, 675 (s) and 625 (vw) cm^{-1} for $(CH_3)_3$ Si $[N(C_2H_5)_2]$, $(CH_3)_2$ Si $[N(C_2H_5)_2]_2$ and (CH_3) (Cl) Si $[N(C_2H_5)_2]_2$, respectively. For all these compounds, N-Si-N deformation bands were found to be situated below 400 cm^{-1}.

After calcination of the TEOS-hydrolysis products (Figure 24), the infrared spectra for the three compounds look identical to the spectrum for silica (Figure 25). The amines are almost entirely eliminated, as evidenced by the absence of bands in the C-H vibration region. Water is present in large amounts in the calcined TEOS-hydrolysis products: there is a broad O-H stretching band centered at 3434 cm^{-1} with a shoulder at 3275 cm^{-1} and an O-H bending vibration at 1631 cm^{-1}. As will be determined by the porosity study, the water molecules are physisorbed in the pores. The Si-O vibrations are assigned to bands at 1080, 953, 803, 567 and 460 cm^{-1}. The 1080 cm^{-1} peak is the most intense : it is also accompanied by a large shoulder toward higher wavenumbers.

The infrared data correlate well the chemical compositions calculated from chemical analysis and thermogravimetric data. After hydrolysis, there are no remaining ethoxy groups or ethanol molecules trapped in the air-dried product ; the amine content increases with the amine chain length. The alkylamine is completely oxidized after calcination. Only in HA100 and OA100 is some water present. After calcination, water molecules are

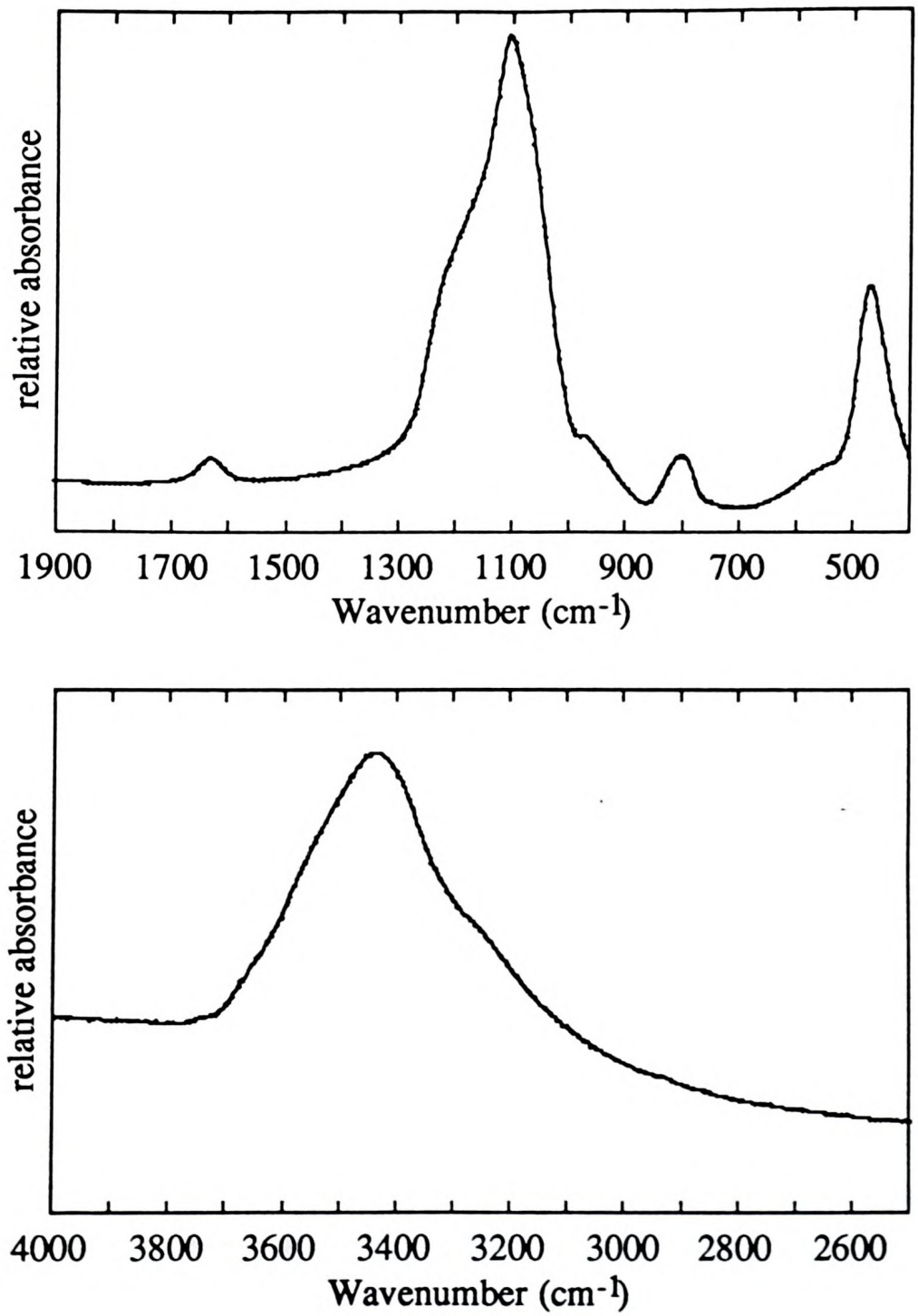

FIGURE 25. Infrared spectra of silica gel Davisil-62 (KBr pellet)

present in the three compounds. Infrared analysis provides two new pieces of information: after calcination, the three products are similar and are silica-like.

^{29}Si nuclear magnetic resonance

The differences between the air-dried products and the similarities of the calcined compounds can also be verified from solid state ^{29}Si nuclear magnetic resonance. The spectra are displayed on Figures 26 and 27 and the data are collected in Table 18.

TABLE 18. ^{29}Si NMR data of the dried and calcined products (450°C) TEOS-hydrolysis products formed in the presence of alkylamines

sample	chemical shifts (ppm *vs.* TMS)		$Q^3 : Q^4$	
	Q^3	Q^4	approximate ratio	peak height ratio
HA100	-102.0	-111.3	0.7	6 : 10
OA100	- 99.3	-109.9	0.7	7 : 10
DA100	- 99.9	-110.2	0.9	8 : 10
CHA100	-102.2	-108.1		
COA100	-102.1	-109.3		
CDA100	-101.1	-108.6		

Pouxviel et al.[51] has determined the liquid ^{29}Si NMR chemical shifts for various Q^n types of silicon tetrahedra.[41] The Q^n peak position depends on the degree of condensation of the silicon tetrahedra. Q^0: -72 to -82 ppm; Q^1: -82 to -89 ppm ; Q^2: -90 to -96 ppm and Q^3: -100 to -104 ppm.

The air-dried TEOS-hydrolysis products before calcination (Figure 26), exhibit ^{29}Si NMR spectra containing two separated peaks. The Q^3 and

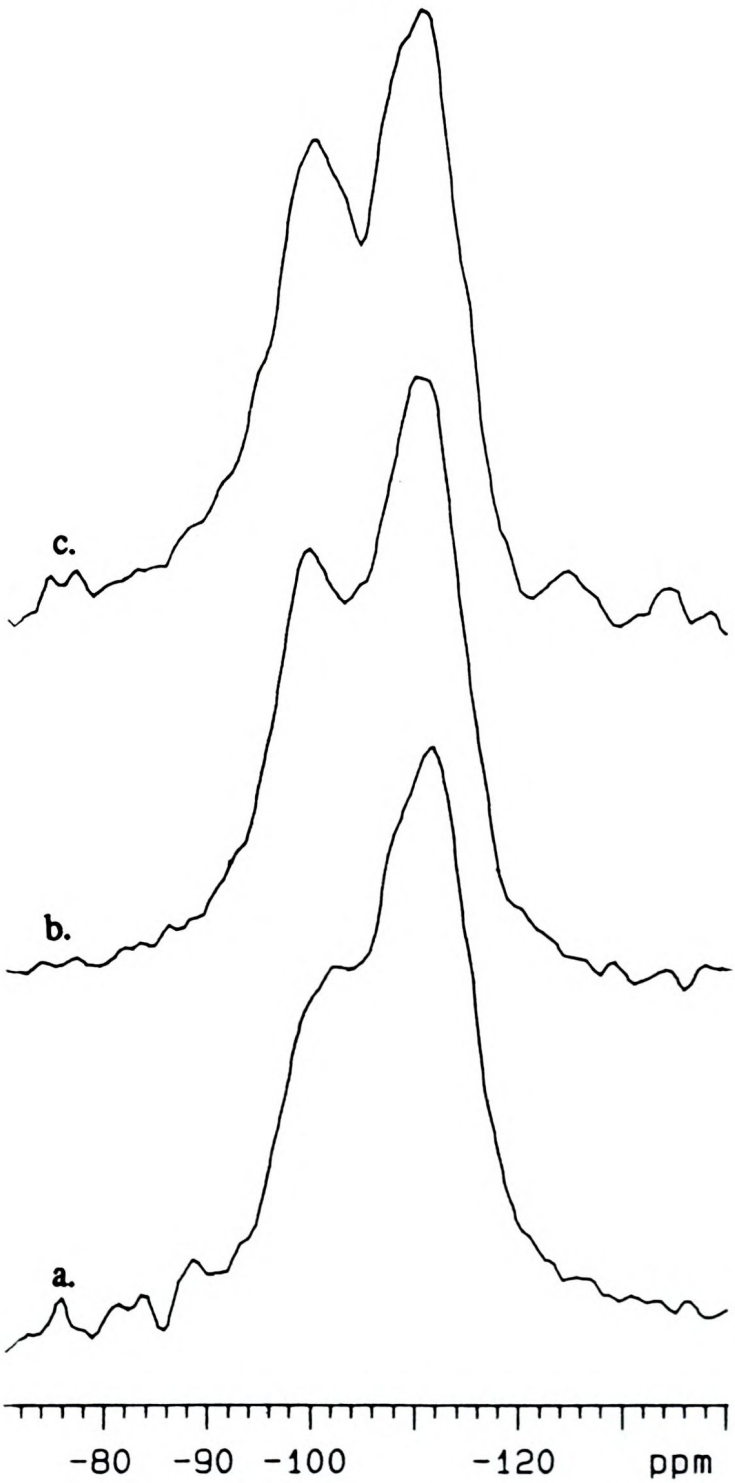

FIGURE 26. ^{29}Si NMR spectra of the air-dried TEOS-hydrolysis products formed in the presence of alkylamines
(delay time: 600 seconds, line broadening: 140, 12 scans)
a. HA100, b. OA100, c. DA100

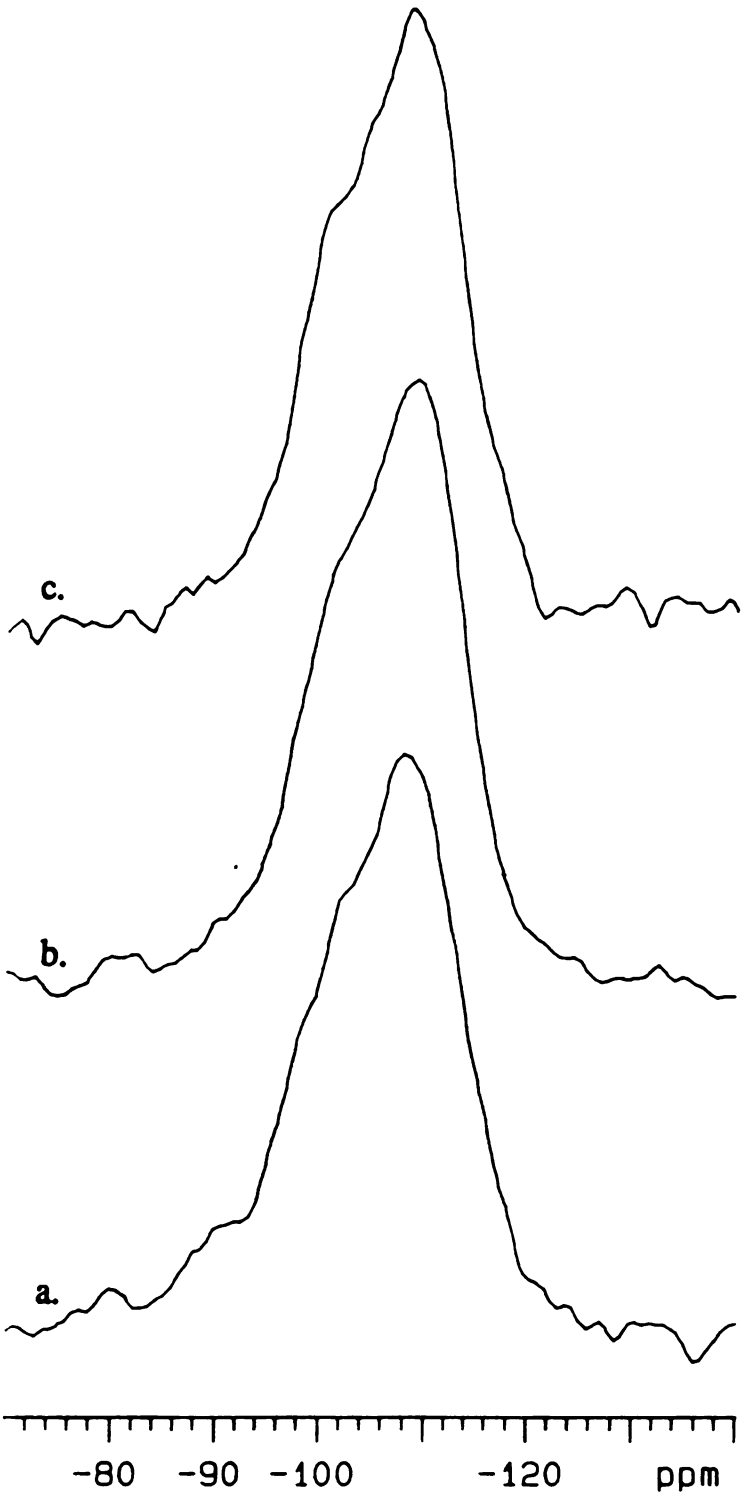

FIGURE 27. ^{29}Si NMR spectra of the calcined (450°C) TEOS-hydrolysis products formed in the presence of alkylamines
(delay time: 600 seconds, line broadening: 140, 12 scans)
a. CHA100, b. COA100, c. CDA100

Q^4 peak assignments have been done according to their chemical shifts. The presence of Q^3 peaks is correlated with the silanols seen on the infrared spectra. The first resonance is situated around -100 ppm and is assigned to silicon tetrahedra in a Q^3 environment: $(SiO)_3\underline{Si}O\text{-}H$. The second line at about -110 ppm can be assigned to silicon tetrahedra in a Q^4 environment: $\underline{Si}(OSi)_4$. The approximate Q^3/Q^4 ratio was obtained by deconvolution of the peaks ; the numerical value should be handled with care due to the poor resolution of the peaks. Peak height ratios can be qualitatively compared (Table 18). The intensity of the Q^3 peak increases from sample HA100 to DA100. Thus, the amine plays a role in determining the arrangement of the hydrolyzed silicon centers.

The calcined (450°C) TEOS-hydrolysis products (Figure 27), exhibit similar ^{29}Si NMR spectra. The Q^4 peak is shifted slightly toward lower values at about -109 ppm, while the Q^3 forms a shoulder on the Q^4 peak at about -102 ppm. The change in the ^{29}Si NMR chemical shifts on calcination suggests the formation of siloxane bridges by silanols condensation that creates Q^4 sites from Q^3 silicons:

$$\underset{Q^3}{(SiO)_3SiO\text{-}H} + \underset{Q^3}{(SiO)_3SiO\text{-}H} \text{ -----> } \underset{Q^4\ \ Q^4}{(SiO)_3Si\text{-}O\text{-}Si(OSi)_3} + H_2O$$

The cross linkage of units and the increasing number of Q^4 sites change the overall environment of every Q^3 which is surrounded by more Q^4 than before calcination. They are still Q^3 sites, but with more Q^4 near-neighbor environments ; the shielding of Q^3 sites by Q^4 sites increases and therefore the Q^3 resonance is shifted upfield.

^{13}C and ^{1}H solid state nuclear magnetic resonance analysis would give us more information about the presence of ethoxy groups or ethanol molecules and the silanols.

The ^{29}Si NMR analysis provides proof that the amine affects the hydrolysis and is probably acting as a template in deciding Q^3/Q^4 ratios and overall structure. Increasing the length of the alkyl chain creates more Q^3 sites in the dried products. However, after calcination, the spectra of the three compounds look similar, regardless of the amine used in the hydrolysis step.

Nitrogen adsorption-desorption

As the hydrolysis of TEOS inside layered materials creates highly microporous products, we decided to study the products of our acid-catalyzed TEOS polymerization in the presence of alkylamine by nitrogen adsorption. This measurement allowed us to determine adsorption-desorption isotherms and t-plots to calculate the total surface area and the porosity (Appendix C). Furthermore, Strawbridge et al.[48] showed that gels made by acid-catalyzed TEOS polymerization exhibit high surface areas. For example, a gel synthesized with a TEOS to H_2O molar ratio of 0.5 in presence of ethanol and concentrated HCl has a microporous volume of 0.36 cm^3/g. He assigned this porosity to interstices caused by particles packing during the gelation. The adsorption-desorption isotherms and the t-plots are displayed in Figures 28, 29 and 30 according to the TEOS to amine molar ratio used in the hydrolysis step. The numerical data are gathered in Table 19.

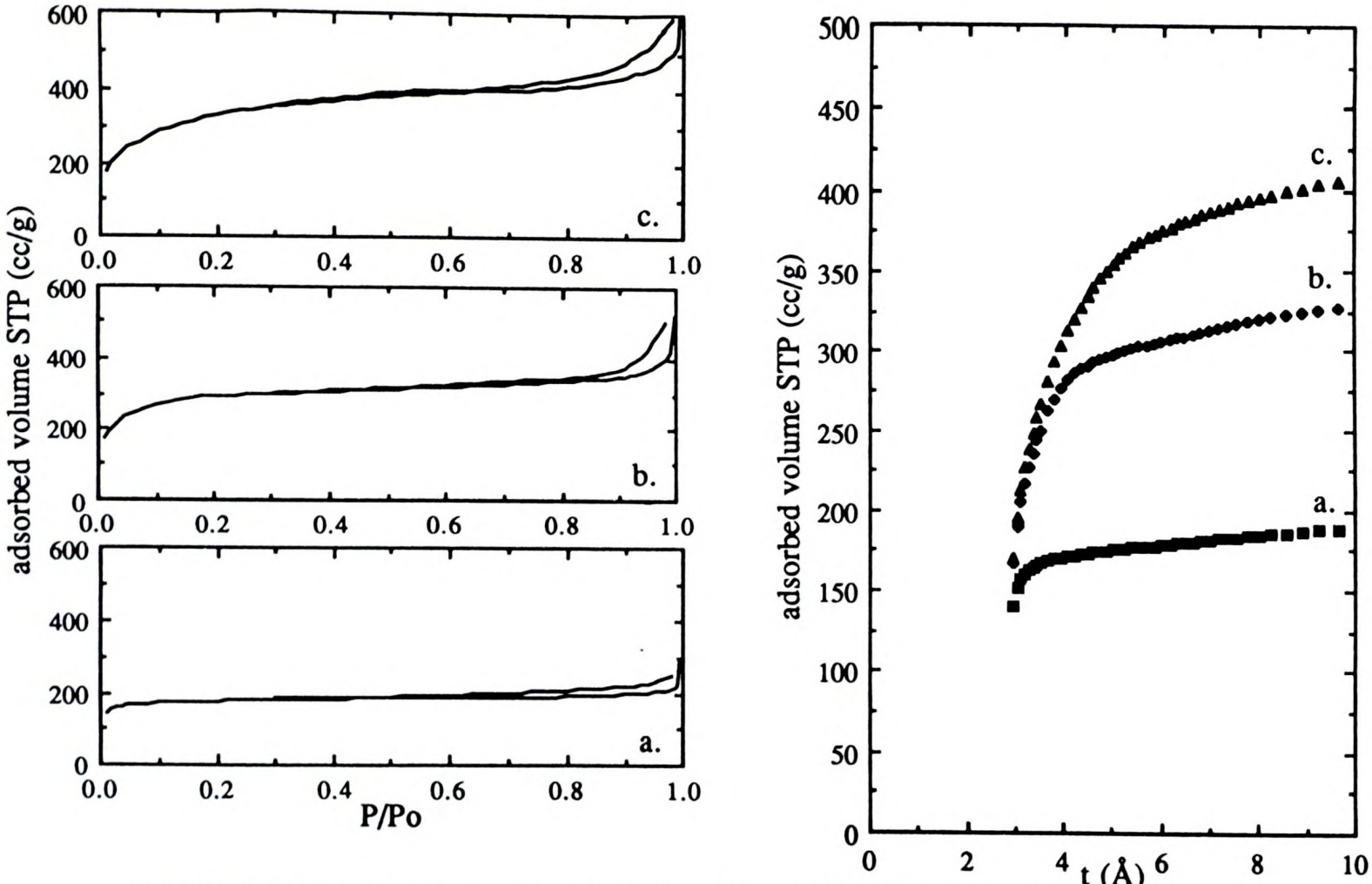

FIGURE 28. N_2 adsorption curves of the calcined (450°C) TEOS-hydrolysis products formed in the presence of alklamines prepared at an initial TEOS to amine molar ratio of 7.5 ; outgassing was carried out under vacuum at 150°C
left: N_2 adsorption-desorption isotherm, right: t-plot
a. CHA200, b. COA200, c. CDA200

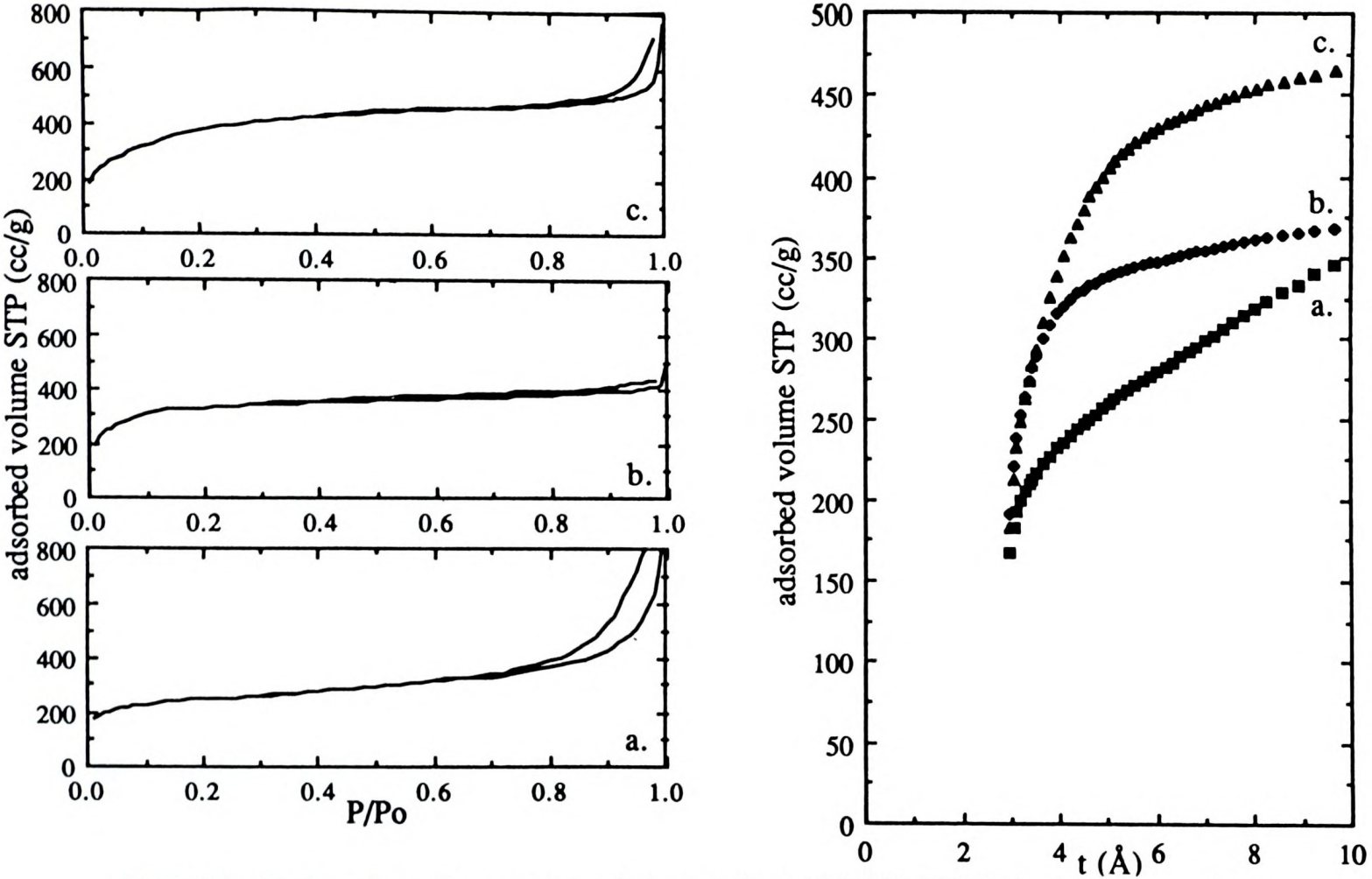

FIGURE 29. N_2 adsorption curves of the calcined (450°C) TEOS-hydrolysis products formed in the presence of alklamines prepared at an initial TEOS to amine molar ratio of 3.7 ; outgassing was carried out under vacuum at 150°C
left: N_2 adsorption-desorption isotherm, right: t-plot
a. CHA100, b. COA100, c. CDA100

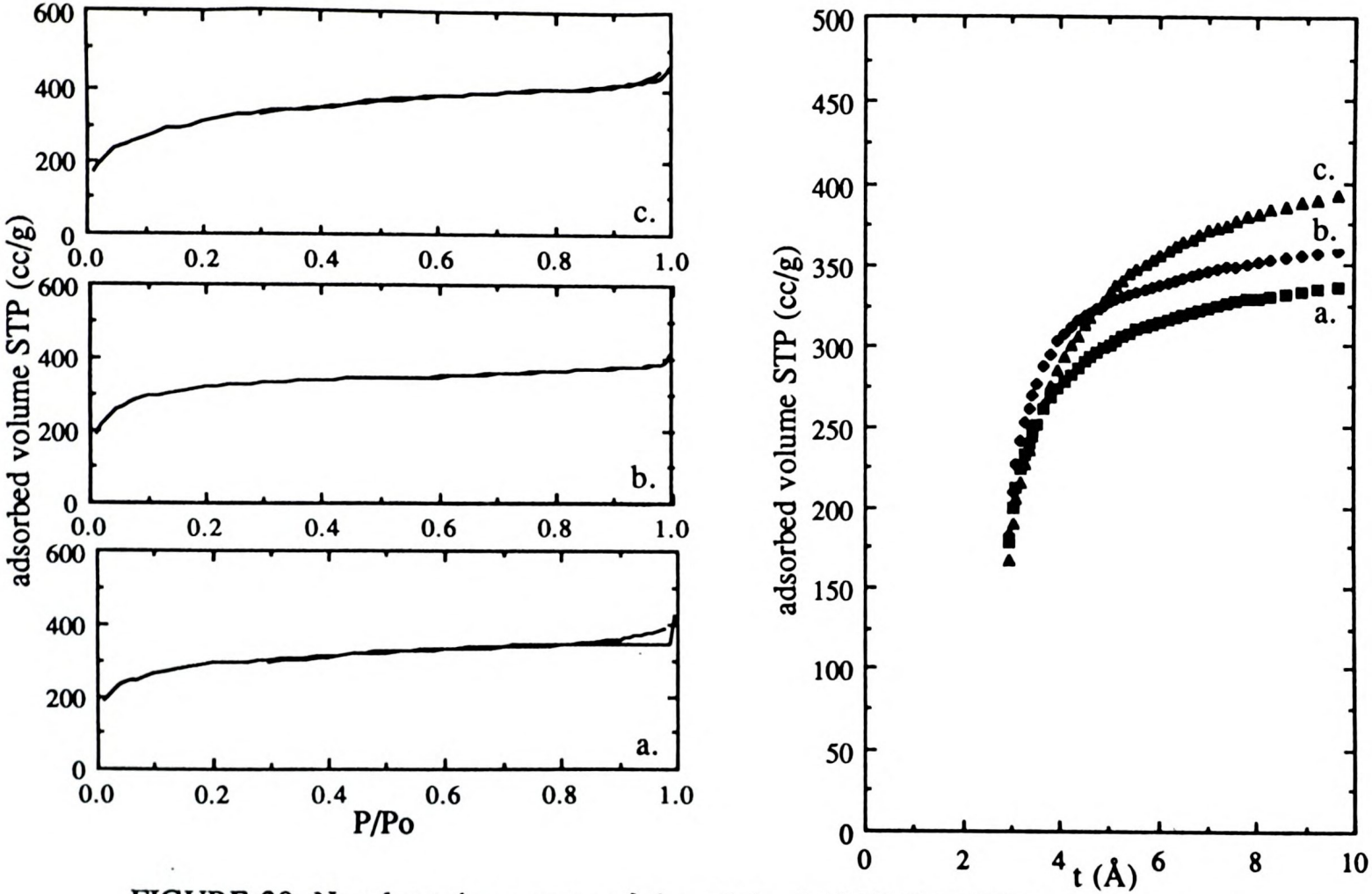

FIGURE 30. N_2 adsorption curves of the calcined (450°C) TEOS-hydrolysis products formed in the presence of alklamines prepared at an initial TEOS to amine molar ratio of 1.9 ; outgassing was carried out under vacuum at 150°C
left: N_2 adsorption-desorption isotherm, right: t-plot
a. CHA50, b. COA50, c. CDA50

TABLE 19. N_2 adsorption data of the calcined (450°C) TEOS-hydrolysis products formed in the presence of alkylamines

	BET[43]		t-plot[44]				
sample	S_{total} m^2/g	C**	S_{total} m^2/g	$S_{non-\mu}$ m^2/g	$S_\mu^{(1)}$ * m^2/g	$S_\mu^{(2)}$ * m^2/g	V_μ liq cm^3/g
CHA200	690	160	770	60	680	710	0.24
COA200	1110	100	1100	130	1110	970	0.39
CDA200	1240	70	1160	170	1350	990	0.48
CHA100	900	310	960	310	690	650	0.24
COA100	1270	120	1260	160	1270	1100	0.45
CDA100	1380	70	1320	210	1520	1110	0.54
CHA50	1080	150	1100	230	980	870	0.35
COA50	1220	110	1220	190	1160	1030	0.41
CDA50	1140	80	1110	190	1230	920	0.43

S_μ: microporous surface area, $S_{non-\mu}$: non-microporous surface area, V_μ: microporous volume

* $S_\mu^{(1)}$ is derived from V_μ by the t-plot method ; $S_\mu^{(2)} = S_{total} - S_{non-\mu}$

** the C value is an energetic constant depending on the chemical behavior of the surface.

The surfaces of the silica products exhibit different chemical behavior for each amine, regardless of the initial TEOS to amine ratios. Indeed, the C value found by the BET method is decreasing from hexylamine- to decylamine-derived products: C~160, 110, 70 for hexylamine-, octylamine- and decylamine-derived products. This is further evidence for the role of the amine during the TEOS-hydrolysis process.

Octylamine- and decylamine-derived products exhibit, for the three TEOS to amine molar ratio, about the same total surface area at ~1200 m^2/g. The total surface areas calculated from the BET equation[43] and the t-plot method[44] agree relatively well. The microporous surface areas $S_\mu^{(1)}$ were determined by the classic de Boer et al.[44] t-plot method. We compared $S_\mu^{(1)}$ with $S_\mu^{(2)}$, the microporous surface area obtained by subtraction of the non-microporous surface area $S_{non-\mu}$ from the total surface area S_{total}. With that method, we found a microporous surface area

of ~1000 m^2/g for the octylamine- and decylamine-derived products at the three different TEOS to amine molar ratios. The disagreement between $S_\mu^{(1)}$ and $S_\mu^{(2)}$ may be due to the fact that the micropores are so large (XRD patterns on Figures 31 to 33 display 29 to 37 Å lines) that they do not match typical micropores (pore < 20 Å) models, but are too small to be treated by mesopores (20 < pore < 500 Å) theory and so do not exhibit hysteresis. A better microporous surface area might be obtained from immersion microcalorimetry. Indeed, the Harkins-Jura method[66] would allow for a precise determination of the external surface area which would be subtracted from the total surface area. However, the microporous volume is always larger for the decylamine derived products than for the octylamine ones. Since the surface areas are identical, but the pore volumes are different, the pores sizes are different. The decylamine-derived products exhibit larger micropore sizes than those of octylamine, because their microporous volume is larger. According to Strawbridge et al.[48], when the two lines derived from the two slopes on the t-plot curve intersect at high t-values, the pore sizes are larger than when the intersection occurs at low t-values. Adsorption of molecules with known kinetic diameters would give a more precise idea of the pore sizes. Thus, regardless of the TEOS to amine molar ratio, octylamine- and decylamine-derived products display high surface areas, due mainly to microporosity. The microporous surface areas are identical for both amine derived products, but in the decylamine case, the pores size is larger because the microporous volume is larger.

The hexylamine-derived products exhibit higher surface areas when the TEOS to amine molar ratio decreases. For the lowest TEOS to amine molar ratio, the surface areas are about equal to the octylamine and

decylamine derived products ones, but the microporous volume is smaller. Again, for an identical surface area, the pore volume and the pore size depend on the amine length: the longer the amine, the larger the pore size. Thus, the size of the alkylamine chain in the TEOS-hydrolysis product serves as a pore size template. The surface area values depend on the amount of hexylamine present: the more hexylamine, the higher surface area. This dependence of surface area on the initial amount of hexylamine is related to other differences on the hexylamine-derived products. Indeed, as the hexylamine vapor pressure is higher than the vapor pressure for octylamine and decylamine, it tends to evaporate more readily during the air-drying process. As we saw before, the amine directs the pore structure of the final silica product. So, if the hexylamine leaves the system before hydrolysis and polymerization are completed, it will be less effective in influencing the size of the final micropores. When the initial amount of hexylamine is increased, it takes more time for the amine to evaporate upon air-drying. Therefore, it can not play a structural role as do octylamine and decylamine.

X-ray powder diffraction

The X-ray diffraction patterns (Figures 31, 32 and 33) are somehow surprising. The calcined samples exhibit one broad peak or no peak. The air-dried sample spectra display one broad peak and/or one sharp peak. The data are gathered in the Table 20.

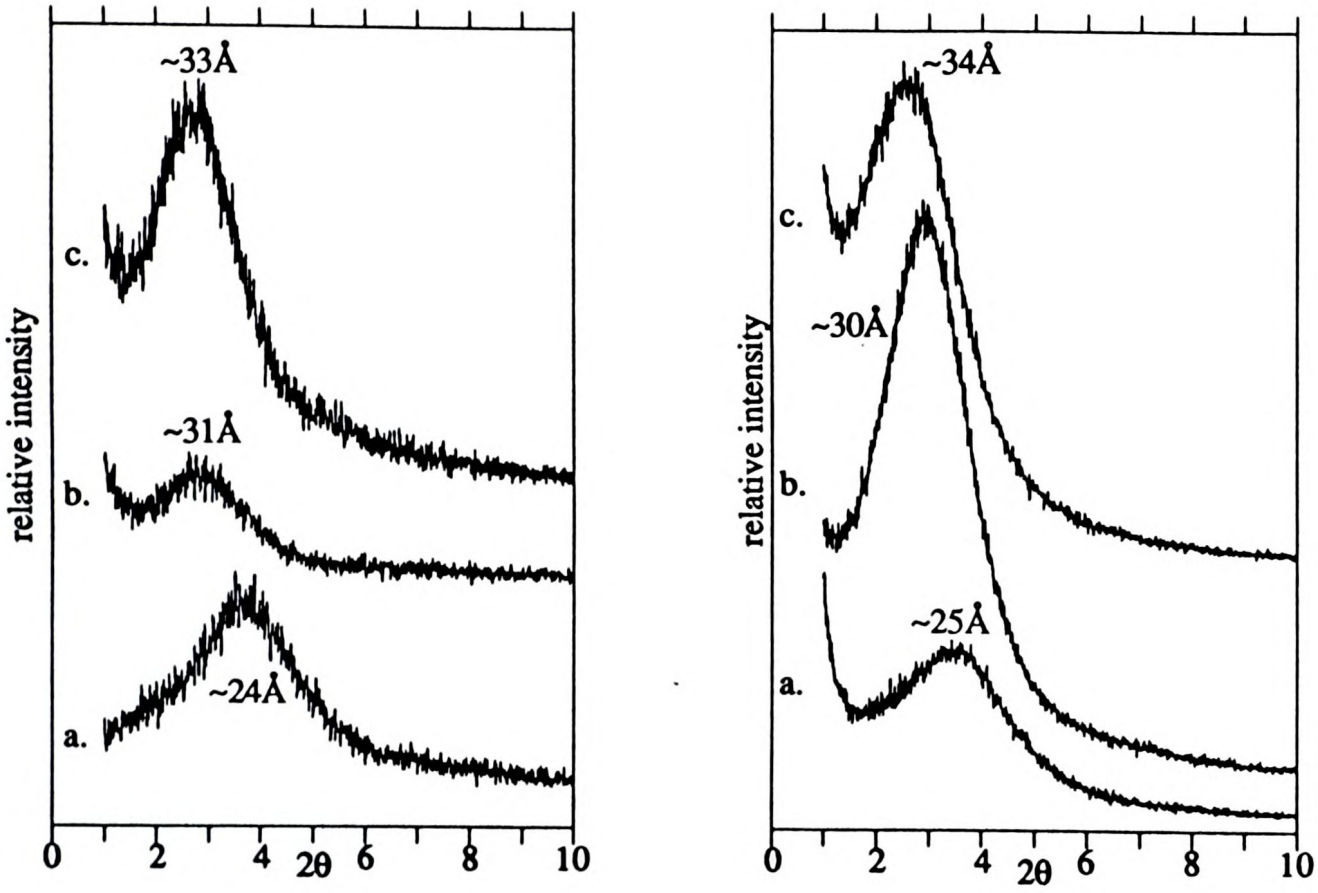

FIGURE 31. X-ray powder diffraction (pwd) patterns of the air-dried and calcined (450°C) TEOS-hydrolysis products formed in the presence of alkylamines prepared at an initial TEOS to amine molar ratio of 7.5
left: air-dried products, right: calcined products
a. HA200 and CHA200, b. OA200 and COA200, c. DA200 and CDA200

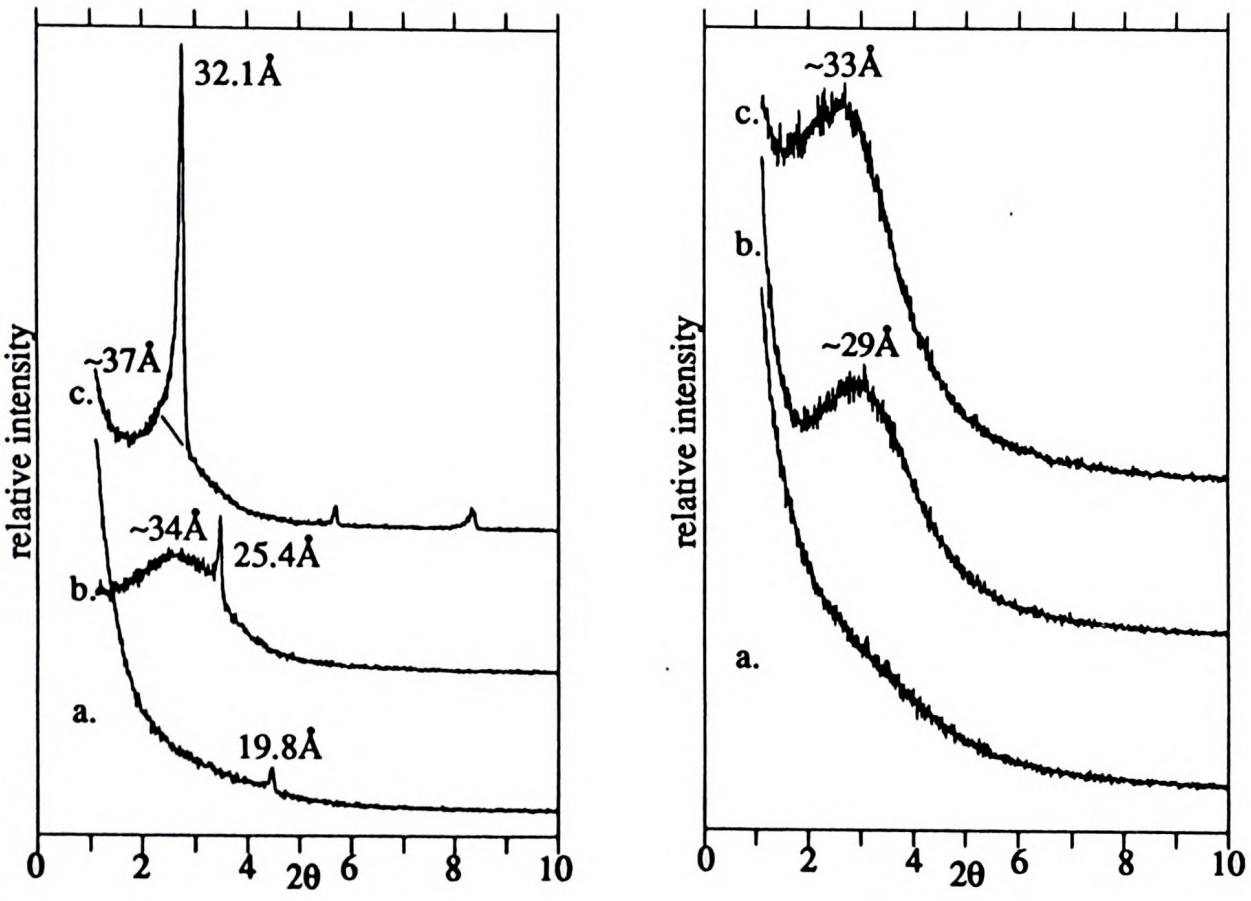

FIGURE 32. X-ray powder diffraction (pwd) patterns of the air-dried and calcined (450°C) TEOS-hydrolysis products formed in the presence of alkylamines prepared at an initial TEOS to amine molar ratio of 3.7
left: air-dried products, right: calcined products
a. HA100 and CHA100, b. OA100 and COA100, c. DA100 and CDA100

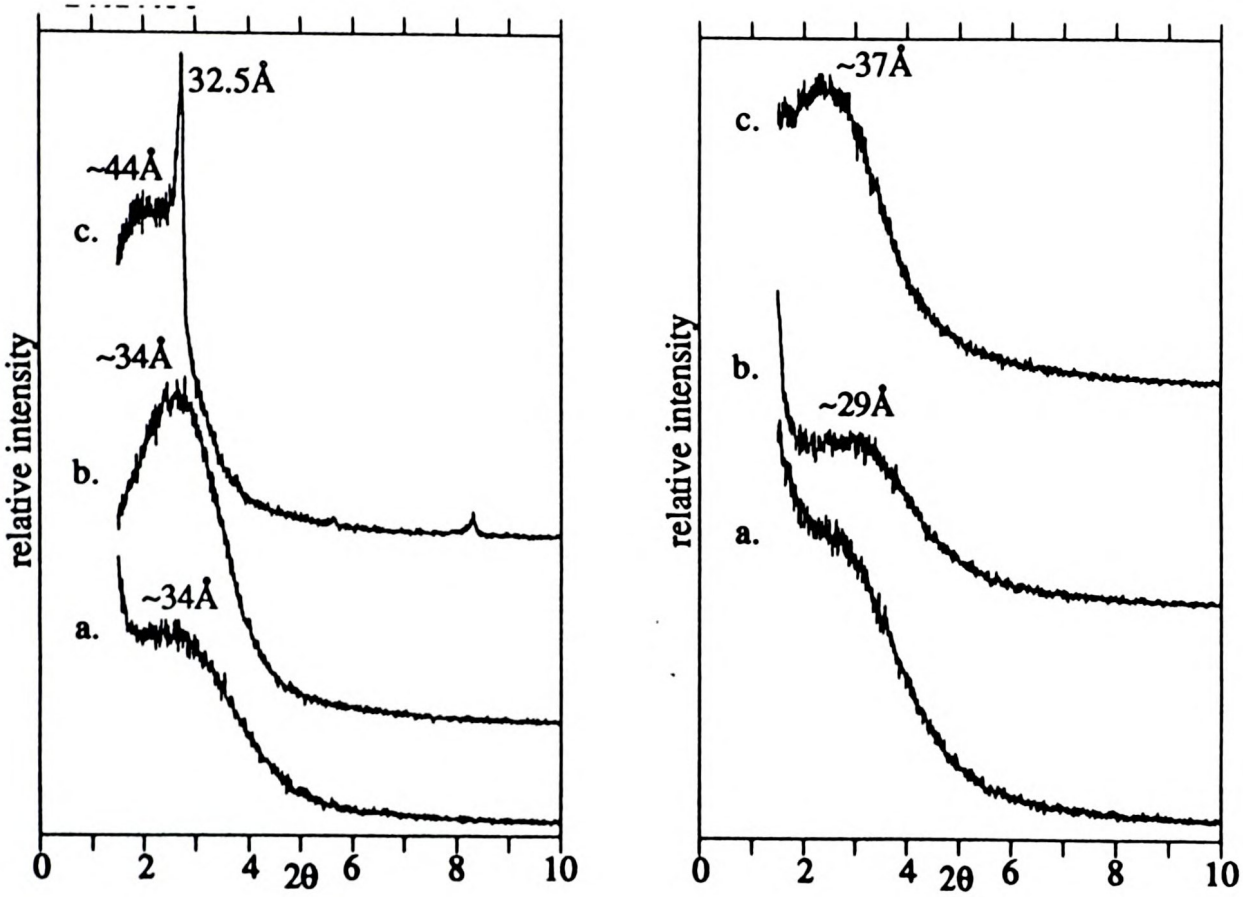

FIGURE 33. X-ray powder diffraction (pwd) patterns of the air-dried and calcined (450°C) TEOS-hydrolysis products formed in the presence of alkylamines prepared at an initial TEOS to amine molar ratio of 1.9
left: air-dried products, right: calcined products
a. HA50 and CHA50, b. OA50 and COA50, c. DA50 and CDA50

TABLE 20. X-ray diffraction data of the air-dried and calcined products

air-dried sample	d_{001} (Å)	calcined sample	d_{001} (Å)
HA200	24 -	CHA200	25
OA200	31 -	COA200	30
DA200	33 -	CDA200	34
HA100	- 19.8	CHA100	-
OA100	34 - 25.4	COA100	29
DA100	37 - 32.1	CDA100	33
HA50	34 -	CHA50	-
OA50	34 -	COA50	29
DA50	44 - 32.5	CDA50	37

The sharp peak at about 19.8, 25.4 and 32.3 Å for the air-dried hexylamine, octylamine and decylamine derived products, respectively, are due to ammonium chloride salt formation (Table 21).

TABLE 21. Amine and ammonium chloride salt dimensions

amine	length (Å)	ammonium chloride basal spacing (Å)
hexylamine	9.2	19.8 (sharp)
octylamine	11.7	25.5 (sharp)
decylamine	14.2	29.3 (sharp)

The presence of the ammonium salt depends on the length of the amine and so on its vapor pressure. The decylammonium salt is more often present and in larger quantities than the octylamine and hexylamine ones. The quantity of amine remaining in the air-dried products might also be related in some extent to the atmospheric conditions and the humidity used to air-

dry as some ammonium bicarbonate salt can also be formed. In all cases, the ammonium salts are completely removed after calcination.

Transmission electron microscopy

The presence of the broad diffraction peaks at high d-spacings suggests some layered organization of the polymer that remains stable even after calcination. Strawbridge et al.[48] TEM pictures of a gel synthesized with a TEOS to H_2O molar ratio of 0.5 in presence of ethanol and concentrated HCl has a layer structure but with no fine structure. It correlated with the fact that under low water content, gelation results from the entanglement of linear chains created during the condensation-polymerization reaction.[67] We have analyzed our sample by transmission electron microscopy (Figure 34) in an attempt to detect some repeating units of dimension equivalent to those found by X-ray diffraction studies. We seek evidence for layers, ribbons or spheric particles.

Some layered structure is evidenced on the edges of the particles. Unfortunately, we can not really draw more conclusions from those pictures. The material seems to have some structure due to the presence of atomic resolution, but no general feature can be seen. Shades are apparent on some pictures, maybe due to interconnecting ribbons. But, up to now, no conclusion can be made: a more intense study should be completed.

FIGURE 34a. CDA50 TEM picture (3x190,000: 1cm=175Å)

FIGURE 34b. CDA50 TEM picture (3x190,000: 1cm=175Å)

FIGURE 34c. CDA50 TEM picture (3x190,000: 1cm=175Å)

FIGURE 34d. CDA50 TEM picture (3x190,000: 1cm=175Å)

CONCLUSION

The acid catalyzed hydrolysis-polymerization of tetraethylorthosilicate in presence of alkylamines generates air-dried precursors which, when calcined are converted to highly microporous silica. The high total surface area and layered structure has been sometimes noticed for acid or base catalyzed polymerization of TEOS in the presence of a solvent. However, the study of our samples demonstrated the influence of alkylamines on the pore structure and exhibited its directing role during the polymerization. We can predict that using a higher amine alkyl chain, we will be able to reach the domain of mesopores. This method could then be used to create silica with determined micropores or mesopores sizes at low temperature and without the use of a solvent. Thus, it seems we created a new form of porous silica. Additional experiments still have to be done to obtain more information on the pore size of these materials. Information can be obtained from adsorption isotherms of molecules with known kinetic diameters and from the study of transmission electron micrographs. Finally, with a better knowledge of this new silica, application studies could be made, eg. by substituting silicon atoms by aluminum atoms to obtain some porous acidic alumina-silica.

POLYMERIZATION OF TEOS INTO LAYERED SILICIC ACID: A NEW POROUS SILICA INTERCALATED IN MAGADIITE LAYERS

INTRODUCTION

Hydrous sodium silicate minerals are layered materials. The layers consist of SiO_4 tetrahedra units linked together. The sheets bear negative charges which are compensated by sodium cations surrounded by an hydration sphere. Adjacent layers are held together by electrostatic interactions between the layers and the gallery cation and/or by hydrogen bondings with interlayer water.[14,16,22,30,33,34] The acid derivatives, called silicic acids, are obtained by proton exchange. Those solid acids retain the layer structure, but some rearrangements occur in the gallery due to the loss of interlayer water molecules (see section on magadiite characterization). The hydrous sodium silicate minerals and their acidic analogs are starting reactants for the synthesis of new layered materials. This synthesis of new lamellar compounds results from the intercalation of

new species in the interlayer space. It is carried out by cation exchange of sodium or protons, by grafting or polymerization into the silicic acid galleries.

Na-magadiite ($Na_2 Si_{14} O_{28} (OH)_2 . 8 H_2O$)[17] and its acid form H-magadiite have been extensively studied. Indeed, Na-magadiite is easily prepared by hydrothermal reaction.[9] It has an intermediate layer thickness (11.2 Å)[38] among the hydrous sodium silicate minerals family. Kanemite ($Na H Si_2 O_4 (OH)_2 . 2 H_2O$)[12] and makatite ($Na_2 Si_4 O_8 (OH)_2 . 4 H_2O$)[15] are lower condensed silicates while kenyaite ($Na_2 Si_{22} O_{44} (OH)_2 . 9 H_2O$)[17] is more condensed. Recently, magadiite cation exchange has been demonstrated for lanthanum,[32] cesium[32] and cobalt sepulchrate.[4] Ruiz-Hitzky et al.[68,69] and Yanagisawa et al.[31] reported the grafting of organosilanes and alkyldisilazane monomers after expansion of the H-magadiite layers by polar organic solvents or by organoammonium intercalation, respectively. Sprung et al.[70] reported direct grafting of organosilane oligomers. Several species have been polymerized into H-magadiite, among them are acrylamide,[28,71] acrylonitrile,[72] caprolactam[28] and tetraethylorthosilicate.[2-4]

The work of Sprung et al.[70] and Landis et al.[3] both yielded silica-pillared magadiite, but they used different pillaring approaches. Sprung et al.[70] used a traditional-derived approach where the pillaring species were prepared separately: an alkyltrichlorosilane was allowed to polymerize before being allowed to interact with a H-magadiite suspension at 0°C. The oligomers were then grafted onto the layers. Landis et al.[3] invented a new pillaring procedure: the pillaring species were introduced as monomers in swelled organoammonium magadiite solution and polymerized *in situ* at 25°C-80°C. The latter method resulted in larger surface areas.

On the basis of our understanding of magadiite chemistry, together with our knowledge of the acid catalyzed polymerization of TEOS in the presence of alkylamines, we decided to study the intercalation-polymerization of TEOS in alkylammonium/alkylamine swelled magadiite.

RESULTS AND DISCUSSION

Synthesis

The intercalation-polymerization of TEOS in alkylammonium magadiite can be divided into several stages. First, Na-magadiite synthesized by hydrothermal reaction[9] is proton exchanged[10] with HCl to obtain its acid-derivative: H-magadiite. The layers of the silicic acid are swelled by the addition of alkylamine. TEOS is added to that amine-solvated alkylammonium/alkylamine magadiite. Polymerization occurs between the layers in the presence of alkylamine to form a siloxane-intercalated magadiite. The remaining alkylamines and ethoxy groups are removed by calcination and the structure is stabilized as silica-intercalated magadiite.

We first carried out amine swelling experiments to better understand the effect of the amine on the H-magadiite structure. We then established the experimental parameters such as washing procedure and calcination temperature. Finally, we studied the effect of amine chain length and TEOS concentration on the intercalation-polymerization reaction.

Alkylammonium/alkylamine-magadiite

TEOS intercalation-polymerization reaction in magadiite galleries is initiated by amine intercalation. As was revealed by the work of Lagaly et al.,[7] amines readily swell H-magadiite. There are several steps in the

swelling mechanism. Firstly, the adsorbate penetrates between the silicate layers, causing a lattice expansion and displacing the initial gallery molecules. For the acid derivative of magadiite, the driving force for amine penetration is protonation. That is, the amine enters the gallery and reacts with a proton to form an ammonium cation. Secondly, solvatation of the resulting onium ions by neutral amine molecules results in an energy gain from van der Waals interactions, allowing the layers to separate. The amine chain length is an important parameter for the stabilization of the final ammonium/amine-magadiite.

The alkylammonium/alkylamine-magadiites have been studied under different conditions using various alkylamines. The alkylamines used were hexylamine, octylamine and decylamine. The alkylammonium/alkylamine-magadiites were studied as amine-solvated products or air-dried compounds. As the amine-solvated products are unstable intermediates, we have only been able to record their X-ray diffraction patterns. However, the air-dried compounds, formed by evaporation of excess amine at room temperature, have been characterized by X-ray diffraction, C, H, N analyses and ^{29}Si NMR.

X-ray powder diffraction

X-ray diffraction analysis has been our main analytical tool for investigating gallery expansion. The data are gathered in Table 22.

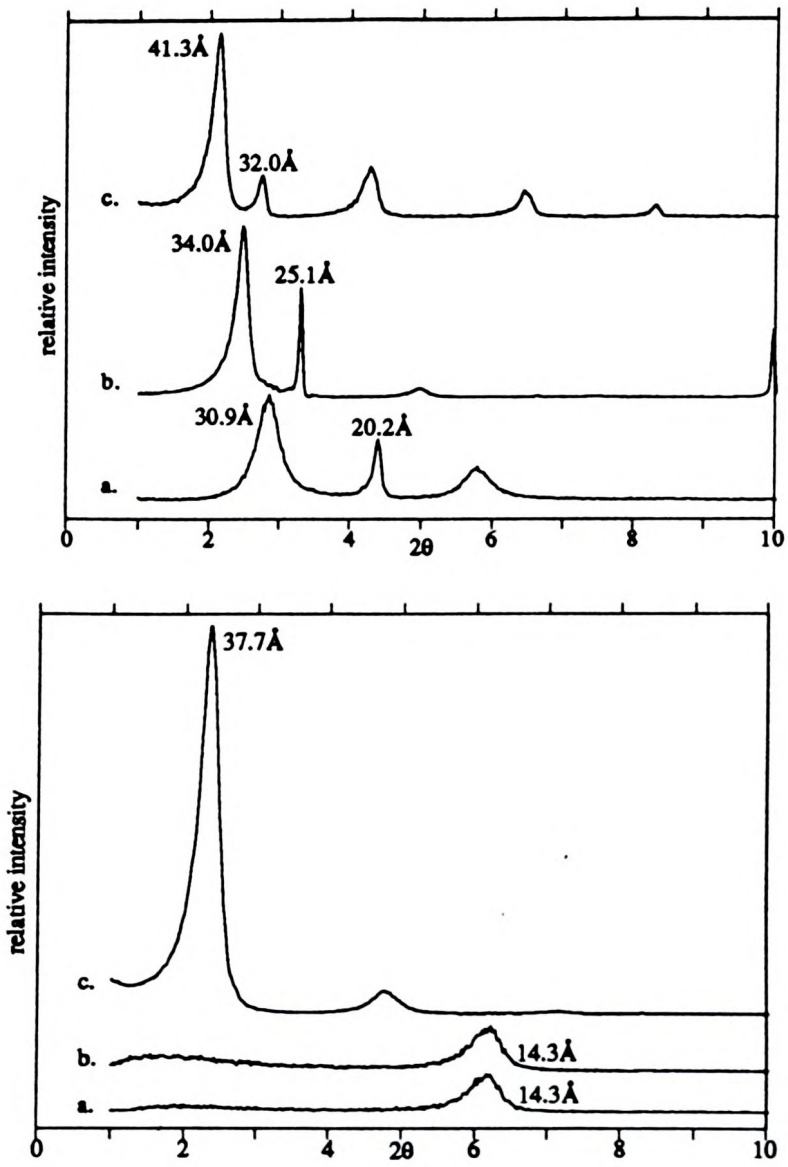

FIGURE 35. X-ray diffraction patterns of alkylammonium/alkylamine-magadiites gels
top: alkylammonium/alkylamine-magadiites in amine suspension
bottom: air-dried alkylammonium/alkylamine-magadiites
a. hexylammonium/hexylamine-magadiite
b. octylammonium/octylamine-magadiite
c. decylammonium/decylamine-magadiite

TABLE 22. X-ray diffraction data for various alkylammonium/alkylamine magadiites

ammonium/amine intercalated magadiite		basal spacing (Å)	crystallinity (Å)
hexylamine	amine suspension	30.9(b) , 20.2(n)	260
	air-dried	14.3(b) , -	200
octylamine	amine suspension	34.0(b) , 25.1(n)	370
	air-dried	14.3(b) , -	180
decylamine	amine suspension	41.3(b) , 32.0(n)	590
	air-dried	37.7(b) , -	340

(b): broad, (n): narrow

The alkylammonium/alkylamine-magadiite patterns in amine suspension are displayed in Figure 35. The narrow peaks at 20.2 Å, 25.1 Å and 32.0 Å for the hexylamine, octylamine and decylamine samples, respectively, are inconsistent with the presence of swelled magadiite. The sharpness of this peak suggested the presence of alkylammonium salts formed by reaction of the amine with atmospheric CO_2 or an atmospheric acid contaminant. To confirm this hypothesis, we first crystallized the ammonium chloride salt by adding concentrated hydrochloric acid to the amine on a microscope slide. The X-ray diffraction patterns exhibited narrow peaks at 19.8 Å, 25.5 Å and 29.3 Å, for hexylammonium, octylammonium and decylammonium chloride, respectively (Table 21). The positions of these narrow peaks are close to those found on the alkylammonium/alkylamine-magadiite patterns. On the basis of the amine dimensions (Table 21), the ammonium salt crystallizes in double layers. In H-magadiite, no counter-anions other than the silicate layers are present for alkylammonium salt formation. Furthermore, the salt peak intensity is dependent on the aging time of the glass slide: the older the preparation,

the less intense the narrow peak. Those two facts support the hypothesis of a reaction related to the atmosphere. We, thus, decided to run a blank experiment with octylamine and amorphous silica. Amorphous silica is made of SiO_2 grains that do not exhibit any acid-base properties. The silica gel served only as a solid support to spread the octylamine on a vertical microscope slide. The pattern obtained contained a narrow peak at 25.4 Å. When the slide was allowed to air-dry, the powder did not stick anymore to the microscope slide: octylamine had evaporated and nothing was linking the silica grains together anymore. No X-ray diffraction pattern could be recorded. This blank experiment confirmed the assignment of the narrow peaks in the alkylammonium/alkylamine-magadiite XRD patterns. They are attributed to the reaction of the amine with atmospheric CO_2 and water to yield a bicarbonate ammonium salt according to the following reactions:

$$\underset{\text{in air}}{H_2O_{(g)} + CO_{2(g)}} \;\underset{\text{drying}}{\xleftarrow{\quad}}\; [H_2CO_3] \;\xleftarrow[\text{drying}]{RNH_{2(liq)}}\; \underset{\text{bicarbonate ammonium salt}}{[RNH_3^+, HCO_3^-]_{(solid)}}$$

(unstable)

As the excess liquid amine evaporates in air, the equilibrium shifts to the left. So, the bicarbonate ammonium salt disappears on aging, as it has been observed for our various samples.

The relatively broad XRD peaks at 30.9 Å, 34.0 Å and 41.3 Å for the amine-solvated samples are assigned to onium ion exchange form of magadiite swollen by hexylamine, octylamine and decylamine, respectively. They arise due to amine intercalation into H-magadiite. The gallery heights (as defined in Figure 4) are 19.7 Å, 22.8 Å and 30.1 Å for hexylamine,

octylamine and decylamine magadiites, respectively. As stated by Lagaly,[29] alkylamines are arranged in double layers within magadiite. Lagaly extensively studied amine intercalation in various silicic acids. The magadiite intercalation of alkylamines having up to 5 carbon atoms in their chains, results in an alkylamine monolayer parallel to the silicate layers (Figure 36a). The resulting basal spacing is 14.4 Å. For alkylamines containing 6 to 9 carbon atoms, intercalation of gauche-block alkylamine bilayers occurs in magadiite (Figure 36b). The resulting basal spacings range from about 30.0 Å for hexylamine to about 34.2 Å for nonylamine. For longer alkylamines, the adsorbate arranges in bilayers perpendicular to the silicate layers (Figure 36c). The resulting basal spacing for the decylamine intercalated magadiite is about 40.0 Å.

The air-dried samples exhibit different basal spacings. The gallery heights, as well as the crystallinity (Appendix B), decreases upon drying. The basal spacings collapse to 14.3 Å, 14.3 Å and 37.7 Å for hexylamine, octylamine and decylamine magadiites, respectively. Hexylamine and octylamine belong to the same amine category as defined by Lagaly et al.. Upon evaporation of the excess amine, the interlayer molecules rearrange to form an alkylamine monolayer parallel to the silicate layers characterized by a 14.3 Å basal spacing. In order to rearrange into a monolayer, excess amine has to be removed and, thus, van der Waals interactions have to be overcome. Although the decylamine-solvated sample already belonged to a different category, the particularity of the decylamine intercalation is better distinguished when the sample is air-dried: the basal spacing is maintained at 37.7 Å after one month at room temperature. For the air-dried hexylamine and octylamine samples, the

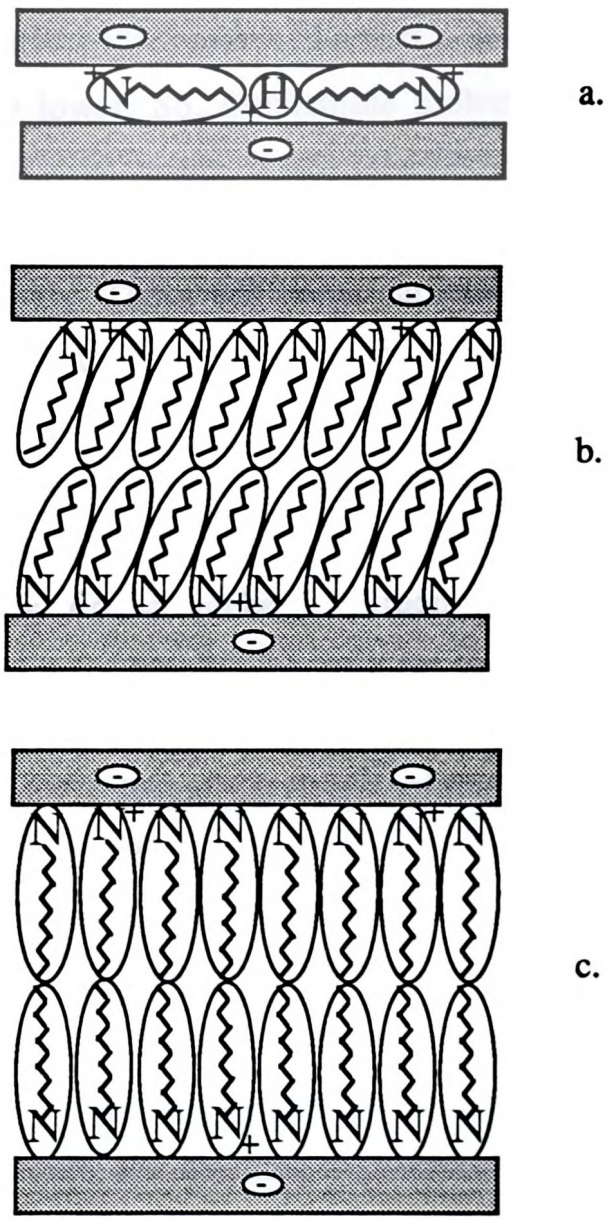

FIGURE 36. Alkylamine intercalation into silicic acids, according to the number of carbon atoms in their chain

a: monolayer
b: gauche-block bilayer
c: perpendicular bilayer

basal spacing collapsed after a few hours. The explanation is certainly related to the longer chain length of decylamine. It results in a higher boiling point for decylamine: 216-218°C. Hexylamine and octylamine boiling points are 131-132°C and 175-177°C, respectively. Its vapor pressure is certainly lower. So, decylamine molecules can not readily escape from the magadiite layers. Also, in a bilayer conformation, the decylamine has 8 or 4 more carbon atoms than the hexylamine and octylamine, respectively. Those additional carbons create more van der Waals interactions that must be overcome to evaporate the excess amine.

Van der Waals interactions between intercalated amine chains are related to crystallinity. The greater the van der Waals interactions, the better the crystallinity. As the number of carbon atoms in the alkylamine chain increases, from 6 for hexylamine, to 8 for octylamine and to 10 for decylamine, the size of the scattering domain along the layer stacking direction of the amine-solvated alkylammonium/alkylamine magadiite increases from 260 Å to 370 Å and to 590 Å, respectively. H-magadiite exhibits a scattering domain of 50 Å. When the amines lie parallel to the layer, and so, when van der Waals interactions are minimal, the air-dried hexylamine and octylamine-magadiites scattering domain sizes are identical at ~190 Å. The gallery order for amine-intercalated magadiite is still better than that for H-magadiite. For air-dried decylamine-magadiite, even if the amine did not evaporate completely, the degree of order changed owing to a decrease in the number of van der Waals interactions. The crystallinity went down to 340 Å. This value is lower than the initial one, but higher than those of the air-dried hexylamine and octylamine-magadiites. This is in good agreement with our general conclusion, namely, for amine-

intercalated magadiite, van der Waals interactions between the chains and crystallinity are related.

Chemical compositions

In order to understand better this phenomenon, we studied the carbon, hydrogen and nitrogen contents. The data are presented in Table 23.

TABLE 23. Chemical composition from elemental analysis for the air-dried alkylamine-intercalated magadiites

air-dried amine-intercalated magadiite	%wt element					%wt composition		
	%wt C*	%wt H*	%wt N*	%wt Si**	%wt O**	%wt SiO_2**	%wt amine**	%wt H_2O**
hexylamine	6.3	1.9	1.2	40	50	86	8	6
octylamine	7.8	2.1	1.1	40	49	85	10	5
decylamine	56	11	6.2	10	17	20	70	10

* measured from C, H, N analysis

** calculated according to the method explained in the text

The C, H, N results from the chemical analyses are given in ppm (μg/l) for C, H and N. By assuming a density of 1 g/l for the analyzed solutions, we can convert those results to %wt.

The amine content has been calculated from the %wt N, given by the analysis:

n_A: moles of nitrogen in 100 g = moles of amines in 100 g

$$n_A = \frac{\%wt\ N}{M_N} = \frac{\%wt\ N}{14}$$

$$\%wt\ amine = n_A * M_A$$

M_A = 101.19 g/mol for hexylamine

M_A = 129.25 g/mol for octylamine

M_A = 157.30 g/mol for decylamine

The water content has been calculated using the %wt H left after deduction of the hydrogen present in the amine:

n_{H2O} is defined as the number of moles of water created by silanol condensation and by desorption of water per 100 g of compound.

$$n_{H2O}=\left(\frac{\%wt\ H}{M_H} - h * n_A\right)/2 = \left(\frac{\%wt\ H}{1} - h * n_A\right)/2$$

h = 15 for hexylamine

h = 19 for octylamine

h = 23 for decylamine

$$\%wt\ H_2O = n_{H2O} * M_{H2O} = n_{H2O} * 18$$

The silicon content in 100 g of compound has been calculated, assuming that after the C, H, N analysis, the remaining product is silica SiO_2.

$$\%wt\ SiO_2 = 100 - \%wt\ amine - \%wt\ H_2O$$

If n_{SiO2} and n_{Si} represent the number of silica molecules and silicon atoms, respectively, in 100 g of compound:

$$\%wt\ SiO_2 = n_{SiO2} * M_{SiO2} = n_{SiO2} * 60.1$$

$$n_{Si} = n_{SiO2} = \frac{\%wt\ SiO_2}{60.1}$$

$$\%wt\ Si = n_{Si} * M_{Si} = n_{SiO2} * 28.1$$

Finally, the total oxygen content in 100 g of compound is determined to complete the elements' weight % to 100:

$$\%wt\ O = 100 - \%wt\ C - \%wt\ H - \%wt\ N - \%wt\ Si$$

As the swelling experiments are intercalation reactions, it is therefore possible to calculate the number of amines remaining per Si_{14} unit after air-drying (Table 24).

TABLE 24. Number of amines present per unit cell for the air-dried alkylamine-intercalated magadiites

air-dried amine-intercalated magadiite	hexylamine	octylamine	decylamine
Si	14	14	14
amine	0.8	0.8	18

The validity of the chemical analysis can be checked: the carbon content should match the amine content as the carbon only comes from the amine aliphatic chain (Table 25).

We should obtain : $\frac{\%wt\ C}{M_C} = \frac{\%wt\ C}{12} = c * n_A$

c = 6 for hexylamine

c = 8 for octylamine

c = 10 for decylamine

TABLE 25. Validity of the C, H, N analysis

air-dried amine-intercalated magadiite	hexylamine	octylamine	decylamine
%wt C/12	0.52	0.65	4.6
$c * n_A$	0.50	0.61	4.4
% error	4	7	5

As the ideal H-magadiite formula is $H_2 Si_{14} O_{28} (OH)_2 . x H_2O$ (alternatively written: $Si_{14} O_{26} (OH)_4 . x H_2O$), the maximum number of ammonium molecules produced by the acid-base reaction between amines and hydrogens from silanol groups and from the interlayer protons is 4. It appears (Table 24) that air-dried hexylamine- and octylamine-intercalated magadiites lose not only all the neutral amines, but also some of the ammonium molecules. In the case of a C_6 or C_8 chain, the alkylammonium interaction with the layers is not strong enough to maintain the layers apart in the absence of neutral amine. To balance the charges, the alkylammonium cations deprotonate before leaving the layers. They dissociate into amine and protons, and leave the protons between the layers to balance the charges.

As for the air-dried decylamine-intercalated magadiite, alkylammonium cations and neutral amines still form a bilayer, we took into account geometrical considerations. Using molecular graphics to simulate molecule configuration and size, we find the distance between two hydrogen atoms linked to the nitrogen to equal 1.747 Å. By projection and geometrical considerations, we calculated the radius of the amine head surface: r_N~1 Å (1.747/2*cos30°). Thus, the surface area required per amine in the vertical position is at least 3.2 Å^2 (πr_N^2). However, there are

some unoccupied spaces. Assuming a closest-packed arrangement, we consider the stacking hexagonal. Accounting for the unoccupied spaces, we find a needed surface per amine of at least 4 $Å^2$ ([2*1/tan30°]^2*3/9). According to Brindley,[38] the lattice parameters in the sheet plane are a=b=7.25 Å. So, the available space for an amine double layer is 105 $Å^2$ (a*b*2sheets) per Si_{14} unit. If, as has been calculated from chemical analyses, there are 18 decylamines per Si_{14} unit, they would occupy, in the closest-packed configuration, 72 $Å^2$ (18amines*4$Å^2$). So, when the decylamine-intercalated magadiite is air-dried, the remaining decylamines are not in a close-packed vertical configuration. This fact can account for the loss in crystallinity and basal spacing.

^{29}Si nuclear magnetic resonance

The air-dried decylamine-intercalated magadiite is stable and exhibits a large basal spacing. We thus have been able to obtain ^{29}Si nuclear magnetic resonance spectra and to determine precisely the Q^3/Q^4 ratio without any interlayer interaction (Table 26). The air-dried decylamine-intercalated magadiite solid state ^{29}Si NMR spectrum is displayed in Figure 37.

TABLE 26. Various cation-magadiites ^{29}Si NMR data

sample	Si chemical shifts (ppm *vs.* TMS)				Q^3/Q^4	per unit cell	
	Q^3	Q^4			ratio	Q^3	Q^4
Na-magadiite	-99.5	-110.0	-111.4	-114.1	0.39	3.9	10.1
H-magadiite	-101.2	-110.9	-111.7	-114.3	0.29	3.2	10.8
air-dried decylamine-intercalated magadiite	-100.8		-111.6	-114.9	0.29	3.2	10.8

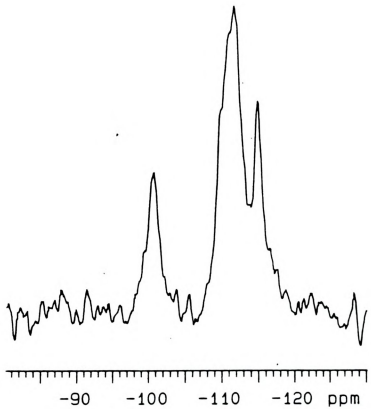

FIGURE 37. Air-dried decylamine-intercalated magadiite solid state ^{29}Si NMR spectrum
(delay time: 1200 seconds, line broadening: 40, 12 scans)

The air-dried decylamine-intercalated magadiite basically exhibits the same NMR spectrum as H-magadiite (Figure 14c). The Q^3/Q^4 ratio, as defined in the section on magadiite characterization is identical. It proves that the Q^3/Q^4 ratio calculated from the H-magadiite spectrum is not perturbed by the hydrogen bondings between the layers. It also tells us that the amine intercalation only separates the layers and does not have any effect on the layer structure. This is a noticeable difference in comparison to the effect of aqueous alkyltrimethylammonium intercalation into kanemite.[42,73] As kanemite is constituted of a single sheet of SiO_4 tetrahedra, its ^{29}Si NMR spectrum only displays one resonance at -97.2 ppm[42] or -101 ppm[14] assigned to Q^3 silicon atoms. However, upon intercalation of dodecyltrimethylammonium[42] (hexadecyltrimethylammonium),[73] the Q^3 peak shifts to higher values: -100.3 ppm (-100.8 ppm) and one Q^4 peak appears at -109.2 ppm (-110.2 ppm). This behavior did not occur for Na-magadiite and K-kenyaite treated in the same conditions.[31] This difference was said to be due to the deformation of the single SiO_4 tetrahedral sheet that allows for natural condensation upon alkyltrimethylammonium intercalation.[42]

Conclusion

To conclude on this set of experiments, it is worth noticing that the three alkylamines exhibit similar magadiite swelling behavior in the presence of excess amine. They incorporate a bilayer configuration inside the gallery when fully solvated by excess amine. The intercalation is initiated by an acid-base reaction between the amines and hydrogen ions from silanol groups and interlayer protons. The structure is stabilized by van der Waals interactions between the aliphatic chain of the

alkylammonium cations and the neutral amine. Air-dried hexylamine- and octylamine-intercalated magadiite exhibit a monolayer structure. However, air-dried decylamine-intercalated magadiite still retains an amine bilayer configuration. Therefore, it would not be surprising if the products resulting from TEOS polymerization in pre-swollen magadiite exhibit properties dependent on the alkylamine reactant.

Experimental conditions for TEOS polymerization in H-magadiite

An important parameter in the final design of the silica-intercalated magadiite is the calcination temperature. Indeed, heat treatment stabilizes the system, in particular, by eliminating the organic molecules. We thus carried out experiments at various calcination temperatures to establish the best calcination temperature for the further studies. As one purpose of the heat treatment is to eliminate organic molecules, we also carried out syntheses where an ethanol washing procedure was included before calcination. In this set of experiments, the silica-intercalated magadiite was synthesized from 5.04 g ($5.6*10^{-3}$ mol) of H-magadiite, 20.2 g (0.16 mol) of octylamine and 120 g (0.58 mol) of tetraethylorthosilicate. The TEOS:octylamine:magadiite molar ratio was 103:28:1.

Thermogravimetric analysis

In order to choose a suitable calcination temperature, we obtained first thermogravimetric analysis curves (Figure 38). The numeric data are gathered in Table 27. The %wt SiO_2 determined from thermogravimetric analysis has been calculated assuming the remaining mass left after heating at 800°C is pure silica.

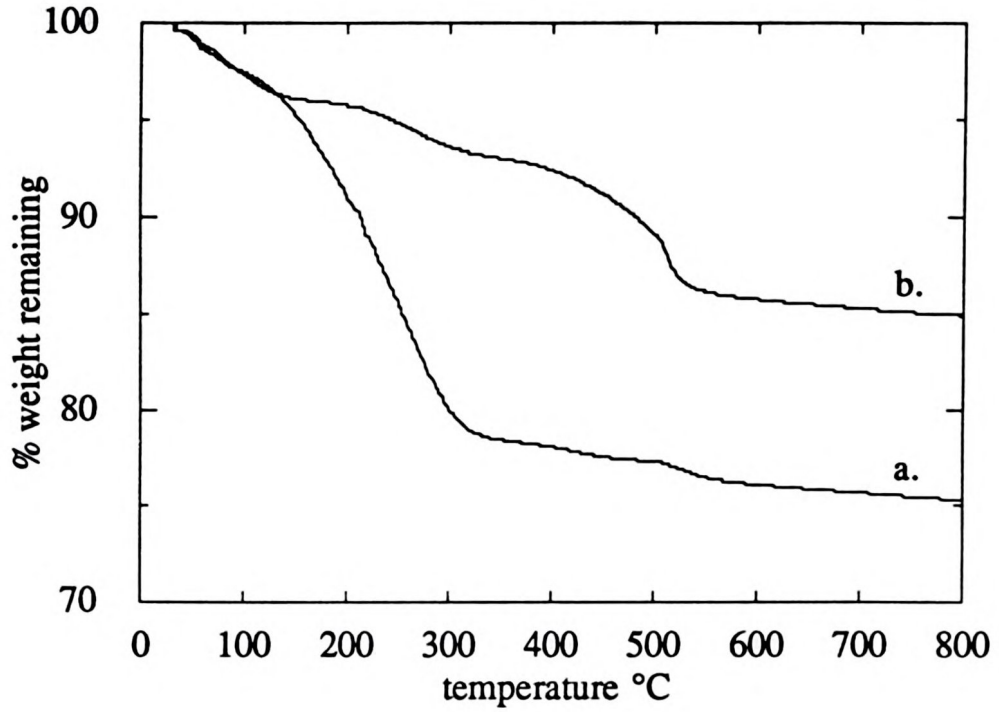

FIGURE 38. Thermogravimetric analysis curves for octylamine-derived siloxane-intercalated magadiites
a. unwashed octylamine-derived siloxane-intercalated magadiite
b. octylamine-derived siloxane-intercalated magadiite washed once with ethanol

TABLE 27. Chemical composition from thermogravimetric analysis for unwashed and ethanol-washed octylamine-derived siloxane-intercalated magadiites

octylamine-derived siloxane-intercalated magadiite	first %wt loss: external water	second %wt loss: octylamine	third %wt loss: dehydroxylation	%wt SiO_2
unwashed	1.6	20	2.7	76
ethanol-washed	3.7	3.1	7.9	85

The thermogravimetric curves show a three-step weight loss. The first one from room temperature to about 150°C is assigned to external water loss. It is almost identical for the unwashed and the ethanol-washed samples. The second weight loss from ~150°C to ~350°C is assumed to be due to the octylamine elimination. This second step is much larger in the case of the unwashed sample, suggesting that washing, indeed, removes the amine. The last slope occurring between 350°C and 800°C is assigned to silanol dehydroxylation. We thus studied samples formed at the following calcination temperatures: 100°C, after water elimination ; 250°C, after partial amine evaporation ; 450°C, when amine elimination is complete ; 800°C, after partial dehydroxylation.

Chemical compositions

The assignments of the various weight loss have been confirmed by C, H, N analysis (Table 28).

As was found from the thermogravimetric analysis, the unwashed octylamine-derived siloxane-intercalated magadiite contains much more octylamine than its washed counterpart. The octylamine content found by the two methods are in agreement: 20% and 3.1% from the thermogravimetric analysis, 18% and 3.2% from the C, H, N analysis, for the unwashed and washed samples, respectively. Also, the comparison of the SiO_2 content quantity measured by thermogravimetry (Table 27: 76% and 85%) and the one found by calculation from the C, H, N analysis (Table 28: 75% and 85%) proves the reliability of our calculations.

TABLE 28. Chemical composition from elemental analysis for unwashed and ethanol-washed octylamine-derived siloxane- and silica-intercalated magadiites at various calcination temperatures

	%wt element					%wt composition			
sample	%wt C*	%wt H*	%wt N*	%wt Si**	%wt O**	%wt amine**	%wt ethoxy**	%wt H_2O**	%wt SiO_2**
unwashed	14	4.0	2.0	35	45	18	1.5	5.8	75
100°C	13	3.4	1.7	35	47	16	2.0	7.0	75
250°C	5.8	2.1	0.66	39	52	6.1	2.4	8.1	84
450°C	0.78	1.6	0.09	40	57	0.83	0.31	13	86
800°C	0.32	1.4	0.14	41	57	1.3	0.00	11	88
washed	4.4	1.8	0.35	40	54	3.2	3.7	7.5	85
100°C	5.8	2.0	0.83	40	52	7.7	0.17	7.3	85
250°C	4.4	1.7	0.23	40	53	2.1	5.3	6.3	86
450°C	0.37	0.99	0.14	43	55	1.3	0.00	7.2	92
800°C	0.17	0.57	0.07	45	55	0.65	0.00	4.3	95

* measured from C, H, N analysis

** calculated according to the method explained in the section acid-catalyzed TEOS polymerization in the presence of alkylamines

Furthermore, the water composition is found to be larger in the case of the washed sample by the two analysis: from Table 27, we find a total water composition of 4.3% and 11.6% ; Table 28 gives the water %wt of 5.8% and 7.5%. The amount of octylamine is always larger in the unwashed samples, even at various calcination temperature. This quantity decreases when the calcination temperature is increased, but octylamine is still present even at 800°C. However, the ethoxy-ethanol groups are completely eliminated after calcination at 450°C.

X-ray powder diffraction

We next look at the X-ray diffraction data (Table 29) to determine if the layer structure is retained. The X-ray diffraction patterns for the unwashed and ethanol-washed octylamine-derived siloxane- and silica-intercalated magadiites are displayed in Figure 39.

TABLE 29. X-ray diffraction data of unwashed and ethanol-washed octylamine-derived siloxane- and silica-intercalated magadiites at various calcination temperatures

sample	unwashed		ethanol-washed	
	d_{001} (Å)	gallery height (Å)	d_{001} (Å)	gallery height (Å)
siloxane-intercalated	36.0	24.8	18.9	7.7
silica-intercalated 100°C	34.7	23.5	18.9	7.7
silica-intercalated 250°C	34.5	23.3	18.9	7.7
silica-intercalated 450°C	33.2	22.0	17.1	5.9
silica-intercalated 800°C	31.3	20.1	15.9	4.7

The octylamine-derived siloxane- and silica-intercalated magadiites display large basal spacings (Table 29) which are confirmed by the presence of the d_{002} peaks (Figure 39: left). Upon calcination, the gallery height (= basal spacing - layer thickness = d_{001} - 11.2) slightly decreases up to a calcination temperature of 250°C. But, when the temperature is increased to 450°C and 800°C, the d_{001} decreases further. As it has been seen by thermogravimetric and chemical analyses, the amine is essentially eliminated at 450°C. Thus, up to 250°C, the alkylamine might still play a role in propping apart the layers. Then, the basal spacing decreases due to the stacking of the layer onto the gallery species (450°C) and drops further because of the condensation-dehydroxylation of the gallery species onto the layers (800°C). Ethanol-washing not only eliminate some of the amines

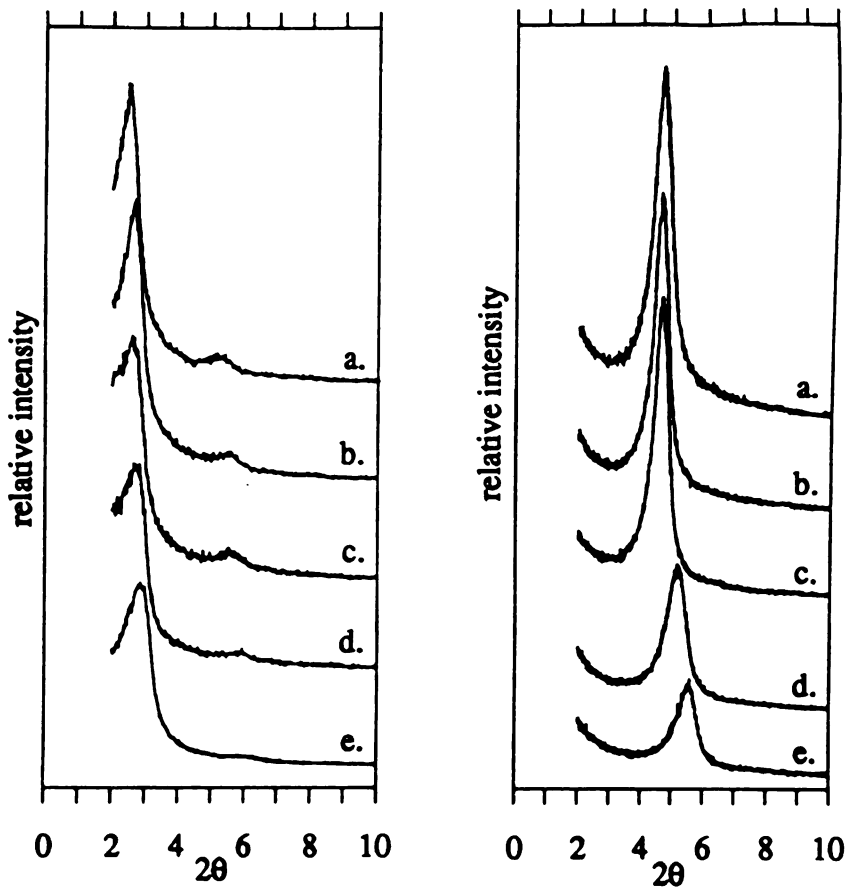

FIGURE 39. X-ray diffraction patterns of unwashed and ethanol-washed octylamine-derived magadiites at various calcination temperatures
left: unwashed octylamine-derived siloxane- and silica-intercalated magadiites (film)
right: ethanol-washed octylamine-derived siloxane- and silica-intercalated magadiites (pwd)

a. siloxane-intercalated magadiite
b. silica-intercalated 100°C
c. silica-intercalated 250°C
d. silica-intercalated 450°C
e. silica-intercalated 800°C

(Table 28) but it also decreases the basal spacing. As some amines are eliminated, they can not play their role as well as if they are more numerous. But, this phenomenon can be understood if we recall the acid-catalyzed TEOS polymerization in the presence of alkylamine (see the section on acid catalyzed TEOS polymerization in the presence of alkylamines). Indeed, the silica-product of the polymerization was found to dissolve in ethanol and to crystallize upon evaporation of the solvent. The same phenomenon, most probably, also is occurring for the siloxane formed inside the magadiite layers. However, we do not know how well the silica-product recrystallizes and also, at that point, the recrystallization occurs in the absence of amine.

Nitrogen adsorption

As we studied the TEOS polymerization inside the H-magadiite layers in order to be able to tailor new microporous solids, we ran some nitrogen adsorption experiments. The N_2 adsorption isotherms are displayed in Figures 40 and 41. The surface areas data are gathered in Table 30 (Appendix C).

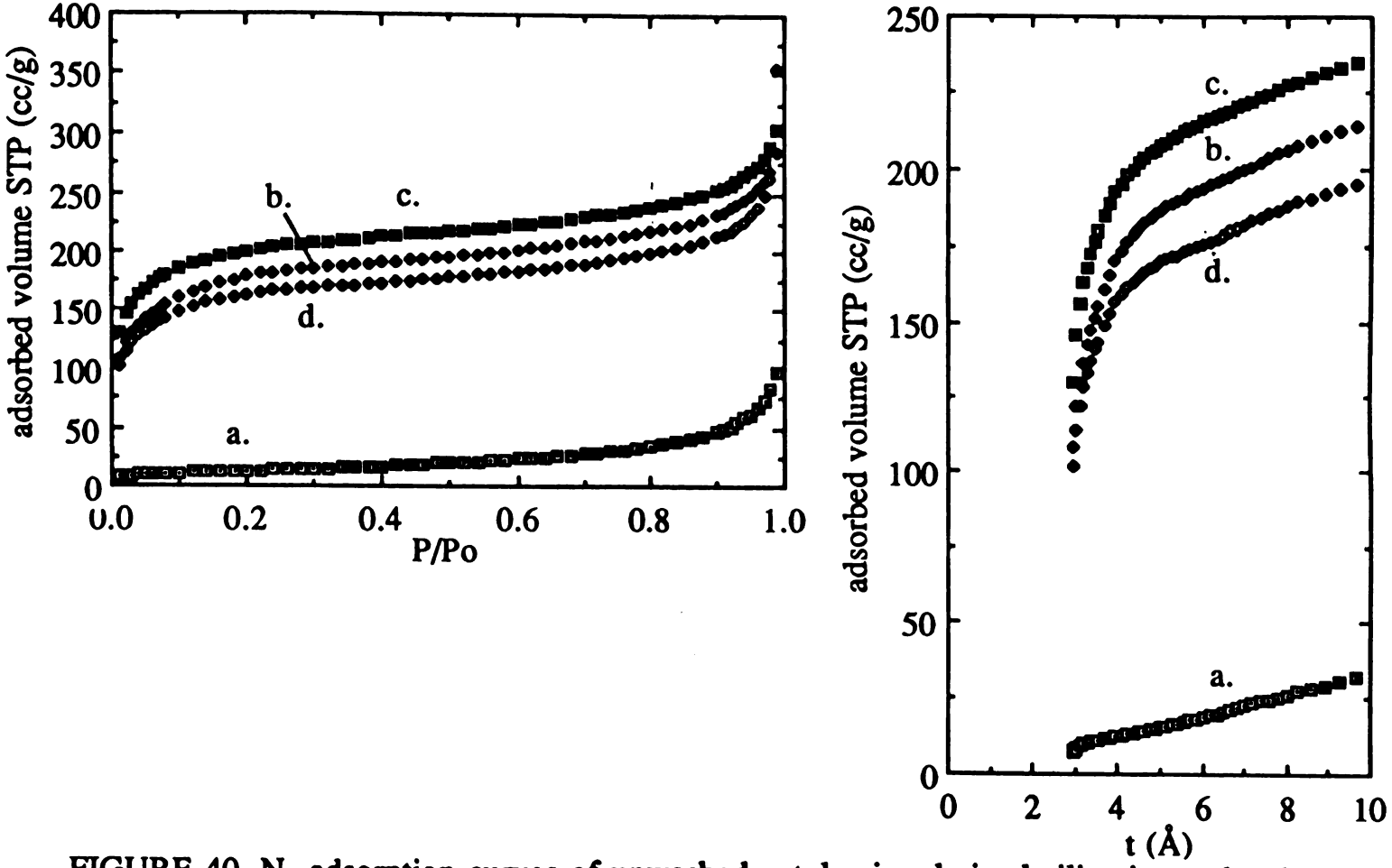

FIGURE 40. N_2 adsorption curves of unwashed octylamine-derived silica-intercalated magadiites at various calcination temperatures
left: N_2 adsorption isotherm, right: t-plot

a. siloxane-intercalated magadiite
b. silica-intercalated 100°C
c. silica-intercalated 250°C
d. silica-intercalated 450°C
e. silica-intercalated 800°C

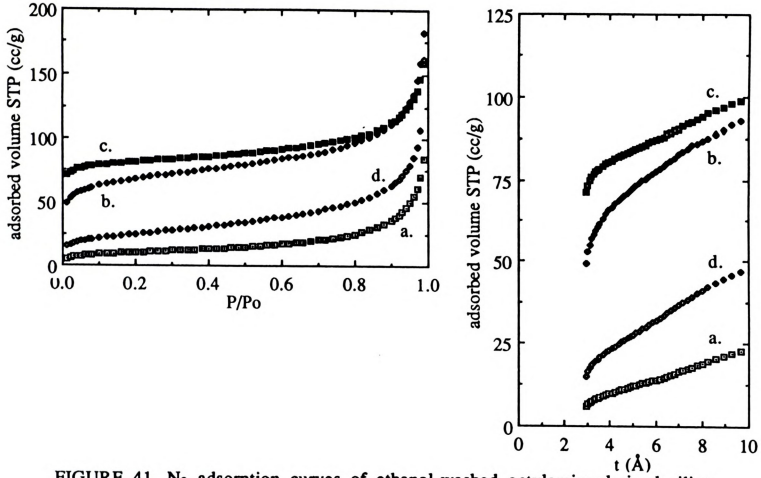

FIGURE 41. N_2 adsorption curves of ethanol-washed octylamine-derived silica-intercalated magadiites at various calcination temperatures
left: N_2 adsorption isotherm, right: t-plot
a. siloxane-intercalated magadiite b. silica-intercalated 100°C
c. silica-intercalated 250°C d. silica-intercalated 450°C
e. silica-intercalated 800°C

TABLE 30. N_2 adsorption data of unwashed and ethanol-washed octylamine-derived silica-intercalated magadiites at various calcination temperatures

octylamine-derived silica-intercalated magadiite	BET[43]	t-plot[44]				
	S_{total} m^2/g	S_{total} m^2/g	$S_{non-\mu}$ m^2/g	$S_{\mu}^{(1)}$ * m^2/g	$S_{\mu}^{(2)}$ * m^2/g	V_{μ} liq cm^3/g
unwashed precursor						
100°C	70	50	50	0	0	0
250°C	670	690	100	680	590	0.24
450°C	760	790	100	770	690	0.27
800°C	620	630	90	610	540	0.21
washed precursor						
100°C	40	40	40	0	0	0
250°C	250	280	80	200	200	0.07
450°C	320	380	50	300	330	0.10
800°C	90	90	80	20	10	0.01

S_{μ}: microporous surface area, $S_{non-\mu}$: non-microporous surface area, V_{μ}: microporous volume

* $S_{\mu}^{(1)}$ is derived from V_{μ} by the t-plot method ; $S_{\mu}^{(2)} = S_{total} - S_{non-\mu}$

As we already saw in the section on acid-catalyzed TEOS polymerization in the presence of alkylamines, the total surface areas calculated from the BET equation[43] and the t-plot method[44] agree relatively well. However, the unwashed samples' microporous surfaces determined by the classic de Boer et al.[44] t-plot method are always higher than the difference between the total surface area and the non-microporous surface area. This might be due to the fact that the micropores are so large (see XRD patterns on Figure 39: left, display gallery height of 20 to 23 Å) that they do not match typical micropores (pore < 20 Å), but are too small to be assigned to mesopores (20 < pore < 500 Å). On the other hand, $S_{\mu}^{(1)}$ and $S_{\mu}^{(2)}$ values for the ethanol-washed samples (XRD patterns on Figure 39: right, display gallery height of 5 to 8 Å) are in agreement.

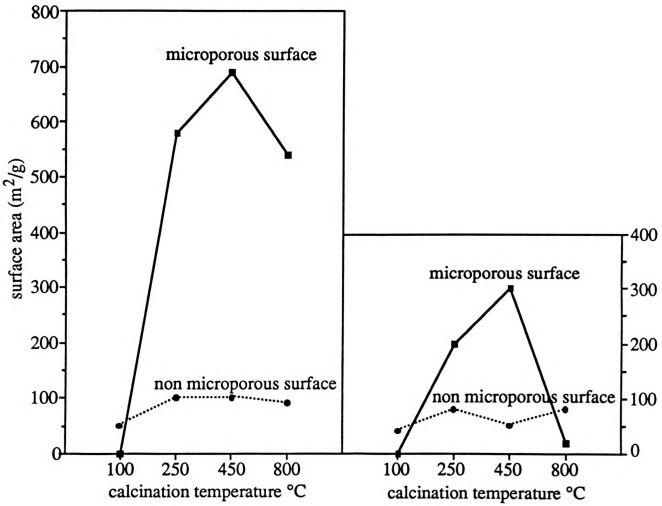

FIGURE 42. Dependence of the microporous and non-microporous surface areas on the calcination temperature
left: unwashed octylamine-derived silica-intercalated magadiites
right: ethanol-washed octylamine-derived silica-intercalated magadiites

Figure 42 is a plot of the microporous ($S_{\mu}^{(2)}$) and non-microporous ($S_{non\text{-}\mu}$) surface area data from Table 30 as a function of the calcination temperature. Clearly, as we eliminate the octylamine upon heating from 100°C to 450°C, the pores are unplugged and the nitrogen gas molecules can access them. So, the pores are shaped by the octylamine. However, when the calcination temperature is increased to 800°C, the total surface area decreases, almost certainly due to a collapse of the structure. The non-microporous surface area is about the same for each samples: ~80 m^2/g. It is independent of the calcination temperature and on the washing procedure. For the two washing procedures, the maximum surface area is obtained for the 450°C calcination temperature. Also, we can see that ethanol-washing decreases the total surface areas. This result can be related to the depletion of amine and the loss of gallery height seen in Table 29. So, either the microporous surface area is dependent on the size of the gallery height, or after dissolution of the siloxane in ethanol, the silica recrystallizes in a different way.

Infrared spectroscopy

We set the experimental parameters to 450°C for the calcination temperature with no ethanol-washing according to structural analyses. We then tried to relate these physical behaviors to chemical properties. First, we carried out infrared spectroscopy experiments. The spectra are displayed in Figures 43 and 44. The data are gathered in Table 31.

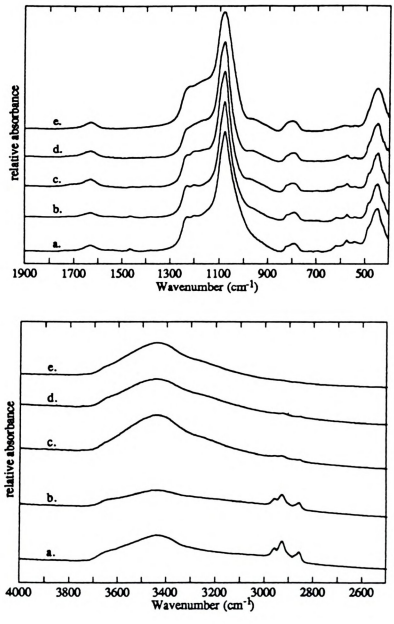

FIGURE 43. Infrared spectra of unwashed octylamine-derived siloxane- and silica-intercalated magadiite (KBr pellet, room temperature)

a. siloxane-intercalated magadiite
b. silica-intercalated 100°C
c. silica-intercalated 250°C
d. silica-intercalated 450°C
e. silica-intercalated 800°C

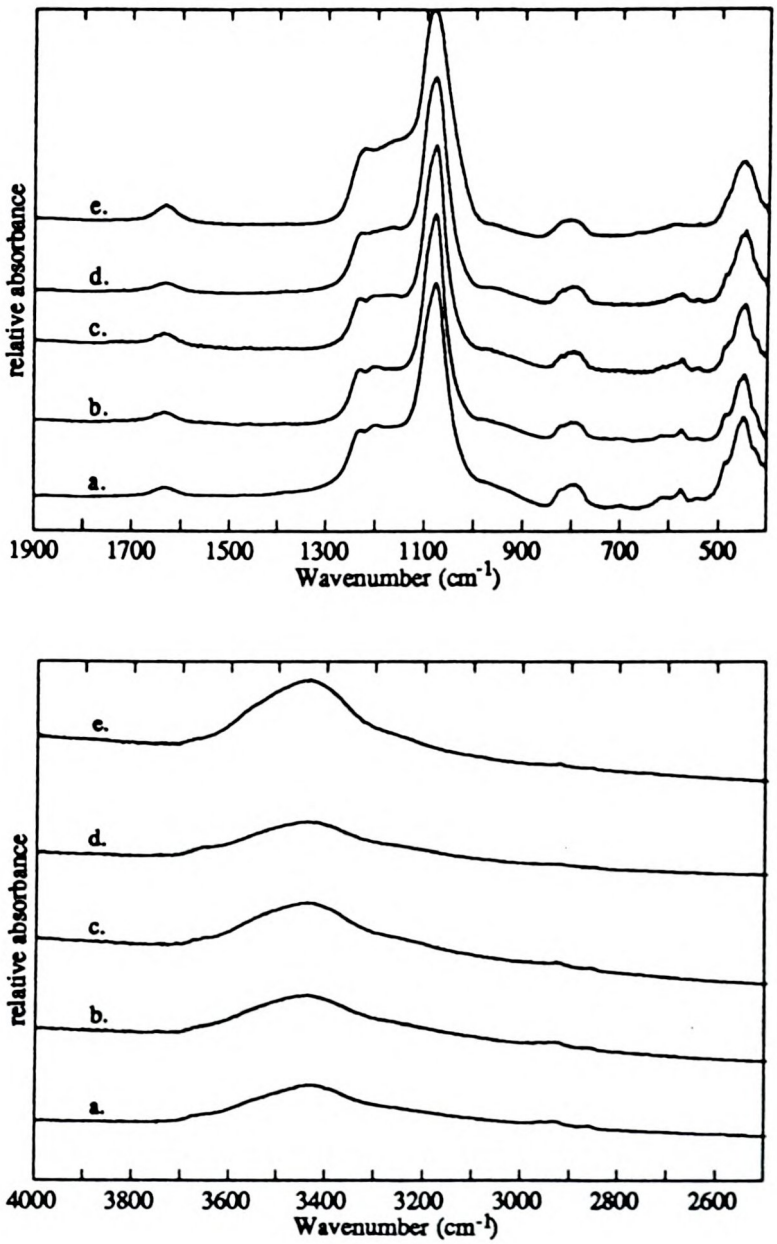

FIGURE 44. Infrared spectra of ethanol-washed octylamine-derived siloxane- and silica-intercalated magadiite (KBr pellet, room temperature)

a. siloxane-intercalated magadiite
b. silica-intercalated 100°C
c. silica-intercalated 250°C
d. silica-intercalated 450°C
e. silica-intercalated 800°C

TABLE 31. Infrared data of unwashed and ethanol-washed octylamine-derived siloxane- and silica-intercalated magadiites

octylamine-derived silica-intercalated magadiite	wavenumber (cm^{-1})									
	ν(O-H)	ν(CH_2,CH_3)		δ(H_2O)	ν(C-C)	ν(Si-O)				
unwashed precursor	3620 3440	2959 2928	2872 2857	1631	1469	1233 1200	1078		821 796	613 576 542 483 450
100°C	3620 3440	2959 2928	2872 2857	1631	1469	1233 1200	1078	975	821 796	619 576 542 483 450
250°C	3440	2928	2857	1631		1233 1194	1078	975	821 796	613 576 542 483 450
450°C	3440			1631		1226	1078	975	821 796	576 542 483 450
800°C	3440			1631		1226	1078	969	803	588 542 450
washed precursor	3650 3440	2959 2928	2872 2857	1631		1233 1200	1078	975	821 796	613 576 542 483 440
100°C	3658 3440	2959 2928	2872 2857	1631		1233 1200	1078	975	821 796	613 576 542 483 450
250°C	3650 3440	2928	2857	1631		1233 1200	1078	975	821 796	613 576 542 483 450

450°C	3658 3440		1631		1233	1078 975	803	576 542 483 450
800°C	3669 3440		1631		1223	1078 969	803	592 450

There are only small differences in the infrared spectra of the unwashed (Figure 43) and ethanol-washed samples (Figure 44). The only difference, as well as the one between the calcination temperatures is the amount of octylamine. There is almost no octylamine present (Figure 22b : 2959, 2928, 2872, 2857 and 1469 cm^{-1}) in the ethanol-washed samples. However, in the unwashed samples, the amine is almost completely removed at 450°C. In the Si-O vibration region, we can recognize the bands originating from the magadiite layer structure: 1233-1223, 1200, 1078, 975, 821, 613, 576-579, 542 and 483 cm^{-1} (Figure 12). The bands at 1237 and 1210 cm^{-1} for Na-magadiite were assigned by Garces et al.[22] to the presence of SiO_4 units forming five-member rings. Also, the 579-576 and 542 cm^{-1} bands represent the presence in the structure of double rings.[22,37] The Si-O asymmetric stretch vibration at 1078 cm^{-1} is the most intense band in the Na-magadiite and H-magadiite spectra as well as on the octylamine-derived siloxane- and silica-intercalated magadiite.The 975 cm^{-1} vibration is a Si-OH stretching band for isolated silanols.[40] This set of infrared experiments tells us that the silicate structure is retained after the polymerization of TEOS inside the magadiite layers. To get information about the silanols, we performed some infrared measurements

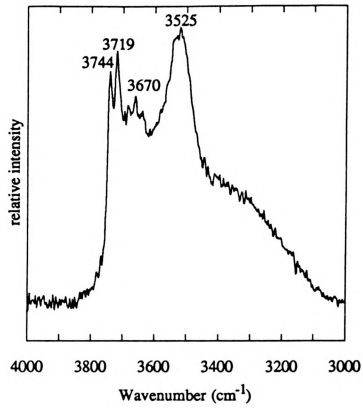

FIGURE 45. Hydroxyl stretch FTIR bands under vacuum at 150°C for unwashed octylamine-derived silica-intercalated magadiite (450°C) (1 mg of sample in a 100 mg KBr pressed pellet)

under vacuum at 150°C to eliminate the water molecules filling the pores (Figure 45).

Four hydroxyl stretch bands can be seen at 3744, 3719, 3670 and 3525 cm^{-1}. By comparing with the data for Na-magadiite and H-magadiite samples (Table 8), we find that the sharp bands at 3744 and 3719 cm^{-1} were already present in the pure Na-magadiite pressed pellet sample. These two bands, however, were absent in the Na-magadiite KBr pellet and H-magadiite samples. These sharp peaks are indicative of isolated silanols. They are regenerated during the intercalation reaction. The two broad peaks at 3670 and 3525 cm^{-1} could be assigned to the two 3595 and 3497 cm^{-1} peaks from the Na-magadiite structure. They are shifted to higher wavenumbers because of the presence of the intercalated silica.

^{29}Si nuclear magnetic resonance

To obtain further information for the silanol groups, we conducted some ^{29}Si nuclear magnetic resonance experiments. The spectra are displayed in Figures 46 and 47.

By comparing the spectra with those of H-magadiite and the products of the acid-catalyzed reaction of TEOS in presence of alkylamines, we can see that the peaks shapes and positions are close to those of H-magadiite. The retention of the magadiite structure found by infrared spectroscopy is confirmed by ^{29}Si nuclear magnetic resonance. We can also notice, for the unwashed and washed samples, that the Q^3 peak relative to $(SiO)_3\underline{Si}O\text{-}Z$ ($Z \neq Si$) silicon environment[41] is decreasing in intensity and broadening as the calcination temperature is increased. It even displays a tail to lower

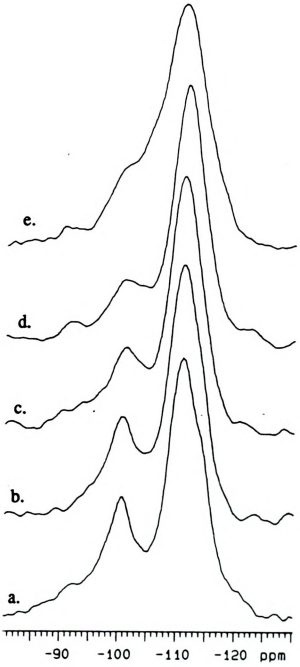

FIGURE 46. ^{29}Si NMR spectra of unwashed octylamine-derived siloxane- and silica-intercalated magadiites
(delay time: 600 seconds, line broadening: 40, 12 scans)

a. siloxane-intercalated magadiite
b. silica-intercalated 100°C
c. silica-intercalated 250°C
d. silica-intercalated 450°C
e. silica-intercalated 800°C

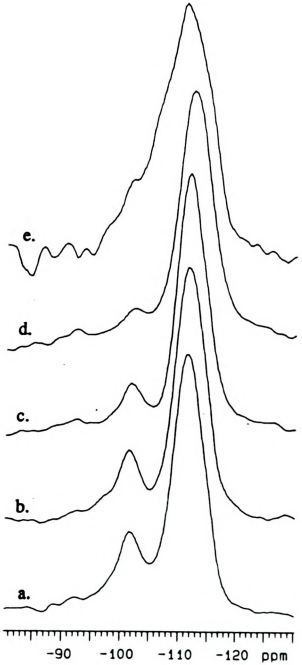

FIGURE 47. ^{29}Si NMR spectra of ethanol-washed octylamine-derived siloxane- and silica-intercalated magadiites
(delay time: 600 seconds, line broadening: 40, 12 scans)

a. siloxane-intercalated magadiite
b. silica-intercalated 100°C
c. silica-intercalated 250°C
d. silica-intercalated 450°C
e. silica-intercalated 800°C

field, suggesting the presence of the Q^2 silicon environment $(SiO)_2\underline{Si}(O\text{-}Z)_2$ ($Z \neq Si$). This tail is confirmed on the 450°C samples, and sometimes the 250°C ones, by the presence of a peak at about 92 ppm. However, upon calcination at 800°C, the Q^2 peak weakens and the Q^3 peak gets shifted toward the Q^4 peak: they can not be differentiated anymore. So, when the octylamine-derived silica-intercalated products are calcined at too a high temperature, the magadiite layers start becoming destroyed. The asymmetry of the Q^4 silicon environment $\underline{Si}(OSi)_4$ peak suggest several contributions to that kind of tetrahedra. Because of those overlaying Q^4 peaks as well as the shallow Q^2 peak and the overlapping of the Q^3 and Q^4 peaks, the ratio of the different silicon environment by deconvolution is complex and can lead to various conclusions. Up to this point, only qualitative conclusions can be drawn: upon increasing the calcination temperature, more silanol groups (Q^3) condense to form siloxane bridges (Q^4) ; the magadiite layer is altered at 800°C.

Conclusion

In conclusion, X-ray diffraction analysis and nitrogen adsorption analysis helped us to choose the optimum experimental parameters: in the further study we did not include a washing procedure during the synthesis and the calcination temperature was set to 450°C. Indeed, ethanol-washing, even though apparently not changing the general chemical features of the products, dissolves the product of the TEOS polymerization. As it recrystallizes in absence of alkylamine upon evaporation, the arrangement inside the layers is disturbed. According to ^{29}Si nuclear magnetic resonance, calcining the siloxane-intercalated silica at too a high temperature, not only converts the siloxane into silica, but also partly

destroys the magadiite structure. That is why, upon increasing the calcination temperature up to 450°C, the pores are freed from octylamine and the surface area increases. But then, with no more amine in the structure above 450°C, the surface area decreases due to a collapse of the structure.

Alkylamine and TEOS to magadiite molar ratio effects

The synthesis of new porous materials is a fast developing field, in particular in the silicon domain.[2-4,42,70,73,74] The goal of those studies is to tailor microporous and mesoporous compounds in a wide range of specific and uniform pore sizes. Indeed, zeolites only exhibit homogeneous pore sizes in the range 4 Å to 15 Å. Thus, crystalline materials with well-defined pore sizes in the range 15 Å to 30 Å are not available for industrial applications. Different approaches have been used. One route is to use a layered starting material. Porous material is created either by polymerizing inside the layers of metal alkoxides $M(OR)_x$,[2-4] either by grafting oligomer species[70] or by generating partial condensation of the layers.[42,73] A more recent procedure is to polymerize metal alkoxide $M(OR)_x$ in the presence of an onium ions.[74] In the preceding chapter on the acid-catalyzed TEOS $Si(OCH_2CH_3)_4$ polymerization in the presence of alkylamines, we studied the synthesis of microporous materials with sizable pore sizes. After establishing the experimental parameters, we are going to study a parallel approach making use of layered materials. We are then going to relate the products to those from the acid-polymerization of TEOS in the presence of alkylamine.

In order to vary the pore sizes, we studied the polymerization of TEOS into H-magadiite in the presence of three different amines:

hexylamine, octylamine and decylamine. The increase in the amine length is expected to increase the pore size in the c-axis direction. We also used various TEOS:amine:magadiite molar ratios of 200:27:1, 100:27:1 and 50:27:1, as defined in Table 32.

TABLE 32. Experimental conditions for the study of the polymerization of TEOS into H-magadiite

sample	amine	calcination temperature	molar ratio		
			TEOS	amine	magadiite
HAMAG50	hexylamine	none	50	27	1
CHAMAG50		450°C	50	27	1
OAMAG50	octylamine	none	50	27	1
COAMAG50		450°C	50	27	1
DAMAG50	decylamine	none	50	27	1
CDAMAG50		450°C	50	27	1
HAMAG100	hexylamine	none	100	27	1
CHAMAG100		450°C	100	27	1
OAMAG100	octylamine	none	100	27	1
COAMAG100		450°C	100	27	1
DAMAG100	decylamine	none	100	27	1
CDAMAG100		450°C	100	27	1
HAMAG200	hexylamine	none	200	27	1
CHAMAG200		450°C	200	27	1
OAMAG200	octylamine	none	200	27	1
COAMAG200		450°C	200	27	1
DAMAG200	decylamine	none	200	27	1
CDAMAG200		450°C	200	27	1

Chemical compositions

We first studied the effect of the amine on the chemical composition of the siloxane- and silica-derived magadiites (Table 33).

TABLE 33. Chemical composition from elemental analysis for unwashed alkylamine-derived siloxane- and silica-intercalated magadiites at the TEOS:amine:magadiite molar ratio = 100:27:1

	%wt element					%wt composition			
sample	%wt C*	%wt H*	%wt N*	%wt Si**	%wt O**	%wt amine**	%wt ethoxy**	%wt H_2O**	%wt SiO_2**
HAMAG100	7.4	2.5	1.4	39	49	13	0.0	5.3	84
OAMAG100	14	3.5	2.0	35	45	18	1.5	5.8	75
DAMAG100	19	4.5	2.1	31	43	19	9.5	4.2	67
CHAMAG100	0.47	1.4	0.05	41	57	0.46	0.24	11	88
COAMAG100	0.78	1.6	0.09	40	57	0.83	0.31	13	86
CDAMAG100	0.63	1.3	0.01	41	57	0.09	1.1	10	88

* measured from C, H, N analysis

** calculated according to the method explained in the section acid-catalyzed TEOS polymerization in the presence of alkylamines

Contrary to our findings for the TEOS-derived silica precursor (Table 14), the change in the amine dimension does not greatly affect the chemical composition of the siloxane-intercalated magadiites. The only significant change is in the increasing presence of ethoxy-ethanol groups with the increase of the amine chain length. It should be noticed, from a comparison of Tables 14 and 33, that the amount of alkylamine present is much lower than in the case of the polymerization without any layered support. In some extent, this can be understood by the presence of the silicate layers which contribute to the %wt SiO_2. After calcination, most of the amine is removed as well as most of the ethoxy groups which are most probably converted to hydroxyl groups. The resulting chemical composition is close to those found for the TEOS-derived silica (Table 14).

^{29}Si nuclear magnetic resonance

To further investigate the ethoxy-ethanol and silanol groups, we conducted some ^{29}Si nuclear magnetic resonance experiments (Figures 48 and 49).

To obtain the correct Q^4:$(SiO)_4\underline{Si}$, Q^3:$(SiO)_3\underline{Si}O$-Z and Q^2:$(SiO)_2\underline{Si}(O\text{-}Z)_2$ (Z≠Si) peak ratios,[41] the spectra were recorded with a time interval of 600 seconds. This delay time is about four times larger than the relaxation times found to be 141 ± 11 s for a Q^4 environment and 44 ± 5 s for a Q^3 environment.[4] Each unwashed amine-derived siloxane-intercalated magadiite spectra exhibits one Q^3 peak at -100.6 ppm and a Q^4 peak centered at -110.9 ppm. However, the HAMAG100 Q^3 peak is broader than the OAMAG100 and DAMAG100 ones. Moreover, as the Q^4 to Q^3 intensity ratio is about the same for the three samples, we can say that the hexylamine-derived sample possesses more silanols (Q^3) than the two other samples. After calcination at 450°C, the unwashed amine-derived silica-intercalated spectra exhibit less defined Q^3 and Q^4 peaks due to the Q^3 peak upfield shift and smaller intensity ; the separation of those two peaks is improved when the amine chain length is increased. Also, as we saw in Figure 46 and on the samples studied at 360°C,[4] the resolution of the peaks gets worse as the calcination temperature is increased. However, a Q^2 peak appears at about -91 ppm. Thus, upon calcination at 450°C, rearrangements occur: some silanol groups (Q^3) are converted to siloxane bridges (Q^4) by condensation, but, surprisingly, some Q^2 silicon environments appear. The presence of those Q^2 peaks in the calcined samples and their absence in the uncalcined samples have been checked by Dailey[4] through proton cross-polarization. Proton cross-polarizationenhances the resonance of nuclei

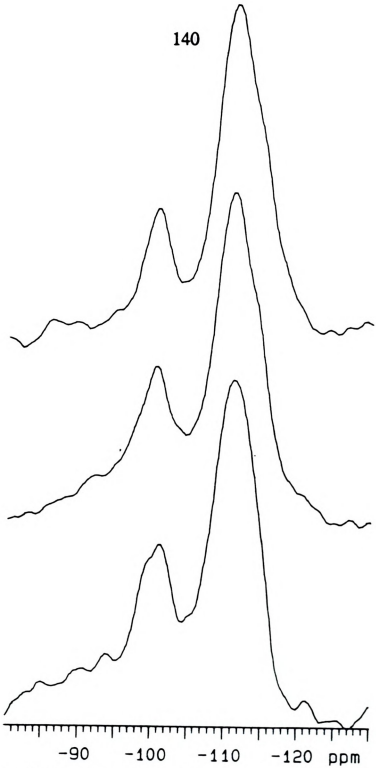

FIGURE 48. ^{29}Si NMR spectra of unwashed amine-derived siloxane-intercalated magadiites with initial TEOS: amine:magadiite molar ratio = 100:27:1 (delay time: 600 seconds, line broadening: 140, 12 scans)

a. hexylamine-derived: HAMAG100
b. octylamine-derived: OAMAG100
c. decylamine-derived: DAMAG100

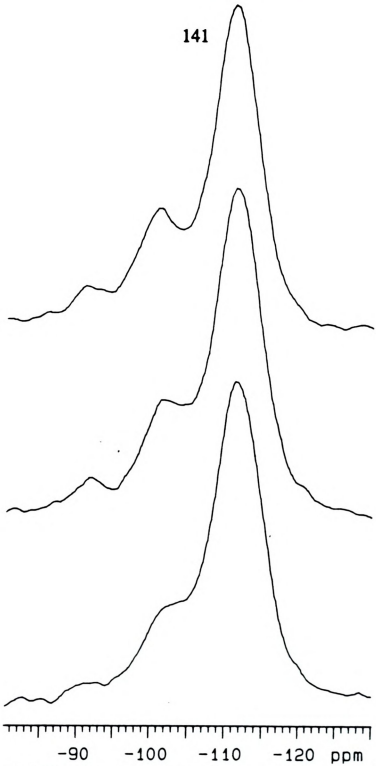

FIGURE 49. ^{29}Si NMR spectra of unwashed amine-derived silica-intercalated magadiites with initial TEOS: amine:magadiite molar ratio = 100:27:1 (delay time: 600 seconds, line broadening: 140, 12 scans)

a. hexylamine-derived: CHAMAG100
b. octylamine-derived: COAMAG100
c. decylamine-derived: CDAMAG100

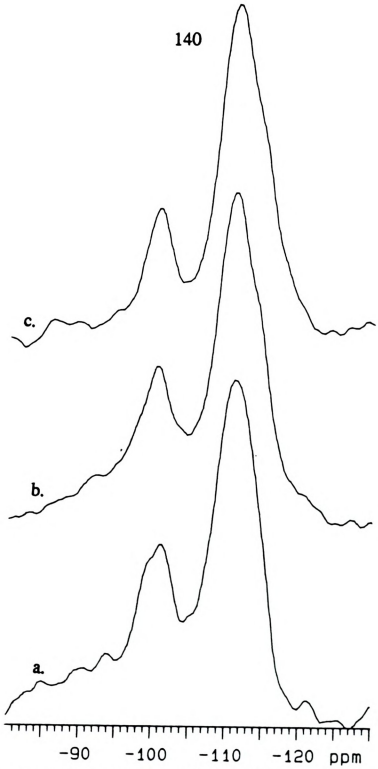

FIGURE 48. ^{29}Si NMR spectra of unwashed amine-derived siloxane-intercalated magadiites with initial TEOS: amine:magadiite molar ratio = 100:27:1 (delay time: 600 seconds, line broadening: 140, 12 scans)

a. hexylamine-derived: HAMAG100
b. octylamine-derived: OAMAG100
c. decylamine-derived: DAMAG100

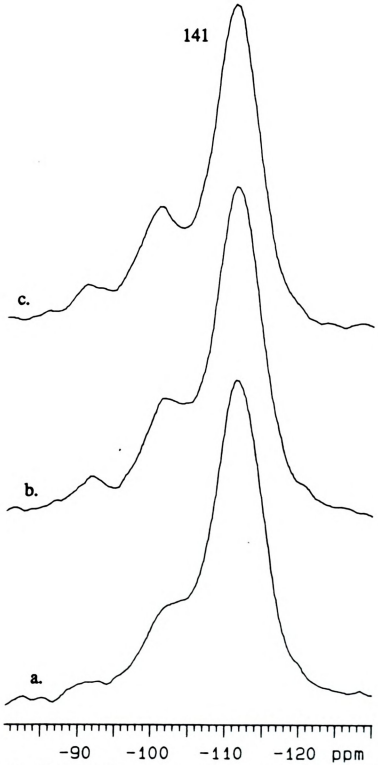

FIGURE 49. ^{29}Si NMR spectra of unwashed amine-derived silica-intercalated magadiites with initial TEOS: amine:magadiite molar ratio = 100:27:1 (delay time: 600 seconds, line broadening: 140, 12 scans)

a. hexylamine-derived: CHAMAG100
b. octylamine-derived: COAMAG100
c. decylamine-derived: CDAMAG100

neighboring protons. Dailey[4] proposed the presence of Q^2 environments in the uncalcined samples as ethoxys: $(SiO)_2\underline{Si}(O\text{-}CH_2CH_3)_2$ instead of silanols: $(SiO)_2\underline{Si}(O\text{-}H)_2$ in the calcined ones. The Q^2 peak lack of enhancement was then due to an absence of coupling because of the increasing number of bonds between the two interacting atoms. Pouxviel et al.[51] took the ^{29}Si NMR spectra of two commercial TEOS. The pure $\underline{Si}(O\text{-}CH_2CH_3)_4$ with no bridging oxygen (Q^0) peak appears at -82 ppm ; disilicic and trisilicic ester ending groups (Q^1) $SiO\underline{Si}(O\text{-}CH_2CH_3)_3$ peak were located at -89 ppm ; peaks at -95.2 ppm and -96.4 ppm were assigned to cyclotetrasilicic and the middle group (Q^2) of linear trisilicic ester ; peaks at -103 ppm and -104 ppm corresponded to branched groups (Q^3) of polysilicic ester ; Q^4 silicon atoms were expected to be located at -110 ppm. Thus $(SiO)_2\underline{Si}(O\text{-}CH_2CH_3)_2$ Q^2 peaks for oligomer species are expected to be located at about -96 ppm. However $(SiO)_2\underline{Si}(O\text{-}CH_2CH_3)_2$ Q^2 peaks for polymers are expected to be shifted upfield due to a greater shielding. This shift might be the explanation for the absence of Q^2 peaks for the uncalcined samples. Even though the Q^2 silicon environments due to ethoxy groups should be more numerous in the uncalcined samples, they might be overlapping the Q^3 peak due to silanols. The comparison of the intercalated magadiite samples (Figures 48 and 49) and the TEOS-derived silica samples (Figures 26 and 27) is the proof for the magadiite layer retention effect during the TEOS polymerization. Indeed, the intercalated magadiite ^{29}Si NMR spectra are more similar to the Na-magadiite and H-magadiite (Figure 14) ones than to the TEOS-derived silica spectra.

X-ray powder diffraction

The alkylamine and TEOS:amine:magadiite molar ratio effects can be easily followed by X-ray diffraction. The patterns of the unwashed alkylamine-derived siloxane- and silica-intercalated magadiites are displayed according to the initial TEOS:amine:magadiite molar ratio in Figures 50, 51 and 52. The basal spacing and gallery height (= basal spacing - layer thickness = basal spacing - 11.2) are gathered in Table 34. A summary graph is represented in Figure 53.

TABLE 34. X-ray diffraction data of unwashed alkylamine-derived siloxane- and silica-intercalated magadiites

sample	TEOS:amine magadiite = 50:27:1		TEOS:amine: magadiite = 100:27:1		TEOS:amine: magadiite = 200:27:1	
	d_{001} (Å)	gallery height (Å)	d_{001} (Å)	gallery height (Å)	d_{001} (Å)	gallery height (Å)
HAMAG	27.6	16.4	28.0	16.8	27.8	16.6
CHAMAG	23.9	12.7	25.5	14.3	24.2	13.0
OAMAG	35.7	24.5	36.0	24.8	37.0	25.8
COAMAG	30.1	18.9	34.6	23.4	35.3	24.1
DAMAG	43.4	32.2	41.9	30.7	41.4	30.2
CDAMAG	28.2	17.0	39.2	28.0	38.8	27.6

As the X-ray diffraction patterns exhibit one 001 peak and sometimes a 002 reflection, only one phase is present in our unwashed alkylamine-derived siloxane- and silica-intercalated magadiites. It proves that TEOS polymerized inside the magadiite layers. If it had polymerized outside the layers, we would get a two-phase X-ray diffraction pattern: one for the H-magadiite at 12.0 Å and one for the TEOS-derived silica. The

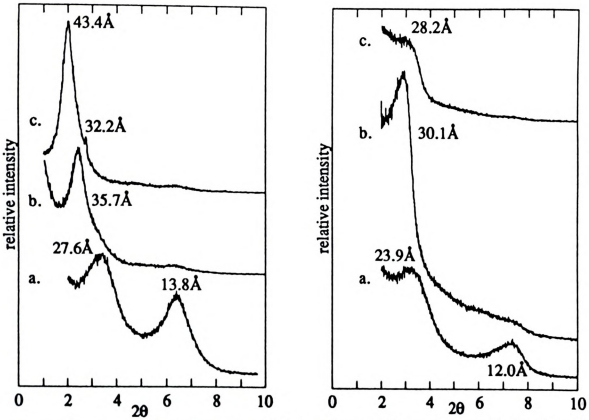

FIGURE 50. X-ray powder diffraction (pwd) patterns of unwashed alkylamine-derived siloxane- and silica-intercalated magadiites with initial TEOS:amine:magadiite molar ratio = 50:27:1

left: unwashed alkylamine-derived siloxane-intercalated magadiite

right: unwashed alkylamine-derived silica-intercalated magadiite

a. hexylamine-derived: HAMAG50 and CHAMAG50

b. octylamine-derived: OAMAG50 and COAMAG50

c. decylamine-derived: DAMAG50 and CDAMAG50

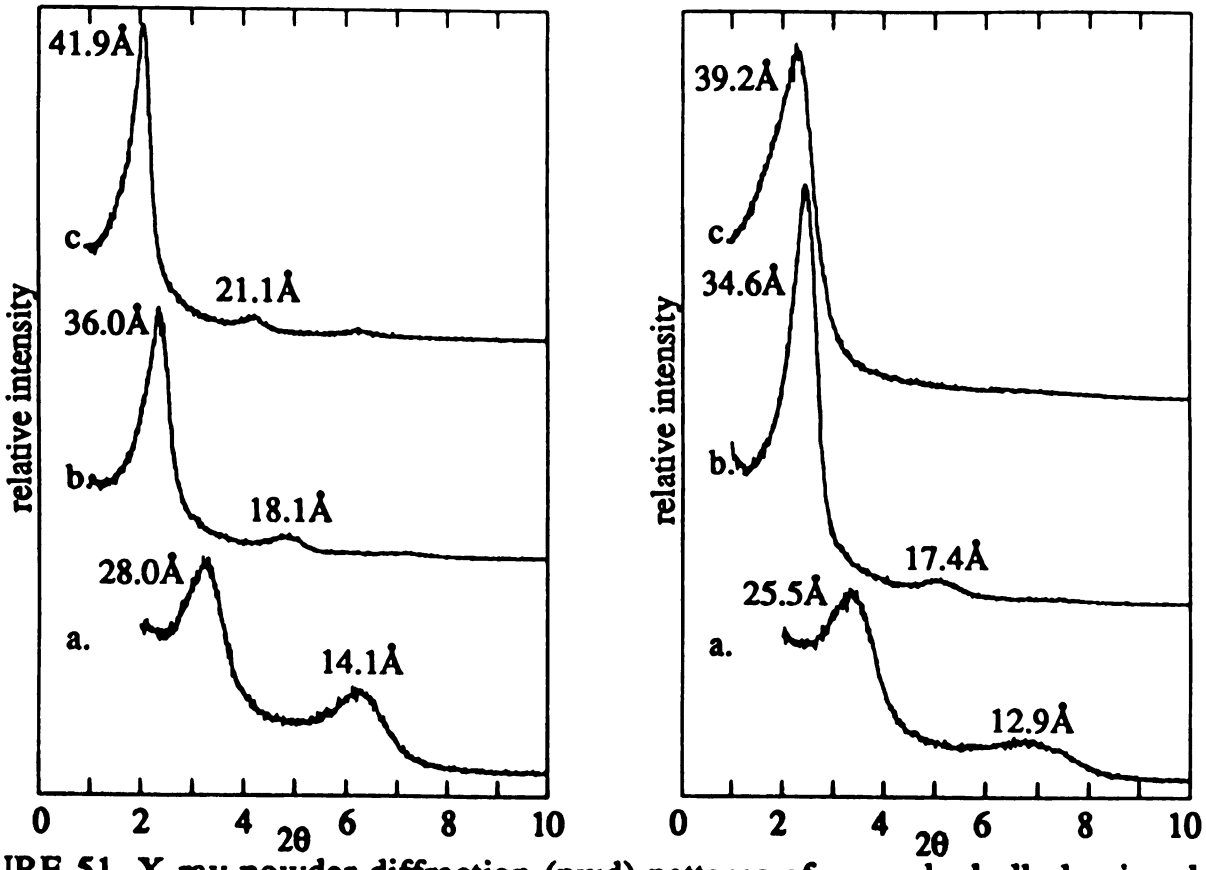

FIGURE 51. X-ray powder diffraction (pwd) patterns of unwashed alkylamine-derived siloxane- and silica-intercalated magadiites with initial TEOS:amine:magadiite molar ratio = 100:27:1

left: unwashed alkylamine-derived siloxane-intercalated magadiite

right: unwashed alkylamine-derived silica-intercalated magadiite

a. hexylamine-derived: HAMAG100 and CHAMAG100

b. octylamine-derived: OAMAG100 and COAMAG100

c. decylamine-derived: DAMAG100 and CDAMAG100

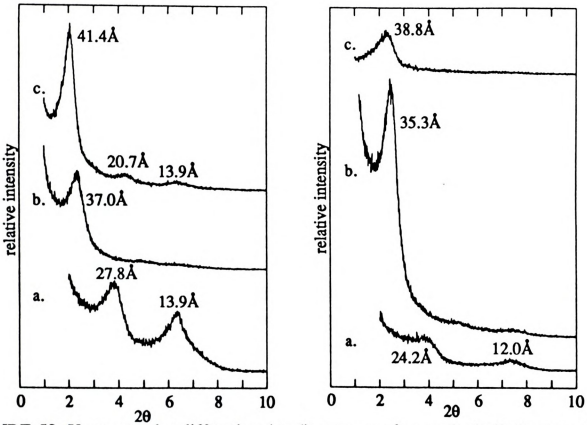

FIGURE 52. X-ray powder diffraction (pwd) patterns of unwashed alkylamine-derived siloxane- and silica-intercalated magadiites with initial TEOS:amine:magadiite molar ratio = 200:27:1

left: unwashed alkylamine-derived siloxane-intercalated magadiite

right: unwashed alkylamine-derived silica-intercalated magadiite

a. hexylamine-derived: HAMAG200 and CHAMAG200

b. octylamine-derived: OAMAG200 and COAMAG200

c. decylamine-derived: DAMAG200 and CDAMAG200

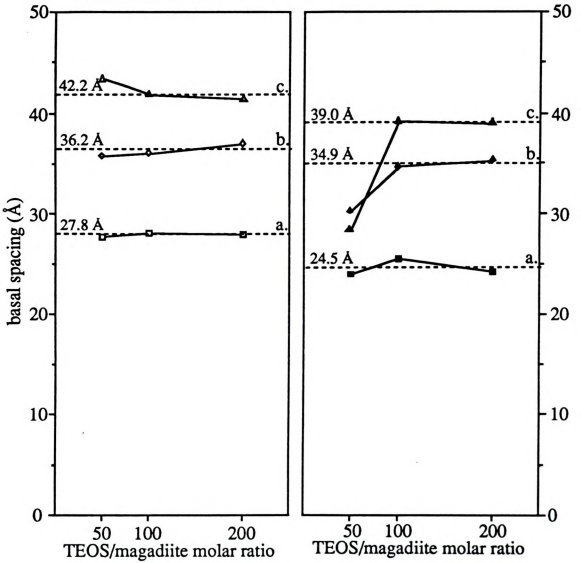

FIGURE 53. Dependence of the basal spacing of the unwashed alkylamine-derived siloxane- and silica-intercalated magadiites on TEOS:magadiite molar ratio
left: unwashed alkylamine-derived siloxane-intercalated magadiites
rigth: unwashed alkylamine-derived silica-intercalated magadiites
a. hexylamine-derived: HAMAG and CHAMAG
b. octylamine-derived: OAMAG and COAMAG
c. decylamine-derived: DAMAG and CDAMAG

alkylamine effect is readily seen on the unwashed alkylamine-derived siloxane-intercalated magadiites. As the amine chain length is increased, the basal spacing and gallery height are increased. The basal spacing for a given amine is independent of the TEOS:amine:magadiite molar ratio. Whatever this ratio is, the unwashed alkylamine-derived siloxane-intercalated magadiites display a basal spacing of about 27.8 Å, 36.2 Å and 42.2 Å for the hexylamine-, octylamine- and decylamine-derived samples, respectively. These d_{001} values closely correspond to the basal spacings found for the amine-solvated alkylammonium/alkylamine magadiites (Table 22): 30.9 Å, 34.0 Å and 41.3 Å for hexylamine, octylamine and decylamine, respectively. Thus the basal spacings determined for the unwashed alkylamine-derived siloxane-intercalated magadiites reflect the amine-solvated alkylammonium/alkylamine magadiites spacings. The slight variations might be due to the different methods of sample preparation. The XRD patterns for the amine-solvated alkylammonium/alkylamine magadiites were recorded for gels spread onto a microscope glass slide while those for the unwashed alkylamine-derived siloxane-intercalated magadiites were recorded as oriented powders. However, upon calcination at 450°C, two types of behavior can be determined. Except for the octylamine- and decylamine-derived samples at the lowest TEOS:magadiite molar ratio, the basal spacing of the unwashed alkylamine-derived silica-intercalated magadiites is independent on the initial TEOS:magadiite molar ratio. The basal spacing is only slightly decreased to 24.5 Å, 34.9 Å and 39.0 Å, for hexylamine, octylamine and decylamine, respectively. This fact demonstrates the importance of the choice of the amine for the TEOS polymerization along the c-axis direction. Regardless of the TEOS:magadiite molar ratio chosen, the gallery height will not be larger

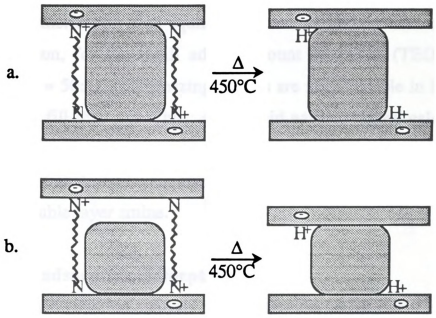

FIGURE 54. Schematic representation of the role of alkylamine on the basal spacing of unwashed alkylamine-derived siloxane- and silica-intercalated magadiites

than the length of the alkylamine bilayer. The octylamine- and decylamine-derived products at the initial TEOS:magadiite molar ratio of 50:1 samples exhibit a different behavior. Upon calcination at 450°C, the basal spacing drops to about the same 24.8 Å value for the two samples. The fact that this latter behavior only occurs for the longest amines and lowest TEOS addition leads us to the conclude it was due to the limited polymerization of TEOS, as shown on Figure 54. For the octylamine- and decylamine-derived samples, the TEOS-derived silica needs to fill the gallery space

opened by the amine, namely 24.0 Å and 30.0 Å for octylamine and decylamine, respectively, in comparison of 15.6 Å for hexylamine. As the TEOS polymerization is an equilibrium reaction and depends on the TEOS concentration, for the small added amount of TEOS (TEOS:magadiite molar ratio = 50:1), polymerizing species are not available in large enough quantity to fill that gap. Thus, as we said earlier, before calcination, the layers are still pushed apart by the amine ; but after removal of the amine by heat treatment, the layers are stacked onto the polymer which is shorter than the double layer amine.

Nitrogen adsorption-desorption

X-ray diffraction analysis showed that the amine chain length has an effect on the c-axis dimension of the TEOS polymerization inside the magadiite galleries. However, at sufficiently large amount of TEOS, no effect was observed on the basal spacing. TEOS stoichiometry could have an effect on the filling of gallery space along the other two directions, namely along the a-axis and b-axis. So, some changes should occur in the surface area analysis. We thus performed some nitrogen adsorption-desorption experiments. The curves for the unwashed alkylamine-derived silica-intercalated magadiites are displayed according to the initial TEOS:amine:magadiite molar ratio in Figures 55, 56 and 57. The surface areas data are gathered in Table 35.

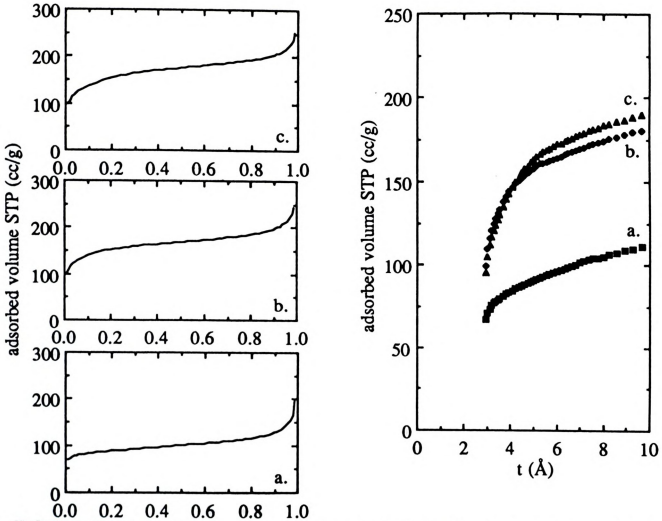

FIGURE 55. N_2 adsorption curves of unwashed alkylamine-derived silica-intercalated magadiites with initial TEOS:amine:magadiite molar ratio= 50:27:1
left: N_2 adsorption isotherm, right: t-plot
a. hexylamine-derived: CHAMAG50, b. octylamine-derived: COAMAG50
c. decylamine-derived: CDAMAG50

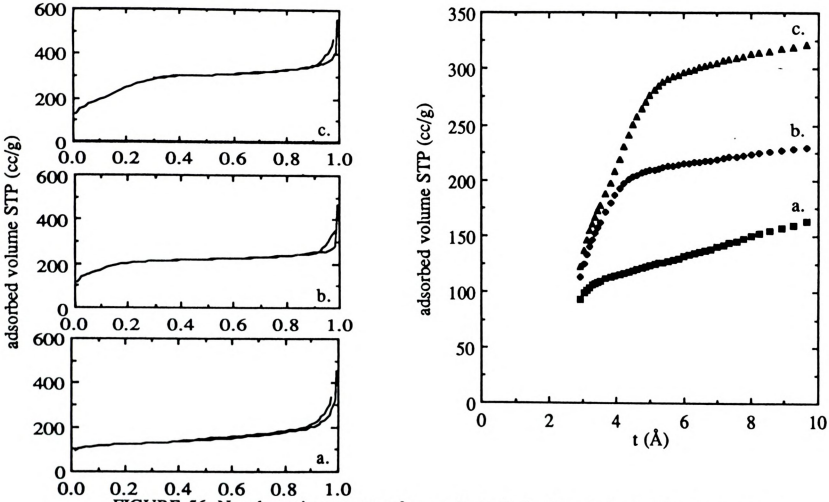

FIGURE 56. N_2 adsorption curves of unwashed alkylamine-derived silica-intercalated magadiites with initial TEOS:amine:magadiite molar ratio= 100:27:1
left: N_2 adsorption-desorption isotherm, right: t-plot
a. hexylamine-derived: CHAMAG100, b. octylamine-derived: COAMAG100
c. decylamine-derived: CDAMAG100

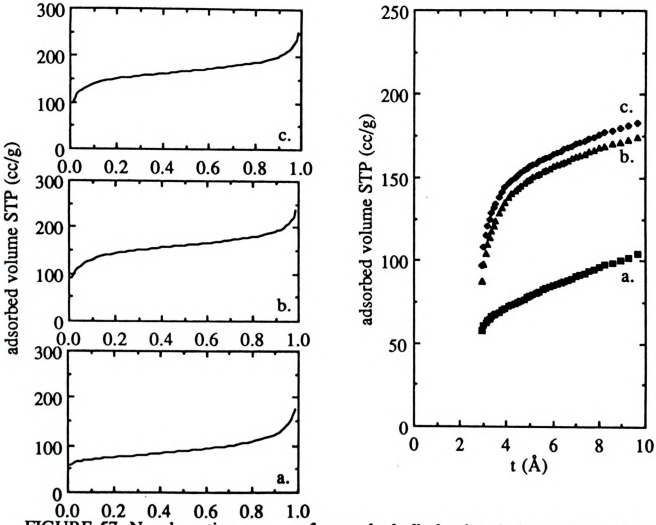

FIGURE 57. N_2 adsorption curves of unwashed alkylamine-derived silica-intercalated magadiites with initial TEOS:amine:magadiite molar ratio= 200:27:1
left: N_2 adsorption isotherm, right: t-plot
a. hexylamine-derived: CHAMAG200, b. octylamine-derived: COAMAG200
c. decylamine-derived: CDAMAG200

TABLE 35. N_2 adsorption data of unwashed alkylamine-derived silica-intercalated magadiites

alkylamine-derived silica-intercalated magadiite	BET[43]	t-plot[44]				
	S_{total} m^2/g	S_{total} m^2/g	$S_{non-\mu}$ m^2/g	$S_{\mu}^{(1)}$ * m^2/g	$S_{\mu}^{(2)}$ * m^2/g	V_{μ} liq cm^3/g
TEOS:magadiite=50:1						
CHAMAG50	320	370	90	270	280	0.10
COAMAG50	560	580	100	560	480	0.20
CDAMAG50	550	570	100	580	470	0.20
TEOS:magadiite=100:1						
CHAMAG100	440	500	130	350	370	0.12
COAMAG100	760	790	100	770	690	0.27
CDAMAG100	820	840	130	1070	710	0.38
TEOS:magadiite=200:1						
CHAMAG200	270	310	100	200	210	0.07
COAMAG200	540	540	100	510	440	0.18
CDAMAG200	570	590	110	530	480	0.19

S_{μ}: microporous surface area, $S_{non-\mu}$: non-microporous surface area, V_{μ}: microporous volume

* $S_{\mu}^{(1)}$ is derived from V_{μ} by the t-plot method ; $S_{\mu}^{(2)} = S_{total} - S_{non-\mu}$

The total surface areas found by the BET equation[43] and t-plot[44] method agree relatively well (Appendix C). The non-microporous surface areas are about the same ~100 m^2/g for all the samples, regardless the amine used and the TEOS concentration. The high total surface areas are due to the presence of micropores. The unwashed octylamine- and decylamine-derived silica-intercalated magadiites exhibit almost the same surface areas while the hexylamine-derived samples always exhibit surface areas half as large. The similarity of the octylamine- and decylamine-derived surface areas has already been noted for the TEOS-derived silica (Table 19). Assuming the silica gallery species and magadiite silicate layers have the same density, we calculated the expected microporous surface areas if the gallery space is completely stuffed and if the microporosity is

only coming from the TEOS-derived silica. The results are displayed in Table 36.

TABLE 36. Calculated alkylamine-derived silica-intercalated magadiite microporous surface area assuming the interlayer space is stuffed with TEOS-derived silica

alkylamine-derived silica-intercalated magadiite	ratio$_{c\text{-}axis}$ = d_{001}/ gallery height (Table 34)	T19: TEOS-derived silica $S_{\mu}^{(2)}$ * m^2/g (Table 19)	alkylamine-derived silica-intercalated magadiite	
			T36**: calculated $S_{\mu}^{(2)}$ * m^2/g	T35: $S_{\mu}^{(2)}$ * m^2/g (Table 35)
TEOS:magadiite=50:1				
CHAMAG50	0.53	870	460	280
COAMAG50	0.63	1030	650	480
CDAMAG50	0.60	920	550	470
TEOS:magadiite=100:1				
CHAMAG100	0.56	650	360	370
COAMAG100	0.68	1100	750	690
CDAMAG100	0.71	1110	790	710
TEOS:magadiite=200:1				
CHAMAG200	0.54	710	380	210
COAMAG200	0.68	970	660	440
CDAMAG200	0.71	990	700	480

* S_{μ}:microporous surface area, $S_{non\text{-}\mu}$:non-microporous surface area, $S_{\mu}^{(2)} = S_{total} - S_{non\text{-}\mu}$

** T36 = ratio$_{c\text{-}axis}$ * T19

Calculated microporous surface areas assuming a stuffed interlayer space (T36) give a higher microporous area than the one obtained experimentally from the t-plot method (T35). Thus, the interlayer space is not completely stuffed with the highly microporous TEOS-derived silica. Some holes might be present, possibly as large pores between entities that are acting like pillars. However, a difference with the TEOS-derived silica can be noticed: the surface areas are dependent on the initial

TEOS:amine:magadiite molar ratio. The total surface area reaches a maximum for the ratio 100:27:1 and the surface areas are about the same for the 50:27:1 and 200:27:1 ratio. The surface areas increase from the TEOS to amine molar ratio = 50:1 to 100:1 reflects the increase in the basal spacings. The maximum surface area values for an identical gallery height (Table 34) for the TEOS to magadiite molar ratios = 100:1 and 200:1 can be understood in terms of different mechanisms of TEOS polymerization. The interlayer space available for TEOS polymerization is constant, but there are more polymerizable species, the TEOS-derived silica formed at the 200:1 ratio might be more dense due to enhanced TEOS polymerization on the internal surface of the pores.

CONCLUSION

The polymerization of TEOS in the galleries of layered silicic acid affords highly microporous materials. The polymerization is done in presence of alkylamines that swell the magadiite layers. Indeed, for TEOS polymerization to start inside the layers, the TEOS molecules have to reach the interlayer protons. As the diameter of TEOS is about 9 Å, the molecules can not access the H-magadiite protons because the interlayer space is less than 1 Å. When H-magadiite layers are swelled by alkylamines, the protons are converted into ammonium cations in presence of excess amine, and the gallery space is expanded, depending on the amine chain length. The polymerization of TEOS can then start. However, as we saw in the case of acid-catalyzed TEOS polymerization in the presence of alkylamines, the amine used to swell the layers will also play a further role in the polymerization. As ethanol washing dissolves the TEOS-derived precursors, as well as the siloxane-intercalated magadiite, and the surface

areas conclusions are identical, we conclude that the magadiite layers are intercalated by our new porous TEOS-derived silica. The calcination temperature used to obtain silica-intercalated magadiite from the siloxane precursor has been found to be optimized at 450°C. Indeed, below 450°C, some amine is still present in the structure, and above 450°C, the magadiite structure starts collapsing or rearranging. The alkyl chain length of the amine affects the basal spacing of the final silica-intercalated magadiite. Indeed, when enough TEOS species are present, the limiting factor for the polymerization growth in the c-axis direction is the amine bilayer space created between the magadiite layers. However, when too many TEOS molecules are present, the silica-intercalated magadiite looses some of its microporosity, probably due to a densification of the silica-intercalated species.

CONCLUSIONS AND SUGGESTIONS FOR FUTURE WORK

The study of Na-magadiite, H-magadiite and the conversion of the sodium to the proton form leads us to a better understanding of the structural importance of the intergallery space. Indeed, for various sodium contents Na-magadiite exhibits substantially longer range order along the stacking axis in comparison to H-magadiite. Furthermore, the stacking order of Na-magadiite decreases as water is removed from the gallery upon heating. Removal of water from Na-magadiite by heat treatment is equivalent to proton exchange with regard to effects on stacking order. In the known makatite structure, water molecules connect consecutive layers as part of the hydration sphere around the sodium cation and are situated at specific locations in the gallery space. We thus assigned the loss of order in H-magadiite to a rearrangement of the gallery space due to the absence of water molecules. This assignment could be confirmed by a study of other

members of the hydrous sodium silicate minerals family where the stabilizing effect of the gallery water molecules on the structure should also be manifested as a general trend for the whole family. An additional improvement to elucidate the Na-magdiite structure would be the synthesis of single crystals and the X-ray crystallographic determination of the structure.

The acid-catalyzed hydrolysis-polymerization of tetraethylorthosilicate in the presence of alkylamines generates precursors, which, when calcined, afford highly microporous silica. The pore size is controlled by the length of the amine alkyl chain. Further studies with longer amines would probably lead to pore sizes in the domain of mesoporosity. This method could then be used to create silica with determined micropores or mesopores sizes. More information on the final silica product could be obtained from adsorption isotherms of molecules with known kinetic diameters and from the study of transmission electron micrographs. A better knowledge of the reaction would be gained by liquid ^{29}Si NMR studies on the supernatant and photon correlation spectroscopy to determine particle growth. Porous acidic alumina-silica for catalytic purposes could then be synthesized by substitution of silicon atoms by aluminum atoms.

The polymerization of tetraethylorthosilicate into alkylamine-swollen layered silicic acid affords materials with large surface areas, due to the silica-intercalated porosity. The hydrolysis is catalyzed by the interlayer protons. Alkylamines are used to swell the layers in order for the protons to be accessible. However, the alkylamines also play a further role in

designing the pore sizes and the basal spacing of the final silica-intercalated magadiite. The optimum calcination temperature of 450°C is used to obtain silica-intercalated magadiite from the siloxane precursor. The surface areas exhibited a maximum value for a TEOS:magadiite molar ratio of 100:1. This optimal surface area could be explained by a difference in the density of the intercalated species. Density experiments and measurements of the unreacted silicon centers left in solution by liquid ^{29}Si NMR studies would bring a better understanding of the silica-intercalated magadiite compounds.

APPENDICES

APPENDIX A

Electron diffraction analysis[75]

The electron diffraction lattice dimension are given by the Bragg's relation and the small angle approximation.

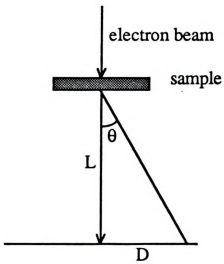

FIGURE 58. Electron diffraction analysis parameters

The Bragg's relation gives:

$$\frac{n.\lambda}{2\ d} = \sin\theta \sim \mathrm{tg}\theta = \frac{D}{L} \qquad \text{for } \theta \sim 0$$

so, $$d = \frac{n \lambda L}{2 D}$$

- d is the lattice dimension
- L is the camera length -> we used L=83 cm
- λ is the electron wavelength -> for a 100 kV voltage, λ=0.037 Å
- D is the measured length on the diffractogram -> between two consecutive points, D=0.369 cm
- n is the order -> between two consecutive points, n=1

thus, $d = 4.16$ Å

APPENDIX B

Scherrer equation[76]

This equation is used to calculate the crystallinity of a material using its X-ray diffraction spectrum.

$$D_{hkl} = \frac{k\,\lambda_{Cu}}{2\,l_{hkl}\cos\theta}$$

- D_{hkl}: crystallinity or coherent scattering domain (Å)
- k: constant close to unity -> if we take k=1, we are going to obtain proportional values for the crystallinity
- λ_{Cu}: copper K_α radiation wavelength (in nm) -> λ_{Cu} = 1.542 nm

- l_{hkl}: corrected half-height width of the sample hkl peak

  $l'^2_{hkl} = l''^2_{hkl} + l^2_{hkl}$

  l'_{hkl}: measured half-height width of the sample hkl peak

  l''_{hkl}: measured half-height width of the reference hkl peak

  for the phlogopite reference, l''_{hkl} = 0.0023 radian

- θ: half the angle (in radian) at which the hkl peak occurs

APPENDIX C

Gas adsorption analysis

The gas adsorption analysis *experimental data* is the adsorption-desorption isotherm. Usually, the isotherm is set at 77 K, the temperature of liquid nitrogen. It is a plot of the adsorbed volume: V_{ads} in cc/g at STP versus the relative pressure: P/P_0 (Figure 59).

- P_0 is the saturating pressure of the adsorbed gas.

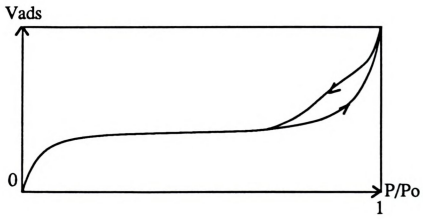

FIGURE 59. Adsorption-desorption isotherm

Three kinds of pores are defined:

- micropores: pores inferior to 20 Å in diameter
- mesopores: pores whose diameter is comprised between 20 Å and 500 Å
- macropores: pores superior to 500 Å in diameter

As the sides of the micropores are close to one another, the interaction energy is large and the adsorption will be rapid. The microporous data can be derived from the t-plot method using the first points of the isotherm.

The presence of mesopores can be noted if there is an hysteresis in the region of the last points on the adsorption isotherm. Indeed, as mesopores are larger than micropores, they are filled with liquid due to capillarity condensation. They will thus exhibit a delay time during the desorption that will create the hysteresis. The determination of the mesopores is derived from the Kelvin's law.

The presence of macropores cannot be detected from gas adsorption. The determination of the macropores, as well as the mesopores, is done by mercury porosity.

The total surface area can be calculated by applying the *BET theory*.[43] The BET equation converts the isotherm adsorption curve to a straight line by changing the y-axis to $\frac{1}{V_{ads}(P_0-P)}$ (Figure 60).

The BET theory is valid up to $P/P_0=0.35$

BET equation: $$\frac{1}{V_{ads}(P_0-P)} = \frac{1}{C\,V_m} + \frac{(C-1)}{C\,V_m}\frac{P}{P_0}$$

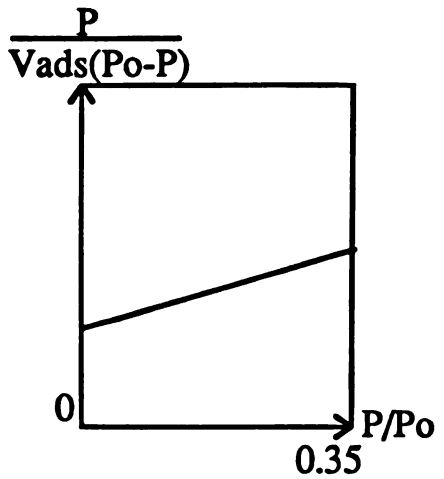

FIGURE 60. BET curve

The slope: $\frac{(C-1)}{C\ V_m}$ and the intercept: $\frac{1}{C\ V_m}$ of the straight line allow for the determination of C and V_m.

- C is an energetical constant: $C = k \exp \frac{(E_1-E_L)}{R\ T}$

  with E_1: filling energy of the first layer of gas adsorbate

  E_L: liquefaction energy of the gas adsorbate

- V_m is the monolayer capacity. It is given in cm^3 of adsorbate / g of adsorbent.

The BET surface area is equal to the total surface area. It is given in m^2/g.

$$S_{BET} = V_m \frac{\mathcal{N}_A}{V_{N2gas}} \sigma_{N2gas} = V_m * 4.37$$

- $\mathcal{N}_A$ is the Avogadro's number -> $6.02\ 10^{23}$ molecules/mol
- V_{N2gas} is the volume of one mole of gas -> 22414 cm^3/mol

- σ_{N2gas} is the average area occupied by a molecule of nitrogen in the completed monolayer -> $16.2*10^{-20}$ m^2/molecule

The microporosity can be determined by using the *t-plot method.*[44] The t-plot is a representation of the adsorption isotherm, where the x-axis is converted to t-values. The t-values are function of P/P_0; as our surfaces are more or less constitued of silicon oxide, we used t-values derived experimentally by de Boer from the study of non microporous oxides. The t-plot is valid up to P/P_0=0.4 This method provides the total surface area (S_{total}), the non-microporous surface ($S_{non-\mu}$) and the microporous volume (V_μ).

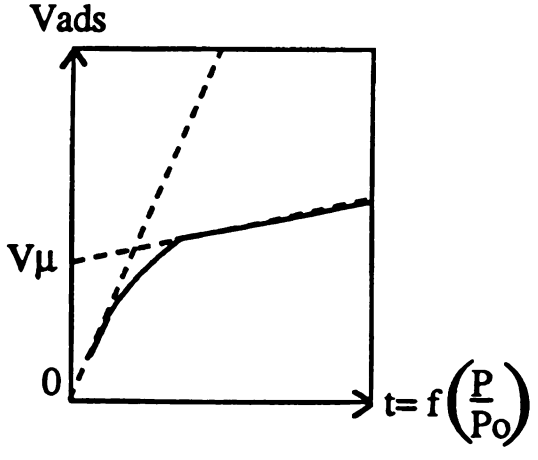

FIGURE 61. t-plot

The total surface area (S_{total}) in m^2/g is calculated from the first slope on the t-plot:

$$S_{total} = \text{1st slope} * \frac{\mathcal{N}_A}{V_{N2gas}} \sigma_{N2gas} * \phi_{N2} = \text{1st slope} * 15.47$$

- ϕ_{N2} is the thickness of a single molecular layer of nitrogen molecules -> $3.54 * 10^{-10}$ m

The non microporous surface area ($S_{non\text{-}\mu}$) in m^2/g is calculated from the second slope on the t-plot:

$$S_{non\ \mu} = \text{2nd slope} * \frac{\mathcal{N}_A}{V_{N2gas}} \sigma_{N2gas} * \phi_{N2} = \text{2nd slope} * 15.47$$

The gaseous microporous volume (V_μ) in cm^3/g is given by the intercept of the second slope. This gaseous volume can be converted to a liquid volume in liq cm^3/g:

$$V_\mu(liq) = \frac{V_\mu(gas)}{V_{N2gas}} * \frac{M_{N2}}{\rho_{N2}} = V_\mu(gas) * 0.00154$$

- ρ_{N2} is the density of liquid nitrogen -> 0.81 g/cm^3
- M_{N2} is the molar mass of nitrogen gas -> 28 g/mol

The microporous surface (S_μ) in m^2/g can be derived from this microporous volume:

$$S_\mu = V_\mu(gas) * \frac{\mathcal{N}_A}{V_{N2gas}} . \sigma_{N2gas} = V_\mu(gas) * 4.37$$

LIST OF REFERENCES

LIST OF REFERENCES

1 T. J. Pinnavaia. *Science*, **220**, 365 (1983).

2 M. E. Landis, C. Pochen, I. D. Johnson, G. W. Kirker, M. K. Rubin and B. Cynwyd. US patent 4,859,648 (1989).

3 M. E. Landis, B. A. Aufdembrink, P. Chu, I. D. Johnson, G. W. Kirker and M. K. Rubin. *Journal of the American Chemical Society*, **113**, 3189 (1991).

4 J. S. Dailey. PhD thesis Michigan State University (1991).

5 T. J. Pinnavaia, M. S. Tzou, S. D. Landau and R. H. Raythatha. *Journal of Molecular Catalysis*, **27**, 185 (1984).

6 R. Burch and C. I. Warburton. *Journal of Catalysis*, **97**, 503 (1986).

7 G. Lagaly, K. Beneke and A. Weiss. *The American Mineralogist*, **60**, 642 (1975).

8 G. Lagaly, H.-M. Riekert and H. H. Kruse. Chemical Reactions in Organic and Inorganic Constrained Systems, Setton edition, Reidel Publishing Company, 361 (1986).

9 R. A. Fletcher and D. M. Bibby. *Clays and Clay Minerals*, **35**(4), 318 (1987).

10 G. Lagaly, K. Beneke and A. Weiss. *Proceedings of the International Clay Conference*, Madrid, 663 (1972).

11 S. J. Gregg and K. S. W. Sing. Adsorption, Surface Area and Porosity, 2nd edition, Academic press, London, (1982).

12 Z. Johan and G. F. Maglione. *Bulletin de la Société française de Minéralogie et de Cristallographie*, **95**, 371 (1972).

13 K. Beneke and G. Lagaly. *The American Mineralogist*, **62**, 763 (1977).

14 T. J. Pinnavaia, I. D. Johnson and M. Lipsicas. *Journal of Solid State Chemistry*, **63**, 118 (1986).

15 R. A. Sheppard and A. J. Gude. *The American Mineralogist*, **55**, 358 (1970).

16 H. Annehed, L. Fälth and F. J. Lincoln. *Zeitschrift für Kristallogaphie*, **159**, 203 (1982).

17 H. P. Eugster. *Science*, **157**, 1177 (1967).

18 W. Schwieger, D. Heidemann and K.-H. Bergk. *Revue de Chimie Minérale*, **22**, 639 (1985).

19 L. McCulloch. *Journal of the American Chemical Society*, **74**, 2453 (1952).

20 V. G. Il'in, L. F. Kirichenko, Y. K. Ivanov, V. Y. Kondrachuk and Z. Z. Vysotskii. *Doklady Physical Chemistry*, USSR. English Translation, **174**, 408 (1967)

21 I. M. Timishenkov, Y. P. Menshikov, L. F. Gannibal and I. V. Bussen. *Zapiski Vsesoyuznogo Mineralogicheskogo Obschchestva*, **104**, 317 (1975). (abstract in M. Fleischer, *The American Mineralogist*, **61**, 339 (1976).

22 J. M. Garces, S. C. Rocke, C. E. Crowder and D. L. Hasha. *Clays and Clay Minerals*, **36**(5), 409 (1988).

23 G.Borbély, H. K. Beyer, H. G. Karge, W. Schwieger, A. Brandt and K.-H. Bergk. *Clays and Clay Minerals*, **39**(5), 490 (1991).

24 M.-T. Le Bihan, A. Kalt and R. Wey. *Bulletin de la Société Française de Minéralogie et de Cristallographie*, **94**, 15 (1971).

25 K. Beneke and G. Lagaly. *The American Mineralogist*, **74**, 224 (1989).

26 A. J. Gude and R. A. Sheppard. *The American Mineralogist*, **57**, 1053 (1972).

27 R. K. Iler. *Journal of Colloidal Science*, **19**, 648 (1964).

28 G. Lagaly, K. Beneke and A. Weiss. *The American Mineralogist*, **60**, 650 (1975).

29 G. Lagaly. *Advances in Colloid and Interface Science*, **11**, 105 (1979).

30 J. M. Rojo, J. Sanz, E. Ruitz-Hitzky and J. M. Serratosa. *Zeitschrift fuer Anorganische und Allgemeine Chemie*, **540-541**, 227 (1986).

31 T. Yanagisawa, K. Kuroda and C. Kato. *Bulletin of Chemical Society of Japan*, **61**(10), 3743 (1988).

32 K.-H. Bergk, C. Schuetz and W. Schwieger. *Silikatlechnik*, **41**(7), 241 (1990).

33 J. M. Rojo, E. Ruiz-Hitzky, J. Sanz and J. M. Serratosa. *Revue de Chimie Minérale*, **20**, 807 (1983).

34 J. M. Rojo, E. Ruiz-Hitzky and J. Sanz. *Inorganic Chemistry*, **27**, 2785 (1988).

35 J. B. Peri. *The Journal of Physical Chemistry*, **70**(9), 2937 (1966).

36 J. L. McAtee, R. House and H. P. Eugster. *The American Mineralogist*, **53**, 2061 (1968).

37 G. Scholzen, K. Beneke and G. Lagaly. *Zeitschrift fuer Anorganische und Allgemeine Chemie*, **597**, 183 (1991).

38 G. W. Brindley. *The American Mineralogist*, **54**, 1583 (1969).

39 Powder diffraction file. Inorganic volume, set ?, JCPDS

40 B. A. Morrow and A. J. McFarlan. *The Journal of Physical Chemistry*, **96**, 1395 (1992).

41 E. Lippma, M. Mägi, A. Samoson, G. Engelhardt and A.-R. Grummer. *Journal of the American Chemical Society*, **102**, 4889 (1980).

42 T. Yanagisawa, T. Shimizu, K. Kuroda and C. Kato. *Bulletin of Chemical Society of Japan*, **63**(4), 988 (1990).

43 S. Brunauer, P. H. Emmet and E. Teller. *Journal of the American Chemical Society*, **60**, 309 (1938).

44 J. H. de Boer, B. C. Lippens, B. G. Linsen, J. C. P. Broekhoff, A. Van den Heuvel and T. J. Osinga. *Journal of Colloid and Interface Science*, **21**, 405 (1966).

45 T. J. Pinnavaia, M. S. Tzou, S. D. Landau and R. H. Raythatha. *Journal of Molecular Catalysis*, **27**, 185 (1984).

46 R. Burch and C. I. Warburton. *Journal of Catalysis*, **97**, 503 (1986).

47 L. C. Klein. *Annual review of Materials Science*, **15**, 227 (1985).

48 I. Strawbridge, A. F. Craievich and P. F. James. *Journal of Non-Crystalline Solids*, **72**, 139 (1985).

49 J. B. Blum and J. W. Ryan. *Journal of Non-Crystalline Solids*, **81**, 221 (1986).

50 K. C. Chen, T. Tsuchiya and J. D. Mackenzie. *Journal of Non-Crystalline Solids*, **81**, 227 (1986).

51 J. C. Pouxviel, J. P. Boilot, J. C. Beloeil and J. Y. Lallemand. *Journal of Non-Crystalline Solids*, **89**, 345 (1987).

52 C. W. Turner and K. J. Franklin. *Journal of Non-Crystalline Solids*, **91**, 402 (1987).

53 K. Kamaiya, T. Yoko and H. Suzuki. *Journal of Non-Crystalline Solids*, **93**, 407 (1987).

54 J. F. Quinson, N. Tchipkam, J. Dumas, C. Bovier and J. Serughetti. *Journal of Non-Crystalline Solids*, **100**, 231 (1988).

55 A. H. Boonstra and T. N. M. Bernards. *Journal of Non-Crystalline Solids*, **105**, 207 (1988).

56 J. C. Ro and I. J. Chung. *Journal of Non-Crystalline Solids*, **110**, 26 (1989).

57 T. Kawaguchi and K. Ono. *Journal of Non-Crystalline Solids*, **121**, 383 (1990).

58 M. T. Haris, R. R. Brunson and C. H. Byers. *Journal of Non-Crystalline Solids*, **121**, 397 (1990).

59 A. H. Boonstra and J. M. E. Baken. *Journal of Non-Crystalline Solids*, **122**, 171 (1990).

60 M. J. van Bommel, T. N. M. Bernards and A. H. Boonstra. *Journal of Non-Crystalline Solids*, **128**, 231 (1991).

61 H. A. Szimanski and R. E. Erickson. Infrared band handbook, 2nd edition, Plenum Press, London, (1970).

62 A. Stock and C. Somieski. *Berichte der Deutschen Chemischen Gesellschaft*, **54**, 740 (1921).

63 A. Stock. Hydrides of Boron and Silicon, Cornell University Press, Ithaca, N.Y., 30 (1933).

64 R. L. Wells and R. Schaeffer. *Journal of the American Chemical Society*, **88**, 37 (1966).

65 H. Bürger and W. Sawodny. *Spectrochimica Acta*, **23**(A), 2827 (1967).

66 W. D. Harkins and G. Jura. *Journal of the American Chemical Society*, **66**, 1362 (1944).

67 C. J. Brinker, K. D. Keefer, R. A. Assink, B. D. Kay and C. S. Ashley. *Journal of Non-Crystalline Solids*, **63**, 45 (1984).

68 E. Ruiz-Hitzky and J. M. Rojo. *Nature*, **287**, 28 (1980).

69 E. Ruiz-Hitzky, J. M. Rojo and G. Lagaly. *Colloid and Polymer Science*, **263**, 1025 (1985).

70 R. Sprung, M. E. Davis, J. S. Kauffman and C. Dyboski. *Industrial and Engineering Chemistry Research*, **29**, 213 (1990).

71 T. Yanagisawa, C. Yokoyama, K. Kuroda and C. Kato. *Bulletin of Chemical Society of Japan*, **63**(1), 47 (1990).

72 Y. Sugahara, K. Sugimoto, T. Yanagisawa, Y. Nomizu, K. Kuroda and C. Kato. *Yogyo Kyokai Shi*, **95**, 117 (1987).

73 T. Yanagisawa, T. Shimizu, K. Kuroda and C. Kato. *Bulletin of Chemical Society of Japan*, **63**(5), 1535 (1990).

74 a. J. S. Beck. US patent 5,057,296 (1991).
b. C. T. Kresge, M. E. Leonowicz, W. J. Roth and J. C. Vartuli. US patent 5,098,684 (1992).
c. C. T. Kresge, M. E. Leonowicz, W. J. Roth and J. C. Vartuli. US patent 5,102,643 (1992).

75 J. R. Fryer. The chemical application of transmission electron microscopy, Academic Press (1979).

76 Scherrer equation